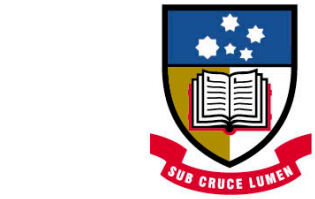


THE UNIVERSITY of ADELAIDE

# An Investigation of Biological Processes Underlying Neratinib-induced Gut Injury

A thesis submitted in fulfilment for the degree of

Master of Philosophy (Medical Science)

in

Discipline of Physiology

School of Biomedicine

The University of Adelaide

by

**Phu Minh Triet Nguyen, BHlthMedSc (Adv)**

May 2023

*I dedicate this research project to my mum, dad, and brother, who inspire me of this work.*

*I saw it (the result) and then interpreted what it meant. In biology, it is very important to be opened to what nature gives you because nature can lead you in directions which you cannot imagine otherwise.*

*-Sir Paul Nurse-*

*The mission of science is to find the truth. As such, the only way for the truth to unveil itself is to let the true data speak louder than noise.*

*-Phu Minh Triet Nguyen-*

# Table of Contents

# Thesis abstract

Neratinib, a small-molecule tyrosine kinase inhibitor (TKI) that irreversibly binds to human epidermal growth factor receptors 1,2, and 4 (HER1, 2 and 4), was recently approved as an adjuvant therapy for patients with *HER2*-amplified or -overexpressed (*HER2*-positive) breast cancer. However, in clinical practice, more than 90% of patients receiving neratinib experience mild-to-severe symptoms of gut toxicity including abdominal pain and diarrhoea. Despite a highly prevalent complication in gut health, the underlying biological processes of how neratinib causes gut injury, especially in the colon, leading to symptoms of gut toxicity remains unclear. Here, using archived colon tissues collected from healthy female Albino Wistar rats dosed with neratinib (50 mg/kg) daily for 28 consecutive days, we found that the severity of colonic injury, especially degeneration of surface lining colonocytes and infiltration of immune cells, was more pronounced in the distal than in the proximal colon.

To better understand biological processes underlying neratinib-induced cell death, we leveraged previously published bulk RNA-sequencing and CRISPR-screening datasets of neratinib-treated mouse TBCP-1 breast cancer and human glioblastoma SF298 cell line and human glioblastoma T895 xenograft. Gene ontology (GO) term and KEGG pathway analyses suggested that a type of cell death induced by neratinib was likely context specific. Specifically, neratinib stimulates ferritinophagy-mediated ferroptosis in TBCP1 and T895 cells, whereas apoptosis in SF298 cells. To identify whether ferroptosis or apoptosis was potentially induced by neratinib in the rat colon, we integrated the analyses from immunohistochemical staining (Caspase-3 to detect apoptosis, FTH1 and 4HNE to detect ferroptosis) on paraffin-embedded rat colons, and RT-qPCR (markers for iron homeostasis: *Fth1* and *Tfrc*; markers for lipid peroxidation: *Acsl4* and *Alox15*; and marker for general ROS: *Nox1*) on cryopreserved rat colons. Our findings suggested that ferritinophagy-mediated ferroptosis, but less likely

apoptosis, was a potential underlying histopathological feature of colonic injury in rat treated with neratinib. We further wanted to ascertain that colonic epithelial cells could undergo ferroptosis as a direct consequence of neratinib treatment by utilising SW48 colorectal cancer cell line. Although SW48 cells were resistant to neratinib treatment, the observation of vacuoles formation at supra-clinical concentration (10 μM) suggests that this cell line could undergo autophagy-mediated cell death. Thus, we switched our efforts to utilise the 3-dimensional (3D) mouse colonic organoids to circumvent the mutation complexities associated with neratinib resistance in SW48 cells. We showed that organoids can be terminally differentiated which might potentially be exploited as a model system for future mechanistic investigations.

In a context of neratinib-induced ferroptosis, such as in mouse TBCP1 and human SKBR3 HER2-positive breast cancer cell lines, by using published LINC-KINOME scan datasets and the alignment of published X-ray crystal structures, we proposed that inhibiting kinase activity of mitogen-activated protein kinase kinase kinase kinase 3 (MAP4K3) by neratinib might be essential for potentiating ferroptosis, but not other TKI, such as lapatinib, which is linked to apoptosis. Overall, the findings from this research suggest that a type of cell death, i.e. apoptosis or ferroptosis, induced by neratinib may be cell-type specific. Ferroptosis is a potential underlying feature of colon injury. Targeting the molecular machinery underlying neratinib-induced ferroptosis, especially the initiating event of cell death such as perturbed redox regulation at specific subcellular compartments, may serve as an exciting platform for future supportive therapies and drug discovery to mitigate toxicity while enhancing the efficacy of similar or emerging anti-cancer therapeutics.

# Thesis declaration

I certify that this work contains no material which has been accepted for the award of any other degree or diploma in my name, in any university or other tertiary institution and, to the best of my knowledge and belief, contains no material previously published or written by another person, except where due reference has been made in the text. In addition, I certify that no part of this work will, in the future, be used in a submission in my name, for any other degree or diploma in any university or other tertiary institution without the prior approval of the University of Adelaide and where applicable, any partner institution responsible for the joint award of this degree.

I give permission for the digital version of my thesis to be made available on the web, via the University's digital research repository, the Library Search, and also through web search engines, unless permission has been granted by the University to restrict access for a period of time.

I acknowledge the support that I have received for my research through The University of Adelaide funded Master of Philosophy (No Honours) International Scholarship.

**Phu Minh Triet Nguyen,**

14th July 2023

# Acknowledgement

**To Professor Joanne (Jo) Bowen** (Jo the *Legend*) – Thanks for being the greatest mentor that a study could have and for being always excited about my research ideas. Through the course of two-year MPhil's study, you had given me generous academic and moral support, especially when my project did not progress at all during the first six months. Thank you for teaching me how to write and for carefully reading and providing me with your constructive feedback on my drafts. I can't wait to have an opportunity to work with you in the near future.

**To Associate Professor Susan (Susi) Woods** (Susi the *Nature*) – Thank you for teaching how to think clearly and critically, articulate what I want to convey, and the power of the controls in the experiments. Thank you for encouraging me to dream high and work hard towards it. I will never forget what you told me 'If you think like *Nature*, you write like *Nature*, [then] you will get into *Nature*'. And of course, thank you for teaching me how to write like *Nature*! Also, I vividly remember when nothing works in the first place, I even considered switching the research. You, as always, calmly asked 'did your rats experience diarrhoea?', I answered 'yes', you said 'Good! That means your drug is doing something; so, hang in there!', and I did. Finally, Thank you very much for welcoming me to your fantastic Gut Cancer Group at SAMHRI. Here, I would like to extend my gratitude to Laura and Jo for their patience to giving me a training on organoid culture. I can't wait to have an opportunity to work with you in the near future.

**To Dr Senthil Arumugam** (Senthil the *Hero*) – I nearly gave up a career in scientific research, but after spending a few months with your fantastic group, you have awakened my research interest and help me realise the beauty of research is the quest of understanding, not repeating like a parrot. I wanted to give a special thanks to Hetvi, Harry, and Ulhas who had generous

with their time to teach me the proper cell culture techniques. I can't wait to have an opportunity to work with you in the near future.

**To everyone in Cancer Toxicities Treatment Group (both past and present)** – Thank you for your immense support both on academic and personal level. *Mrs. Claire Vieyra*, you are truly the wonderful person, a person for 'discussing' drama, and the best drink buddy. Hang in there with your PhD. *Dr. Aurelia Elz*, I owe a lot to you for being the best lab mentor helping me to navigate through the staining, writing, and missing BOX drama; and discuss exciting research in *Cell*, *Nature*, and *Science*. I hope we will see each other again soon! *Dr. Janine Tam*, you really are the best person for assisting me with my cell culture drama even when you were very stressed with your thesis writing. *Dr. Elise Crame and Dr. Courtney Cross*, it is extremely lucky for me to get to know you guys. You guys are the most cheerful persons that I have ever known. Thanks for your great advice on surviving the research study and for always gets excited when I shared my experimental results and gave a presentation. *Dr. Ghanyah Al-Qadami*, thank you for patiently listening to my 'talks'! *Dr. Emma Bateman*, thank you for always reminding me to be calm and breathe! *Ms. Ifeoma Dikeocha*, provider of food and having fun time, especially shopping and discussing science. *Mr. Chris Tay*, thank you for always patiently listening to my discussion. You have done a fantastic job with navigating through all the cell culture ups and downs. Trust me when I am saying that I'm thrilled whenever I heard you said nothing exciting (subtext is contamination) with your cell culture. Hang in there with your Honours' thesis. I sincerely wish you all the best with your future studies; you got this! *Mr. (To-be Dr.) Bailey Deverell and Ms. (To-be Dr.) Micaela Quinn*, thank you for being great friends and for providing me with critical reagents and consumables when they ran out in the middle of my tissue staining and PCR experiments. *Dr. Hannah Wardill*, thank you for always getting excited about my project and your valuable feedback!

**To my collaborators and friends** – *Professor Andrew Abell and Mr. (To-be Dr.) Dion Turner*, thank you for providing me with your constructive feedback on my research from the chemical perspective. We will get our review paper out, I promise! *Professor Scott Ayton*, one of the great things about my MPhil's study is having stimulating discussion on ferroptosis with you and receiving your valuable suggestions in ferroptosis for my research. Thank you for introducing me to all the giants in ferroptosis! I look forward to working with you soon! *Professor Ross Bathgate and Dr. Brad Hoare*, thank you for teaching me valuable lesson on cell culture, especially not giving up on the somewhat disappointing results from the resistant cell line. Especially, thanks, Ross, for putting me in contact with Scott! *Associate Professor Tania Crotti*, thank you for inspiring me to pursue a career in research and for being an amazing post-graduate coordinator helping me navigate through all the challenges in my entire HDR studies. *Associate Professor John Finnie,* the greatest veterinarian pathologist, thank you for your histopathological assessment on all of my tissue sections and for your enthusiasm for my findings. *Dr Christine Chio (Columbia University)*, a legendary ROS lady. Thank you for sharing your passion in ROS biology with me and for our thoughtful discussion on the choice of probes for ROS detection. *Mr. Simon Tang*, my dearest friend and to-go bioinformatician. Thanks for being a great friend, teaching me how to perform RNA-sequencing and troubleshooting everything for me on this aspect that I am completely clueless. *My bestie, Ms. (To-be Dr.) Suet Yee Too*, you are indeed the greatest friend that one could ask for. I feel extremely fortunate to know you personally. Seriously, thank you for always listening to my 'talks' and providing me your unconditional supports. I will never forget our drink that has led us to formulate the conjecture of MAP4K3 modulation. Hang in there with your research; you got this! *To Mr. Jaydon Chai* (my dearest and to-go AlphaFold friend; thanks for the Japanese whiskey by the way!)*, Ms. Christina Karalis and Ms. Chloe Wallent* (my dearest friends and moral support, and deep down from my heart, thank you for showing me how to think positive

when my experiments go south), and *the other members of Amgen Scholar Program*, I sincerely thank you for all the fun, especially all the spontaneous day trips and drinks, that we have together, for always be there for me in both good and bad times, and for always encouraging to pursue my dream in Science. *To the Adelaide microscopy staff - Dr. Agatha Labrinidis, Dr. Jane Sibbons, and Mr. Chris Leigh*, thanks for assisting me with the slide scanners and TEM imaging. You guys are truly remarkable persons!

**Finally, to my wonderful family, *Mum, Dad, and Brother*,** thank you for all your unwavering support, encouragement, and belief in me even when I had doubt about myself. Especially to you, *Mum*, you are the inspiration of my work. You are my hero who always supports whatever decisions I take; and teaches me that nothing is impossible if I am strong, resilient, and full of determination.

# Presentation and abstract arising from the thesis

| Type | Title | Conference |
|---|---|---|
| Poster presentation | Uncovering mechanism of neratinib-induced gut toxicity | 2022 Florey Postgraduate Research Conference, The University of Adelaide, Australia. |
| Poster presentation | Neratinib-induced ferritinophagy is locoregional and cell-type specific in the colon | Iron, Reactive Oxygen Species & Ferroptosis in Life, Death & Disease, Awaji, Japan. (*) |
| Poster presentation | Ferroptosis: an emerging mechanism of gut toxicity induced by neratinib | AusIron 2022, The Florey Institute of Neuroscience and Mental Health, Melbourne, Australia. (**) |

(*) I was awarded the competitive *Adelaide Graduate Research School - Travel Grants* to attend the conference ($2,500).

(**) I was awarded the travel support from the AusIron organiser to attend the conference ($500).

# List of abbreviation

| | |
|---|---|
| $^{\bullet}OH$ | Hydroxyl radical |
| 3D-iLLS | 3-dimensional interferometric lattice light-sheet |
| 4HNE | 4-hydroxynonenal |
| ACSL4 | Acyl-CoA synthetase long-chain family member 4 |
| ADMEM/F12 | Advanced Dulbecco's Modified Eagle's Medium/ Ham's F-12 |
| AKT | Protein kinase B |
| ALOX15 | Arachidonate 15-lipoxygenase |
| AQP8 | Aquaporin 8 |
| ATG5 | Autophagy related 5 |
| ATGA | Australian Therapeutics Goods Administration |
| ATP | Adenosine triphosphate |
| BEX | Brain-expressed X-linked |
| BMP | Bone morphogenetic protein |
| CA1 | Carbonic anhydrase 1 |
| CD43 | Cluster of differentiation 43 |
| CD8 | Cluster of differentiation 8 |
| CDK | Cyclin dependent kinase |
| CEACAM7 | Carcinoembryonic antigen-related cell adhesion molecule 7 |
| CHGA | Chromogranin A |
| CoQ | Coenzyme Q or ubiquinone |
| CRISPR | Clustered regularly interspaced short palindromic repeats |
| Ct | Cycling threshold |

| | |
|---|---|
| $CUL2^{FEM1B}$ | E3 ligase Culin-2-Fem-1-homolog-B |
| DAB | 3,3′-diaminobenzidine |
| DCS | Deep crypt secretory |
| DE | Differential expression |
| DFO | Deferoxamine |
| DHODH | Dihydroorotate dehydrogenase |
| DMSO | Dimethyl sulfoxide |
| DPP4 | Dipeptidyl-peptidase-4 |
| DSS | Dextran sulphate sodium |
| EDTA | Ethylenediaminetetraacetic acid |
| EGF | Epidermal growth factor |
| EGFR | Epidermal growth factor receptor |
| ER | Endoplasmic reticulum |
| ERBB | Erythroblastic leukaemia oncogene B |
| ERK | Extracellular signal-regulated kinase |
| FBS | Foetal bovine serum |
| FNIP1 | Folliculin-interacting protein 1 |
| FTH1 | Ferritin heavy chain 1 |
| GAPDH | Glyceraldehyde 3-phosphate dehydrogenase |
| GES | Genetically encoded sensor |
| GFP | Green fluorescent protein |
| GPX4 | Glutathione peroxidase 4 |
| GRB2 | Growth factor receptor bound protein 2 |
| H&E | Haematoxylin and eosin |

| | |
|---|---|
| $H_2O_2$ | Hydrogen peroxide |
| HCBT | 6-hydroxy-2-cyanobenzothiazole |
| HClO | Hypochlorous acid |
| HEPES | N-2-hydroxyethylpiperazine-N'-2-ethanesulfonic acid |
| HER | Human epidermal growth factor |
| HNF4G | Hepatocyte nuclear factor 4 gamma |
| HPMC | Hydroxypropyl methyl cellulose |
| Hsp70 | 70 kilodalton heat shock protein |
| IETDC | z-Ile-Glu-ThrAsp-d-Cys |
| IFNγ | Interferon gamma |
| IHC | Immunohistochemistry |
| iPSC | induced pluripotent stem cells |
| JNK | c-Jun N-terminal kinase |
| Lgr5 | Leucine-rich repeat-containing G protein-coupled receptor 5 |
| LINCS | Library of integrated network-based cellular signatures |
| LPS | Lipopolysaccharides |
| LSM | Light-sheet microscopy |
| MAP4K3 | Mitogen-activated protein kinase kinase kinase 3 |
| mGluR | Metabotropic glutamate receptor |
| mTOR | Mammalian target of rapamycin |
| MUC2 | Mucin 2 |
| NADPH | Nicotinamide adenine dinucleotide phosphate |
| NCOA4 | Nuclear receptor coactivator 4 |
| NDP | Nanozoomer Digital Pathology |

| | |
|---|---|
| NEUROD1 | Neuronal differentiation 1 |
| NEUROG3 | Neurogenin-3 |
| NIH | National institutes of health |
| NO | Nitric oxide |
| NOX1 | NADPH oxidase 1 |
| NRF2 | Nuclear factor-erythroid factor 2-related factor 2 |
| NRG-1 | Neuregulin 1 |
| $O_2^{\bullet -}$ | Singlet superoxide radical |
| p38MAPK | p38 mitogen-activated protein kinase |
| PBS | Phosphate-buffered saline |
| PCL-2 | Peroxy Caged Luciferin-2 |
| PDGFRα | Platelet-derived growth factor receptor A |
| PI3K | Phosphoinositide 3-kinase |
| PRDX | Peroxiredoxin |
| PUFA | Polyunsaturated fat |
| RNA | Ribonucleic acid |
| ROS | Reactive oxygen species |
| RT-qPCR | Real-time quantitative polymerase chain reaction |
| SIM | Structured illumination microscopy |
| SLC11A2 | Divalent metal transporter 1 |
| SLC26A3 | Solute carrier family 26, member 3 |
| SLC40A1 | Ferroportin-1 |
| SLC7A11 | Solute carrier family 7 member 11 |
| SOS | Son of sevenless |

| | |
|---|---|
| STORM | Single-molecule stochastic optical reconstruction microscopy |
| TA | Transition amplifying |
| TCO-Dye | TCO-modified dye |
| TEM | Transmission electron microscopy |
| TFRC | Transferrin receptor |
| TH17 | T helper 17 |
| TKI | Tyrosine kinase inhibitors |
| TNF | Tumour necrosis factor |
| TXNRD | Thioredoxin reductase |
| UBC | Ubiquitin C |
| US FDA | United States Food and Drug Administration |

# List of figures

# List of tables

# Chapter 1: General introduction

## 1.1. *HER2*-positive breast cancer

Breast cancer is a leading cause of cancer-related mortality and morbidity in Australian women and worldwide [2]. In 2020, nearly 20,000 newly diagnosed cases and 3,000 women died of breast cancer were recorded in Australia [3]. Among all types of breast cancer, the aggressive human epidermal growth factor (HER2)-positive subtype accounts for 20-30% of all diagnosed cases [4]. In the past century, patients diagnosed with *HER2*-overexpressing or -amplified (also referred to as *HER2*-positive) breast cancer were usually associated with the poorest prognosis and outcome, with a high rate of brain metastasis [5-9]. However, this is no longer the case with the recent development of HER2-targeted therapies that precisely target *HER2*-postive cells to inhibit the activation of the receptors and their downstream signalling pathways essential for cell proliferation and survival [10].

## 1.2. HER receptors and their downstream signalling pathways

HER2 receptor belongs to the erythroblastic leukaemia oncogene B (ERBB) receptor family that includes three additional members: epidermal growth factor receptor (EGFR; also known as HER1 or ERBB1), ERBB-3 (or HER3) and ERBB-4 (or HER4). HER downstream signalling pathway is critical for cell proliferation, differentiation, and survival while suppressing cell death mechanisms [11]. In general, HER receptors are activated upon the binding of known cognate ligands such as EGF for HER1 and neuregulin 1 (NRG-1) for HER3 and HER4 to form either homodimer or heterodimer complexes. However, the HER2 receptor does not have any known cognate ligands and only forms heterodimer complexes with another ligand-bound HER receptor [11,12]. Following receptor autophosphorylation at multiple intracellular tyrosine kinase domains, the phosphorylated tyrosine kinases serve as docking sites for GRB2-SOS and PI3K that subsequently potentiates two canonical pathways, RAS-ERK and PI3K-AKT-mTOR,

respectively. Under homeostasis or following damaging stimuli such as chemotherapy treatment, these two pathways are essential for potentiating cell growth, proliferation, and differentiation whilst suppressing cell death mechanisms (Fig. 1) [13]. Mutation in HER receptors and downstream signalling components are frequently observed in tumorigenesis, leading to constitutive activation of this pathway. As such, targeting the HER receptors, especially HER2, has attracted considerable attention as novel targeted anti-cancer therapies for solid tumours including breast cancer with aberrant HER activity [14].

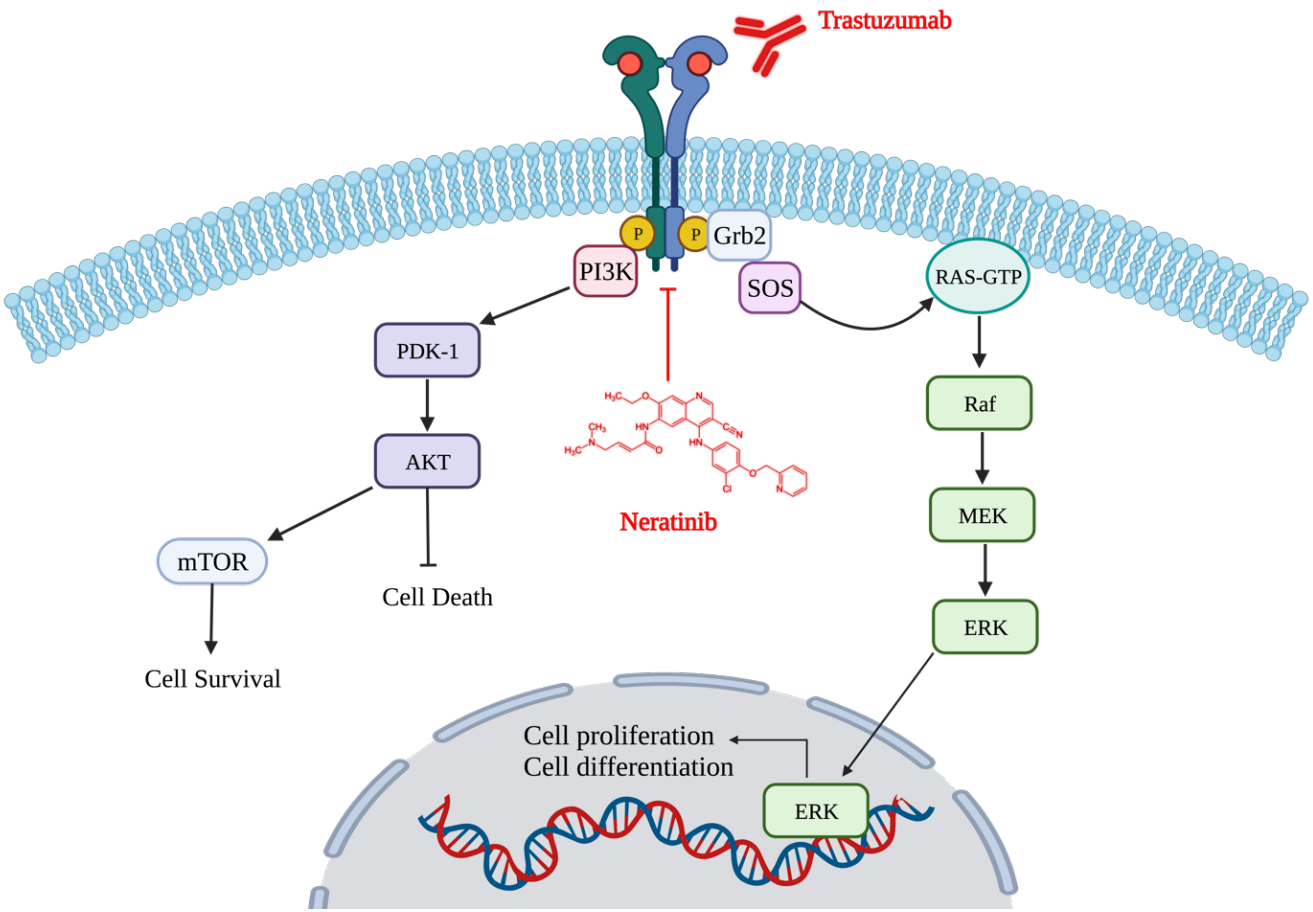


**Figure 1: The activation of HER receptors and their downstream signalling pathways.** Active HER receptor dimer potentiates two canonical RAS-ERK and PI3K-Akt-mTOR pathways that control cell survival, proliferation, differentiation, and death. The binding sites of approved targeted HER2 inhibitors, namely trastuzumab and neratinib, are also demonstrated. Figure created with https://www.biorender.com/

## 1.3. HER2-targeted therapies for HER2-positive breast cancer

HER2-targeted therapies include monoclonal antibodies, such as trastuzumab, and small-molecule tyrosine kinase inhibitors (TKI), such as neratinib (also known as HKI-272). Trastuzumab, which binds to the extracellular domain of HER2 receptor and prevents the formation of HER2 dimer complex, is the gold standard adjuvant therapy in clinical settings (Fig. 1) [15]. Nevertheless, major drawbacks associated with this therapy include: (1) a high incidence of severe-to-life-threatening cardiotoxicities including grade 3-4 congestive heart failure and cardiac dysfunctions [16-18]; (2) a low therapeutic efficacy and response rate in patients with mutated HER2 receptor [19]; and (3) a relatively high resistant rate in adjuvant and neoadjuvant settings [20-22].

In contrast, orally taken neratinib (also known as HKI-272 or Nerlynx), which was originally developed by Pfizer and later optimised by Puma biotechnology, covalently binds to the critical cysteine residue of intracellular kinase domain of HER1/2/4 receptors to suppress their downstream signalling pathways (Fig. 1) [23,24]. Neratinib binds strongly to plasma proteins in the circulation and is metabolised by cytochrome P3A4 [25]. An *in vitro* assay of more than 110 different cancer cell lines demonstrated that neratinib is effective against most *HER2*-positive cancer cell lines, including those insensitive to trastuzumab such as SKBR3 and BT474. However, cancer cells bearing *KRAS* mutations, such as HCT-116, HCT-15, and SW-480 colorectal cancer cell lines, are resistant to neratinib [26]. This indicates that neratinib requires intact HER signalling pathways to exert its therapeutic efficacy. In a pivotal phase III clinical trial, neratinib significantly improved a 2-year survival rate following chemotherapy and trastuzumab treatment [27]. A further 5-year follow-up study reported that neratinib treatment was not commonly associated with long-term toxicity and complications [28].

In May 2020, neratinib was approved by the Australian Therapeutics Goods Administration (TGA) as an extended adjuvant therapy for patients with *HER2*-positive breast cancer who have previously received trastuzumab therapy [29]. In addition to its use as an adjuvant therapy, the combination of neratinib and capecitabine was recently approved for adult patients with advanced or metastatic *HER2*-positive breast cancer by the United States Food and Drug Administration (US FDA), but not by the ATGA [30]. Since then, the therapeutic efficacy of neratinib is currently being assessed for the treatment of other types of cancer in ongoing clinical trials (Table 1).

**Table 1:** A summary of ongoing clinical trials of neratinib treatment beyond *HER2*-positive breast cancers.

| NCI identifier | Phase | Type of cancers | Treatment regime |
|---|---|---|---|
| NCT02932280 | I and II | Central nervous system tumour<br>Lymphoma<br>Leukaemia | Neratinib |
| NCT03457896 | II | Metastatic *KRAS*/*NRAS*/*BRAF*/*PIK3CA* wild-type colorectal cancer | Neratinib +/- Trastuzumab/Cetuximab |
| NCT03919292 | I and II | Colon cancer (*RAS*-mutated)<br>Glioblastoma (*RAS*-mutation or *HER1*-mutated at RP2D)<br>Ocular melanoma<br>Pancreatic cancer (*RAS*-mutated at RP2D) | Neratinib + Divalproex sodium |
| NCT04502602 | I | Advanced ovarian cancer | Neratinib +/- Niraparib |
| NCT05372614 | I | Metastatic malignant solid neoplasm<br>Unresectable malignant solid neoplasm | Neratinib +/- Trastuzumab deruxtecan |
| NCT03065387 | I | Advanced/metastatic/refractory malignant solid neoplasm<br>*HER1/HER2/HER3/HER4* gene amplification/mutation | Neratinib + Everolimus<br>Neratinib + Palbociclib<br>Neratinib + Trametinib |
| NCT05512182 | II | Recurrent/advanced gastric cancer | Neratinib + Pembrolizumab + Paclitaxel |

## 1.4. Neratinib-induced gut toxicity

Despite therapeutic effectiveness against *HER2*-positive breast cancers, over 90% of patients taking neratinib experienced mild-to-severe symptoms of gut toxicity, such as abdominal pain and diarrhoea, which often leads to early dose reduction or termination [31,32]. Given that escalating dose of neratinib leads to a more severe symptom of gut toxicity observed in our preclinical rat models and in clinical trials [33,34], we postulate that inhibition of locally expressed HER receptors in the intestinal epithelial cells which subsequent triggers epithelial cell death is likely the cause of gut toxicity. This is likely due to the gut epithelium naturally expresses HER receptors and is strongly dependent on their downstream signalling pathways for cell survival, differentiation, and proliferation [35-38]. As such, the disruption of HER signalling perturbs intestinal homeostasis leading to intestinal cell death and symptoms of gut toxicity.

In contemporary practice, patients are co-prescribed with loperamide to reduce the incidence of TKI-induced diarrhoea [39]. Loperamide acts by reducing gut motility and secretion by activating the μ-opioid receptors in the muscle wall, thus, reducing diarrhoea [40,41]. However, data from clinical trials suggests that escalating dose of prophylactic loperamide alone, or in combination with other antidiarrhoeic medications only provided modest symptomatic relief following neratinib treatment [42,43]. Specifically, the diarrhoea incidence in patients co-prescribed with loperamide alone or in combination with corticosteroid budesonide or bile acid sequestrant colestipol was reduced by 17.3%, 15.7%, and 41.6%, respectively. This modest relief may be because these prophylactic interventions do not target the underlying cause of neratinib-induced gut toxicity, which remains poorly understood and may be dependent on uncontrolled intestinal cell death, especially in the colon.

## 1.5. The structure of colonic epithelium

The colonic epithelium, which consists of a single layer of polarised columnar epithelial cells, is organised into a crypt structure (Fig.2a). This outermost layer of the colon forms an effective semipermeable barrier for absorbing water and electrolytes while preventing other luminal contents including bacteria from entering inner mucosa. Located at the bottom of the crypt is a population of stem cells expressing *leucine-rich repeat-containing G protein-coupled receptor 5 (LGR5)* [44]. *LGR5*-positive stem cells divide into stem and progenitor cells (Fig.2b). Progenitor cells, then, enter the transition-amplifying (TA) zone, where the proliferative capacity is greatly enhanced, and either self-renew into *LGR5*-positive stem cell or differentiate into post-mitotic cells by entering either absorptive or secretory lineages [44].

The absorptive lineage gives rise to colonocytes whose primary functions is to absorb water, and other selective vitamins and small molecules, to form an effective barrier for mucosal protection [45]. Whereas the secretory lineage gives rise to colonic deep crypt secretory (DCS), goblet and enteroendocrine cells. DCS cells produce essential factors including growth factors and antimicrobials to support the stem cells [46,47]. Goblet cells produce the mucus layer comprised of glycosylated mucins that serves as an effective barrier to further separate the lumina contents from the epithelium and is critical to modulate inflammatory response [48,49]. Enteroendocrine cells produce various hormones, such as serotonin, to regulate the physiology of the colon [50-52]. Therefore, maintaining the cellular composition and integrity of the colonic epithelium is imperative for the homeostasis of colon.

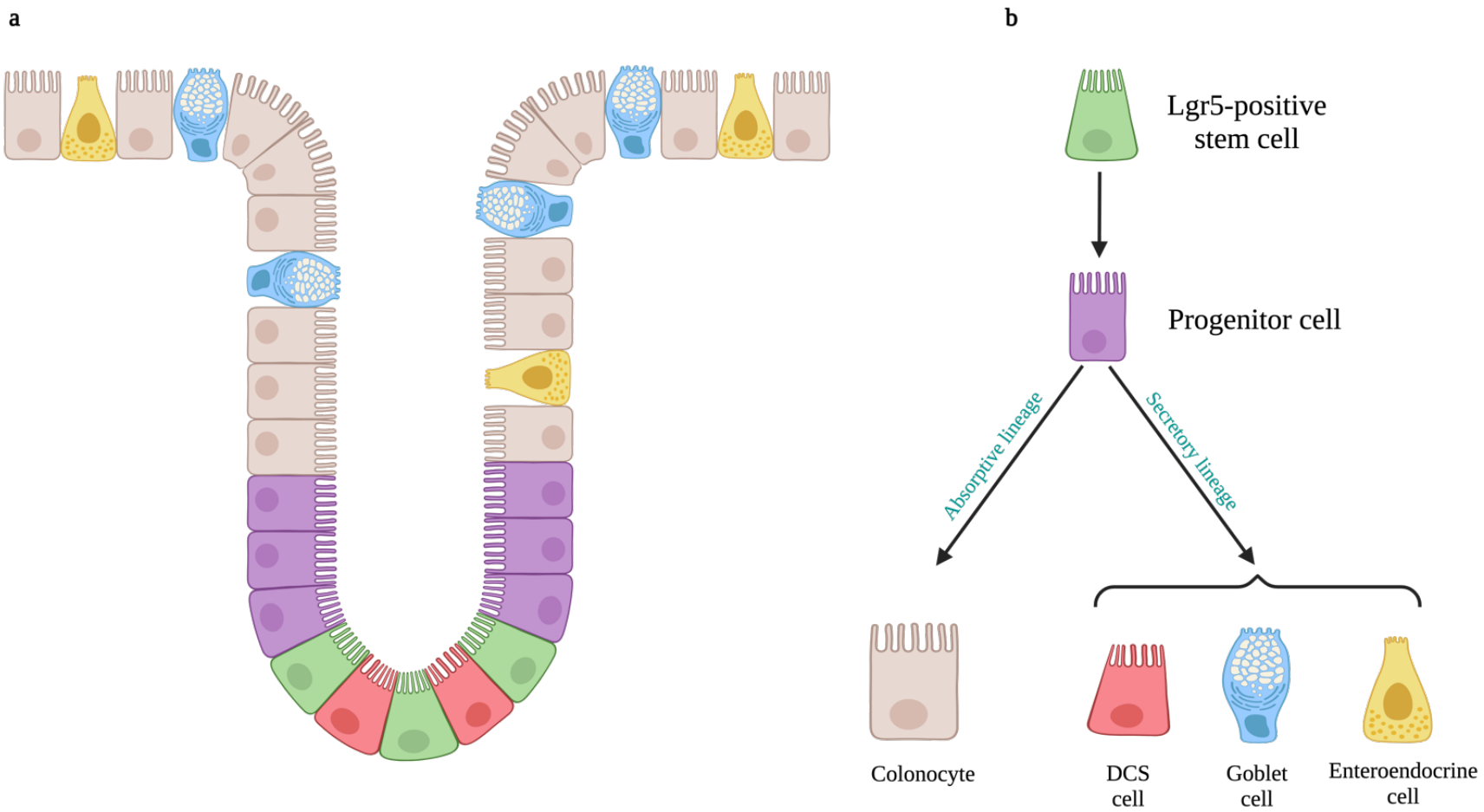


**Figure 2: Colonic epithelium. a,** The organisation of colonic epithelial cells into crypt structure. **b,** A model of colonic stem cell differentiation [1]. Figure created by https://www.biorender.com/

## 1.6. Three-dimensional (3D) colonic organoids

The 3D colonic organoid, which can be generated from isolated colonic stem cells or induced pluripotent stem cells (iPSC), is an *in vitro* model system that precisely recapitulates the heterogenous architecture and functionality of the colonic epithelium [53-57]. Due to their amenability to various experimental techniques ranging from genetic to pharmacological manipulation, an ever-growing list of protocols deviate from the standard organoid culture have been developed to generate customised colonic organoid variants for different experimental purposes [58]. For instance, the use of clustered regularly interspaced short palindromic repeats (CRISPR)-cas9 and lentiviral transduction to generate permanent or transient genetically engineered organoids for unravelling exciting biological questions ranging from identifying rare cell population to illuminating gene functions in different biological processes [59,60].

A standard organoid differentiation requires the inhibition of Wnt signalling pathway by withdrawing Wnt ligand with or without the activation of bone morphogenetic protein (BMP) signalling pathway [1,58,61]. Under these conditions, the differentiation of organoids is non-directional, such that the organoids can give rise to all differentiation lineages. To enrich organoids for a specific cell type of interest, additional pharmacological manipulation of other signalling pathways is therefore required. For example, activating Notch signalling pathways directs stem cells to differentiate into colonocytes; or suppressing MAPK while adding neurogenin-3 (NEUROG3) and neuronal differentiation 1 (NEUROD1) proteins stimulates differentiation towards enteroendocrine cells [61-64].

Given that organoids can recapitulate the heterogeneity of colonic epithelium *in vitro*, this model system is suitable for dissecting biomolecular processes of the epithelium. By integrating bulk multi-omics approaches, Zhou and colleagues [65] strikingly discovered that chromatin

factor special AT-rich sequence-binding protein 2 (SATB2) serves as the safeguard for not only colonocyte differentiation but also the identity of colonic epithelium by maintaining the activity of transcription factors caudal type homeobox 2 (CDX2) and hepatocyte nuclear factor 4 alpha (HNF4A) at the region of colon-specific enhancer. Without SATB2, relocation of CDX2 and HNF4A to ileal-specific enhancer triggers the differentiation of organoids with ileal-like phenotypes. The organoids can also be dissociated into single cells which is then coupled with mass cytometry to delineate the dynamic network of post-translational modification signalling pathways for each individual cell types in organoids [66]. Finally, the use of high-content CRISPR-screening technology, such as Perturb-seq platform, can potentially be exploited to predict the functions of uncharacterised genes and their regulatory networks underlying various physiological and pathological states of the colonic epithelium [67]. Collectively, the 3D colonic organoid presents as a promising *in vitro* model system to bridge the current gaps between *in vitro* cell lines, which lacks cellular heterogeneity, and *in vivo* animal models, which are expensive and ethically challenging [68,69].

## 1.7. HER signalling in the colonic epithelial cells

All epithelial cells in the colonic epithelium depend on HER signalling for cell survival, proliferation, and differentiation [66,70]. HER receptors are strongly expressed in the basolateral membrane of the polarised epithelial cells locating adjacent to subepithelial fibroblasts and other stromal cells, which are considered as the main source of HER ligands (Fig. 3) [35]. For example, EGF, a cognate ligand of HER1 is produced by deep-crypt secretory cells and $CD43^{+}$/PDGFRα cells; and NRG-1, a cognate ligand of HER3 and HER4, produced by $CD43^{-}$/PDGFRα [71]. For a thorough review of HER receptors and ligands, please refer to a recent review by Abud et al. [72].

Extending beyond the role of modulating intestinal homeostasis under normal condition, downstream signalling pathways of HER3 and HER4 receptors are critical for healing following intestinal injury. Frey and colleagues observed that a significant increase in HER3 and HER4 expression following the administration of dextran sulphate sodium (DSS) or tumour necrosis factor (TNF) to induce colitis. The upregulation of these HER receptors correlates with significantly lower number of cleaved caspase-3, an indicator of apoptotic cell death, and suppresses the activation of macrophages to enhance the intestinal resolution of colitis [73,74]. Furthermore, following the treatment of 5-fluorouracil and irradiation, Abud's group showed that NGR-1, a cognate ligand for HER3 and HER4 receptors produced by subepithelial mesenchymal stromal cells, dramatically enhanced the proliferation and differentiation of intestinal stem cells in both *in vitro* organoid and *in vivo* rodents by stimulating both RAS-ERK and PI3K-AKT-mTOR pathways. Together, these results suggest that the expression of HER3 and HER4 and their downstream signalling are essential for intestinal protection and regeneration [75]. As neratinib covalently binds to HER1, HER2 and HER4 receptors and suppresses their downstream signalling pathways, this may explain why patients experience severe symptoms of gut toxicity following neratinib treatment [76,77].

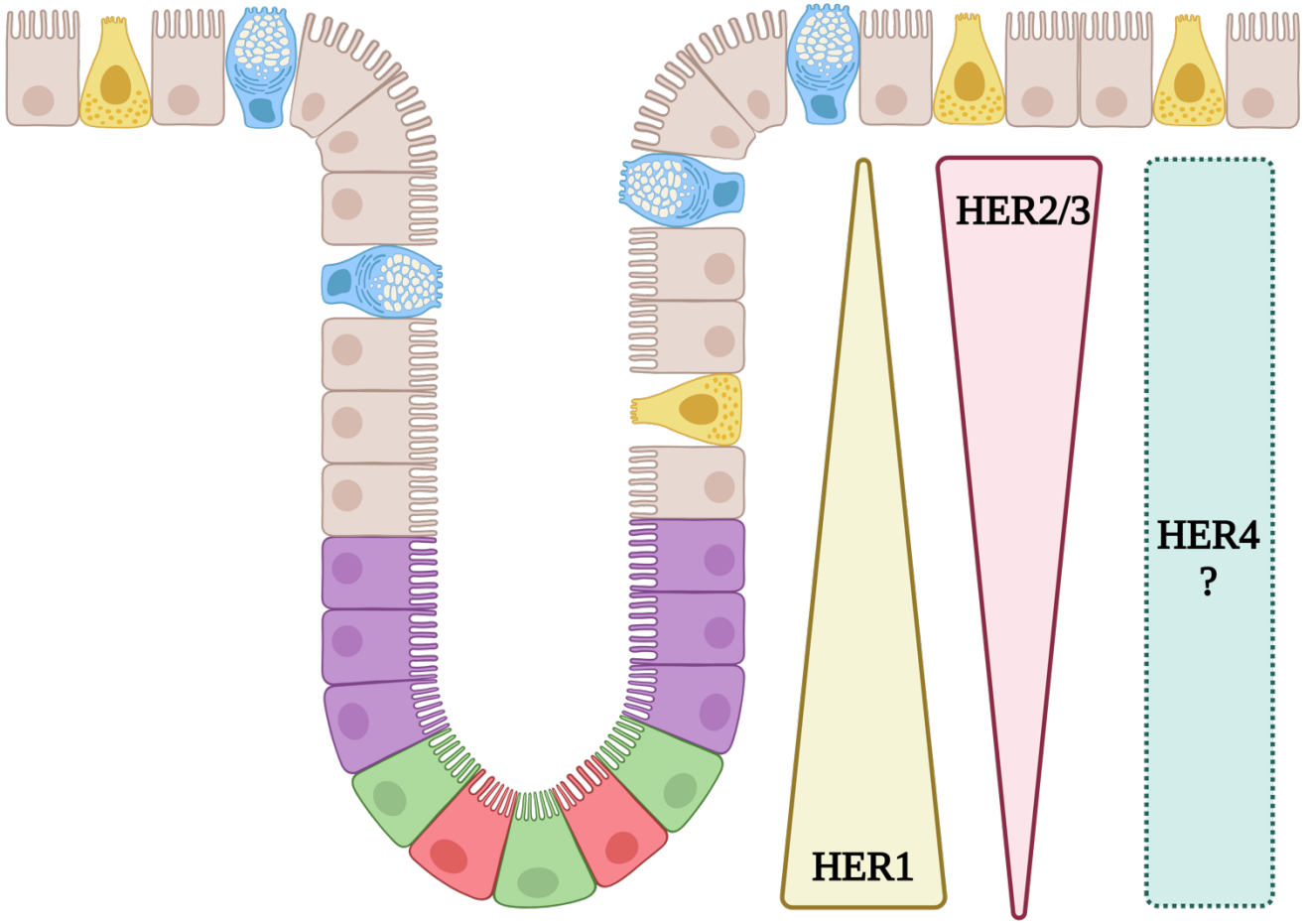


**Figure 3: The expression gradient of HER receptors in a colonic epithelium.** HER1 receptor is primarily enriched in the stem and TA compartment, while HER2 and HER3 receptors are highly expressed in differentiated. HER4 receptor is likely present, but its expression profile is currently unknown under homeostatic condition [72]. Figure created by https://www.biorender.com/

Intriguingly, by exploiting the use of single-cell and spatial transcriptomics, recent studies emerged over the past few years uncovered that the epithelium from different regions of the colon, i.e. proximal versus distal colon, possess molecular regionalisation that determines distinct phenotypes and responses to the same stimulus [78-80]. For example, Parigi et al. noted that the use of oral administration of DSS as a model of colitis resulted in the distal colon being more severely damaged than the proximal colon of treated mice [80]. Their spatial transcriptomic analysis further showed that gene signatures in JAK-STAT and TNFα pathways contributing to inflammation were significantly upregulated in the distal colon but not the proximal colon. Collectively, these findings prompted us to wonder if the response to neratinib treatment may vary among different regions of the colon and if this may be as the consequence of the spatial distribution of HER receptors throughout the entire colon, which unfortunately remains poorly understood.

## 1.8. What is known about the mechanism of neratinib-induced cell death

Neratinib is an approved small-molecule TKI for patients with *HER2*-positive breast cancer. Neratinib induces cell death by covalently binding to tyrosine kinase domains of HER1/2/4 receptors and suppressing the canonical RAS-ERK and PI3K-mTOR-AKT pathways [23,24]. A previous study using *in vitro HER2*-positive breast cancer cell lines, which did not express mutant oestrogen receptor, such as SKBR3, showed that neratinib treatment suppressed the activity of nuclear factor-erythroid factor 2-related factor 2 (NRF2), a master regulator of antioxidant defence, to then promote oxidative-stress-dependent cell death [81]. Oxidative stress is a condition of sustained elevation of intracellular reactive oxygen species (ROS) that may cause reversible and irreversible damage to biomolecules such as lipids, proteins, and nucleic acids [82]. 'ROS' is an umbrella term describing a collection of oxygen-derived radicals, such as

singlet superoxide ($O_2^{\bullet -}$) and hydroxyl radical ($^{\bullet}OH$), and species, such as hydrogen peroxide ($H_2O_2$) and lipid peroxide.

Strikingly, a study from Nagpal et al. revealed that rather than apoptosis as induced by other TKI, such as lapatinib, neratinib promoted ferroptotic cell death in both human (SKBR3) and mouse (TBCP1) *HER2*-positive breast cancer cell lines [83]. Ferroptosis is a type of regulated cell death that arises from perturbed iron and redox homeostasis with excessive lipid peroxidation at the phospholipid membrane [84]. Using Albino Wistar rats dosed with neratinib as a preclinical model system, our previous works demonstrated that neratinib treatment caused severe damage to the epithelium of the distal ileum and stimulated strong inflammation with no profound apoptosis or crypt ablation detected [85,86]. This observation suggests that neratinib may perhaps induce a non-apoptotic cell death in the rat intestine. Nonetheless, whether neratinib-induced ferroptosis is a potential component of intestinal injury, especially in the colon, remains yet to be elucidated.

## 1.9. Hypotheses and aims

Patients receiving neratinib experience mild-to-severe symptoms of gut toxicity, especially diarrhoea. Yet, the precise mechanism of how neratinib induces intestinal injury, especially in the colon, remains unclear. As such, the research carried out in this thesis aimed to address this gap in knowledge. Current findings in the literature have led us to formulate two hypotheses:

- **Hypothesis 1:** The injury induced by neratinib is spatially located and cell-type specific in the colon.

- **Hypothesis 2:** As a consequence of perturbed iron and redox homeostasis, ferroptosis is a likely histopathological feature of neratinib-induced colon injury.

To investigate these hypotheses, the presented work was performed to satisfy the following aims:

- **Aim 1:** To determine the spatially located and histopathological features of neratinib-induced colon injury.

- **Aim 2:** To confirm the features of ferroptosis including perturbed iron and ROS homeostasis in colonic models of neratinib treatment.

# Chapter 2: Methodology

## 2.1. Key reagents or resource

| Reagents or resource | Source | Identifier |
|---|---|---|
| XTT Cell Viability Assay | Roche | 11465015001 |
| Neratinib | Puma Biotechnology | Kindly provided |
| Foetal Bovine Serum | Bovogen | SFBS-AU |
| PBS (pH 7.2; 1X) | Gibco | 20012050 |
| TrypLE™ Select Enzyme (1X), [+] phenol red (500.0 mL) | Gibco | 12605-028 |
| Corning's Falcon Matrigel Basement membrane matrix, growth Factor reduced (GFR), Phenol red-Free, LDEV-Free, 10 ml, 1/Pack, 1/Case | In Vitro Technologies | FAL356231 |
| Advanced DMEM/F-12 (10 x 500.0 mL) | Gibco | 12634028 |
| Antibiotic-Antimycotic (100X; 100.0 mL) | Gibco | 15240062 |
| Gentamicin (10 mg/mL; 100.0 mL) | Gibco | 15710064 |
| GlutaMAX Supplement | Gibco | 35050061 |
| HEPES (1.0 M; 100 mL) | Gibco | 5630080 |
| N-2 Supplement (100X; 5.0 mL) | Gibco | 17502048 |

| | | |
|---|---|---|
| B-27™ Supplement (50X), minus vitamin A (10.0 mL) | Gibco | 12587010 |
| Animal-Free Recombinant Murine EGF (500.0 µg) | PeproTech | AF-315-09 |
| Animal-Free Recombinant Murine Noggin (20.0 µg) | PeproTech | AF-250-38 |
| iPSC Induction Enhancer, Thiazovivin (10.0 mg) | Merck | 420220-10MG |
| GSK-3 Inhibitor XVI (5.0 mg) | Merck | 361559-5MG |
| ROCK Inhibitor (Y-27632; 1.0 mg) | In vitro Technologies | RDS12541 |
| R-spondin 2 | SAHMRI | N.A. |
| Wnt3a | SAHMRI | N.A. |
| NucleoSpin RNA extraction kit | Macherey-Nagel | 740955.50 |
| 2-Mercaptoethanol | Sigma-Aldrich | M6250 |
| iScript cDNA Synthesis Kit (100 x 20 µl reactions) | BIO-RAD | 1708891 |
| DNA Oligos (PCR primers) | Integrated DNA technologies | N.A. |
| QuantiTect SYBR® Green PCR Kits | Qiagen | 204145 |

## 2.2. Animal ethics

This research project involved the use of *in vitro* colon organoids derived from the distal colon of a female C57BL/6 mouse, and *in vivo* paraffin-embedded and frozen Albino Wistar rat colon. The ethics application for the use of mouse colon for organoid generation was previously approved by the animal ethics committee at South Australian Health and Medical Research Institute (SAM322). Colon organoids are maintained from cryopreserved stocks as a standard line in the Gut Cancer Group; and their use for *in vitro* studies does not require further ethics applications and approval. The ethics application for experimental works with healthy female rats dosed with either vehicle control (0.5% hydroxypropyl methyl cellulose; HPMC) or neratinib (50 mg/kg) were previously approved by The University of Adelaide Animal Ethics Committee (M-2019-025).

## 2.3. Tissue collection

All tissues were previously collected and described in Secombe et al. paper [87]. In brief, rats were treated by oral gavage (5 ml/kg) with either HPMC (0.5%) or neratinib (50 mg/kg) every day for 28 days consecutively (n = 6/group). Rats were culled by cardiac puncture while under 4% isoflurane anaesthesia. After colons were dissected and flushed with sterile saline, the length of colon was separated into proximal (the first 3 cm), mid and distal thirds (last 3 cm). While the mid portion of the colon was snap frozen in liquid nitrogen before storage at -80$^{o}$C, the proximal and distal portions were fixed in 10% neutral buffered formalin for 24 hours. After fixation, tissues were processed and paraffin-embedded using standard techniques.

## 2.4. Haematoxylin and eosin (H&E) staining

Tissue H&E staining was carried out to visualise intestinal pathology and score the injury associated with neratinib treatment. Archived paraffin-embedded blocks of proximal and distal colon collected from rats dosed with vehicle control or neratinib were cut into 5 μm sections on a rotary microtome (Leica, Germany). Tissue sections were first de-waxed in xylene (3x5 min) followed by rehydration in a series of graded ethanol concentrations (100% and 90%; 60 s each). Sections were then stained in Harris haematoxylin solution (1:10) for 5 min followed by eosin for 2 min. Sections were subsequently differentiated in acid-alcohol solution (1% concentrated hydrochloric acid in 70% ethanol; 2 quick dips) and Scott's tap water for 2 min. Slides were dehydrated in a series of graded ethanol concentrations (90% and 100%; 30 seconds each) followed by clearing in xylene (3x5 min). Tissue slides were cover-slipped and mounted in Entellan New mounting media. All slides were scanned using Nanozoomer Digital Slide Scanner and viewed using the Nanozoomer Digital Pathology Software (NDP View v2.0, Histalim).

### 2.4.1. Histopathological scoring on H&E slides

Criteria for assessing histopathological features in rat colon previously established by Howarth et al. (1996) were used for histopathological scoring on H&E slides [88]. These criteria included disruption of surface colonocytes, crypt loss or disruption, disruption of crypt cells, infiltration of immune cells, dilation of lymphatics and capillaries, and oedema. Each criterion was scored from 0 to 2, whereby 0 was with no apparent morphological changes, 1 was with mild damage, and 2 was with severe damage. The histopathology of rat colons was additionally assessed by an independent veterinarian pathologist, Associate Professor John Finnie.

## 2.5. Immunohistochemical (IHC) staining

IHC staining was carried out to visualise (1) the changes of markers of surface colonocytes (CA1) and proliferative cells (Ki67) in support for histopathological assessment; and (2) the changes of key markers of ferroptosis, namely ferritin heavy chain 1 (FTH1) and lipid peroxide (4-hydroxynonenal or 4HNE) (Table 2). Archived paraffin-embedded blocks of proximal and distal colon collected from vehicle-control- and neratinib-treated rats were cut into 4μm sections on a rotatory microtome (Leica, Germany). Slides were then processed as follows: de-waxed in xylene/histolene (3x 5 min) followed by rehydration in a series of graded ethanol concentrations (100%, 90% and 70%; 1 min each). Thereafter, slides underwent heat-mediated antigen retrieval in either citrate (pH 6.5) or Tris/EDTA (pH 9.0) buffer depending on the primary antibody used. Refer to table below for a complete list of antibodies including dilution and antigen retrieval buffer used in this study. After pre-heating antigen retrieval buffer to 65$^{o}$C, slides were immersed and heated to 97$^{o}$C for 20 min. Temperature was left to return to 65$^{o}$C before slides were transferred to the Dako Autostainer instrument. Next, endogenous peroxidase was blocked using Dako REAL peroxidase blocking solution for 10 min followed by blocking non-specific protein using DAKO protein block solution for 30 min. Primary antibody diluted in EnVision$^{TM}$ FLEX Antibody Diluent was applied on tissue sections and incubated for 60 min. Primary antibody was then detected using either secondary-HRP labelled mouse or rabbit antibody detection system (Dako EnVision$^{+}$ System-HRP; 30 min) followed by the addition of 3,3′-diaminobenzidine (DAB) chromogen (10 min) was added for visualization. Sections were counter-stained with Harris haematoxylin solution (1:10) for 5.0 minutes followed by differentiating in acid-alcohol solution (1% concentrated hydrochloric acid in 70% ethanol; 2 quick dips) and Scott's tap water for 2 min. Slides were dehydrated in 70%, 90% and 100% ethanol (30 s each) before clearing in xylene (3x5 min). Slides were cover-slipped and mounted in Entellan New mounting media. All slides were scanned using

Nanozoomer Digital Slide Scanner and viewed using the Nanozoomer Digital Pathology Software (NDP View v2.0, Histalim). Qualitative description was carried out to describe the changes of positive IHC signals of **CA1, 4HNE, and FTH1** staining between the neratinib- and vehicle-control-treated rats.

### 2.5.1. Quantification of Caspase-3-stained sections

Caspase-3-positive cells in 10 randomly selected intact crypts per animal were counted and data expressed as the average of positively stained cells per crypt.

### 2.5.2. Quantification of Ki67-stained sections

Ki67-positive cells from 10 randomly selected intact demi (or half) crypts per animal were counted. Data were expressed as the percentage of average of positively stained cells per crypt using the following equation:

$$\%Ki67^{+}\ cells\ per\ crypt = \frac{(Number\ of\ Ki67^{+}\ cells\ per\ demi\ crypt) \times 2}{Total\ number\ of\ cells\ per\ crypt} \times 100\ (\%)$$

**Table 2:** A list of antibodies, and their antigen retrieval buffer and dilution used for IHC staining.

| Antibodies | Source | Identifier | Antigen retrieval buffer | Dilution |
|---|---|---|---|---|
| Rabbit recombinant Anti-Carbonic Anhydrase 1 (CA1) | Abcam | ab267475 | Tris/EDTA buffer | 1:2,000 |
| Rabbit recombinant Anti-Ki67 antibody [SP6] | Abcam | ab16667 | Tris/EDTA buffer | 1:100 |
| Rabbit polyclonal anti-caspase-3 antibody | Abcam | ab4051 | Tris/EDTA buffer | 1:100 |
| Rabbit recombinant Anti-Ferritin (FTH1) antibody | Abcam | ab287968 | Tris/EDTA buffer | 1:2,000 |
| Mouse monoclonal anti-4-hydroxynonenal antibody [HNEJ-2] | Abcam | ab48506 | Citrate buffer | 1:1,500 |

## 2.6. Real-time quantitative polymerase chain reaction (RT-qPCR)

RT-qPCR was utilised to quantify the expression of key markers of ferroptosis in rat colons and to determine the differentiation status of mouse colon organoids (Table 3). All primers were purchased from Integrated DNA Technologies, Inc. (USA). Total ribonucleic acid (RNA) extraction and purification of rat mid colons or Matrigel-containing organoids were carried out using NucleoSpin RNA extraction kit following the manufacturer's instructions. The concentration (ng/ µL) and purity of extracted RNA was determined using Synergy™ Mx reader (BioTek, USA). 1 µg of RNA was reverse transcribed into cDNA using iScript™ cDNA Synthesis Kit using the following sequence – priming at 25°C for 5.0 min, reverse transcription

(RT) at 46ºC for 20 minutes, and RT deactivation at 95ºC for 1.0 minute. RT-qPCR was subsequently carried out using the SYBR-Green system on the Rotor-Gene qPCR cycler (Qiagen). Amplification mix of RT-qPCR contain 1 µL of cDNA (100 ng/ µL), 5 µL of SYBR green dye, 3 µL of nuclease-free water, and 0.5 µL of each forward and reverse primers (50 pmol/L). All samples were run in triplicate. Raw data was plotted as cycle (x-axis) against normalised fluorescent signal (y-axis). Cycling threshold (Ct) value was calculated by Rotor Gene 6 analysis software and used for relative quantification reported in fold difference. The fold difference in gene expression between groups was determined using ΔΔCt method established by Schmittgen and Livak [89]. In rat experiments, all genes were normalised to Ubiquitin C (*Ubc*) housekeeping gene. In mouse organoid experiment, all genes were normalised to glyceraldehyde 3-phosphate dehydrogenase (*Gapdh*) housekeeping gene. The equation to determine fold change as followed. The melting curve analysis was additionally performed to examine the presence of primer-dimers and specificity of PCR product.

$$Fold\ change = 2^{-\Delta\Delta C_T}, in\ which\ \Delta\Delta C_T$$
$$= [(C_T\ gene\ of\ interest - C_T\ housekeeping\ gene)\ treated\ group$$
$$- (C_T\ gene\ of\ interest - C_T\ housekeeping\ gene)\ calibrator\ group]$$

**Table 3:** A list of target mRNA primers used for RT-qPCR. N.A: non-applicable.

| Target mRNA | NCBI reference sequence | Forward primer (5'→ 3') | Reverse primer (5'→ 3') |
|---|---|---|---|
| Ubiquitin C (*Ubc*) - *Rattus norvegicus* | NM_017314.1 (Ref. [90]) | TCGTACCTTTCTCACCACAGTATCTAG | GAAAACTAAGACACCTCCCCATCA |
| Transferrin receptor (*Tfrc*) - *Rattus norvegicus* | NM_022712.1 | CGGCTACCTGGGCTATTGTA | TTCTGACTTGTCCGCCTCTT |
| Ferritin heavy chain 1 (*Fth1*) - *Rattus norvegicus* | NM_012848.2 | ATGATGTGGCCCTGAAGAAC | CACACTCCATTGCATTCAGC |
| Arachidonate 15-lipoxygenase (*Alox15*) - *Rattus norvegicus* | NM_031010.2 | CTTCCTTCTGGATGGGATCA | ATGGCTATGGGCAAGAGTTG |
| Acyl-CoA synthetase long-chain family member 4 (*Acsl4*) - *Rattus norvegicus* | NM_053623.1 | TTGAAGTGAACTGCCGAGTG | CACAGAAAATGGCAATGGTG |
| NADPH oxidase 1 (*Nox1*) - *Rattus norvegicus* | NM_053683.2 | GGCAACATGAGAGCTGCATA | GCAAGTGTCAACCAGCAAAA |
| Glutathione peroxidase 4 (*Gpx4*) - *Rattus norvegicus* | NM_001368043.1 | TACGAATCCTGGCCTTCCCT | CCCTTGGGCTGGACTTTCAT |

| | | | |
|---|---|---|---|
| Glyceraldehyde-3-phosphate dehydrogenase (*Gapdh*) - *Mus musculus* | PMID: 34883119 | CCTCGTCCCGTAGACAAAATG | TCTCCACTTTGCCACTGCAA |
| Carbonic anhydrase 1 (*Ca1*) - *Mus musculus* | NM_001083957.1 | GCTCCGTGGTCTTCTGTCAA | GCTCTGACTGTTCTGCCCTT |
| Aquaporin 8 (*Aqp8*) - *Mus musculus* | NM_001109045.1 | GTCCGAATACTGGGCTCCTG | CCCCAATCAGCCCTCCAAAT |
| Solute carrier family 26, member 3 (*Slc26a3*) - *Mus musculus* | NM_021353.3 | TCCTTCCCACTAGCCACTGT | GGAGCAGCTACAACACCCTT |
| Chromogranin A (*Chga*) - *Mus musculus* | N.A. (Ref. [64]) | GCAACACAGCAGCTTTGAGGAT | GTTAGGCTCTGGAAAGGCCTGA |
| Mucin 2 (*Muc2*) - *Mus musculus* | N.A. (Ref. [64]) | ACCCCAAGCCCTTCTCCTACTA | AGTGGATTGAGAGGTCACAGGC |

## 2.7. Cell culture

Wild-type SW48 colorectal cancer cell line kindly provided by Gut Cancer Group was utilised to assess cytotoxicity of neratinib. SW48 cell was cultured in high-glucose advanced Dulbecco's Modified Eagle's Medium/ Ham's F-12 (ADMEM/F12) supplemented with antibiotic-antimycotic (1X), gentamicin (0.1 mg/mL) and 10% foetal bovine serum (FBS). $SW48^{WT}$ cells were maintained at 37 °C, 5% $CO_2$ and 95% humidity. Cell culture media was refreshed every 2-3 days. Cells were split at least twice every week.

$IC_{50}$ value of neratinib for SW48 cell line (passage number less than 15 in our group) was determined by XTT Cell Viability Assay following the manufacturer's instruction [91]. In brief, 5,000 cells in 100 µL of 10% FBS media were seeded into each well of a clear flat-bottom 96-well plate incubated at 37°C, 95% humidity and 5% $CO_2$ overnight for cell adherence. Old medium was replaced by fresh media spiked with a series of neratinib concentration ranging from 0.01 nM to 10,000 µM, or TX-100 (0.1% in DMSO) as positive control. The 96-well plate was subsequently incubated at 37°C, 95% humidity and 5% $CO_2$ for 24 and 48 hours. After each incubation period, 50µL of XTT mixture was added to each well. The 96-well plate was subsequently incubated for 4 hours. The absorbance was measured on Synergy™ Mx reader (BioTek, USA) at 490 nm with a reference wavelength at 690 nm. Using GraphPad Prism 9 software, the graph of percentage of cell viability was plotted against $\log_{10}$[neratinib] in mol/L (M). The $IC_{50}$ value was determined as a concentration of neratinib at which 50% of cell viability. Non-linear regression was used to fit a sigmoidal dose-response curve, where x-axis represents $\log_{10}$[neratinib] and y-axis is % response compared to DMSO. All experiments were performed in triplicates with two independent experiments.

## 2.8. Transmission electron microscopy (TEM)

All reagents were certified as EM grade. SW48 cells and Matrigel-containing organoids were fixed overnight in TEM fixative (4% paraformaldehyde, 1.25% glutaraldehyde, 4% sucrose in 1X phosphate-buffered saline (PBS), pH 7.2) at 4-8$^{o}$C. Fixed organoids were washed with washing buffer (4% sucrose in 1X PBS; 2x10 min) and post-fixed in 2% osmium tetroxide at room temperature for 1 hour. Afterwards, samples were dehydrated in a series of ethanol concentrations (70%, 95%, and 100%; 3x15 min each). Subsequently, samples were washed with 100% propylene oxide (2x15 min) and incubated in 50% Epon resin in 100% propylene oxide for 60 minutes before the overnight embedding in pure Epon resin. On the next days, the resin was refreshed and polymerised in an oven at 70$^{o}$C for at least 48 hours. Resin-embedded samples were cut to 70.0 nm thickness on rotatory microtome. For imaging Toluene-blue tissue sections, all slides were scanned using Nanozoomer Digital Slide Scanner, and viewed using the Nanozoomer Digital Pathology Software (NDP View v2.0, Histalim). For TEM imaging, all sections were imaged using FEI Tecnai G2 Spirit TEM instrument.

## 2.9. Mouse colon organoid culture

Established protocols by Clevers and colleagues were followed for culturing mouse-derived colon organoids with some modifications [58,92]. The organoid basal media (OBM) was composed of advanced DMEM/F12 supplemented with N-2-hydroxyethylpiperazine-N'-2-ethanesulfonic acid (HEPES; 10 mM), GlutaMAX (1X), antibiotic-antimycotic (1X) and gentamicin (10 mg/ml). Complete organoid culture media contained OBM supplemented with conditioned Wnt-3a (50% v/v) and R-spondin-2 (20% v/v) media, recombinant murine EGF (50 ng/mL), recombinant murine Noggin (100 ng/mL), N2 supplement (1X), B27 supplement (1X), Y-27632 (10 μM), GSK-3 Inhibitor XVI (3 μM), and iPSC enhancer thiazovivin (3 μM).

Conditioned media was produced by Dr. Laura Vrbanac using HEK293T cells either stably transfected to express mouse-Wnt-3a or transiently transfected to express R-spondin-2 vectors [93].

Organoids were derived from the distal region of a healthy female C57BL/6 mouse and cryopreserved by Dr. Laura Vrbanac. After frozen mouse colon organoids were rapidly thawed in a 37°C water bath, organoids were embedded in a dome-shape Matrigel (50 µL/well; Corning; 356231) submerged in complete organoid culture media (500 µL/well) in a 24-well plate. Organoid cultures were maintained at 37°C and 5% $CO_2$. Complete organoid media was refreshed every 2-3 days and organoids were split at 1-2 times a week.

To split organoids, after old medium was removed, 50 µl of Matrigel domes of organoids was dissolved in 1 mL of ice-cold PBS (1X). After leaving on ice for 10 min, the solution was centrifuged at 400 *g* for 5 min at 4°C followed by discarding supernatant. The organoid pellets were resuspended in pre-warmed TrypLE Express (+Y-27632, 10 µM) and incubated for 3 min in 37°C water bath. After the organoids were sufficiently digested, 500 µl of ice-cold FBS was added followed by centrifuging at 400 *g* for 5 min at 4°C and discarding supernatant. Subsequently, Matrigel was added to the pellet and then plated 50 µl of Matrigel domes per well for a 24-well plate. Finally, after polymerizing the Matrigel in a 37°C incubator for 30 min, pre-warmed 500 µl of treatment-specific organoid media was added. The organoid cultures were incubated at 37°C and 5% $CO_2$.

For the induction of differentiation in colon organoids, organoids (15 pieces/µL Matrigel) were first cultured in complete organoid culture media. Two days post-plating, complete organoid medium was removed, and organoids were cultured in different differentiation cocktails to

induce organoid differentiation in comparison to complete medium. Of note, Y-27632, GSK-3 Inhibitor XVI, and thiazovivin were withdrawn in all differentiation cocktails. We tested two main differentiation cocktails, namely $BMP^{high}$ and $BMP^{low}$, in which BMP is denoted for bone morphogenetic protein (Fig. 4).

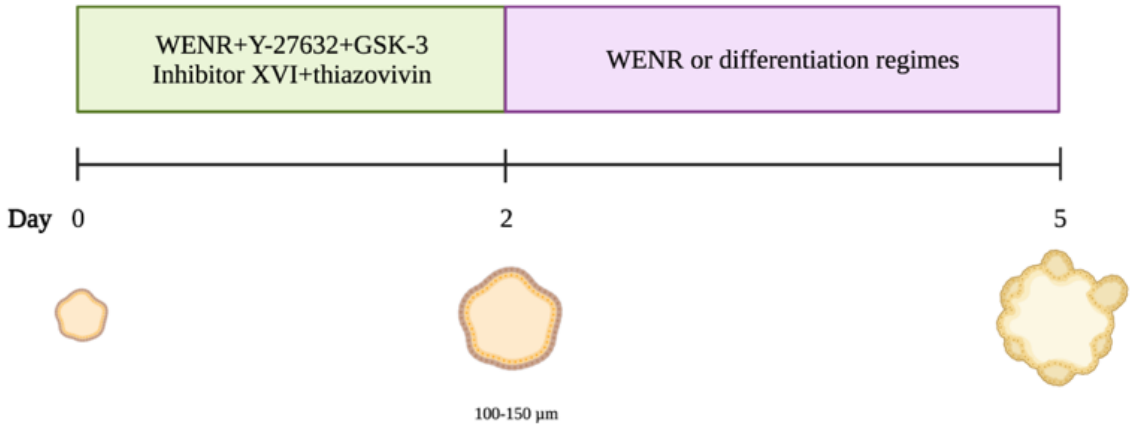


| Condition | Treatment regimes |
|---|---|
| Control | WENR (Wnt3a + EGF + Noggin + R-spondin-2) |
| $BMP^{high}$ | E + BMP2 (EGF + BMP2 (50.0 ng/mL)) |
| | ER + BMP2 (EGF + R-spondin-2 + BMP2 (50.0 ng/mL)) |
| $BMP^{low}$ | EN (EGF + Noggin) |
| | ERN (EGF + R-spondin-2 + Noggin) |

**Figure 4:** The experimental set up for inducing organoid differentiation with different treatment regimes.

## 2.10. RNA-sequencing analysis

RNA-sequencing analysis on previously published datasets was carried out to examine which biological pathways were significantly enriched following neratinib treatment. Processed count tables for protein encoded genes from neratinib-treated mouse breast cancer and human glioblastoma cell lines were kindly provided by Dr Normand Pouliot from Olivia Newton-John Cancer Research Institute and Dr Colin Tang from Weill Cornell Medicine [94,95]. Differential gene expression between neratinib and vehicle control groups were performed using DEseq2 statistical package in R [96]. Unless otherwise stated, a master list of differentially expressed (DE) genes was generated when the P-adjusted value less than 0.05. Subsequently, two lists of significantly upregulated (positive $log_2$FoldChange values) or downregulated (negative $log_2$FoldChange values) genes were generated from the master DE gene list with P-adjusted values or false discovery rate (FDR) below 0.05. Subsequently, these gene lists were inserted into the online database for annotation, visualization, and integrated discovery (DAVID) bioinformatic resource website for gene ontology (GO) terms and Kyoto encyclopaedia of genes and genomes (KEGG) pathway analyses as previously described [97-99]. The computational algorithm used to determine statistical significance of individual pathways was detailed in the original papers [97,100]. Here, GO terms and KEGG pathways were deemed as significantly enriched with P values below 0.05.

## 2.11. CRISPR-screening analysis

As previously described in Tang et al [95], a pool CRISPR screen was performed on neratinib-treated SF268 human glioblastoma cell line to identify genes contributing to neratinib sensitivity. A count table of differentially expressed single-guided RNA and an output file of DrugZ were kindly provided by Dr Colin Tang from Weill Cornell Medicine. Using R script publicly available generated by Dr Colin Tang, drugZ rank plot was generated for normalised

Z score against sgRNA rank [95]. The positive or negative normalised Z score of a gene with FDR below 0.05 confers with either neratinib sensitivity or resistance, respectively.

## 2.12. KINOMEscan search database

KINOMEscan competition assay, which is comprised of kinase-tagged phage, a compound of interest and immobilised ligand, was used to identify the binding affinity of a compound of interest to 442 different kinases [101]. The results from previous scans were deposited on the online National Institutes of Health (NIH) Library of Integrated Network-Based Cellular Signatures (LINCS) KINOMEscan dataset (https://lincs.hms.harvard.edu/db/datasets/) [101,102]. This dataset was then utilised to determine the binding affinity ($K_d$, nM) and percentage of control, where 100% means no inhibitory effect and lower percentage means strong inhibitory effect, of neratinib (10μM, ID: 20195 and 2053) and lapatinib (10μM, ID: 20107 and 20155) to 442 kinases. To be considered as biologically relevant, the $K_d$ value should be lower than the highest plasma concentration ($C_{max}$) of neratinib (84.5 ng/mL equivalent to 152.0 nM [103]) and lapatinib (2.13 μg/mL equivalent to 3.67 μM [104]).

## 2.13. Data analysis and statistics

Descriptions of sample size and statistical tests were detailed in figure legends. Unless otherwise specified, all statistical analyses were carried out using unpaired Student's t-test in GraphPad Prism 9 (version 9.2.0; USA). Statistical values were reported in mean ± standard error of the mean (mean ± s.e.m). Statistical significance, which was reported as exact P values, was considered as followed – for all histological assessment, RT-qPCR, gene ontology and KEGG pathway analyses, P values below 0.05 were deemed significant while for differential gene expression and Drug-Z analyses, P-adjusted values, or false discovery rate (FDR) below 0.05 were deemed significant. In RT-qPCR experiments on frozen rat colons, we excluded two

samples in the vehicle-control-treated group (n = 4) and one sample in the neratinib-treated group (n = 5) due to poor RNA quality.

# Chapter 3: Results

## 3.1. Neratinib-induced injury is spatially located and cell-type specific in rat colon

As previously reported, all rats dosed with neratinib (50 mg/kg), which is clinically relevant for symptomology in human based on our previously published pilot study [33], experienced common signs of gut toxicity including substantial weight loss and moderate diarrhoea [87]. To determine the spatial effect of neratinib on the rat colon, we performed histopathological assessment, namely histopathological scoring, and measurement of crypt length, using haematoxylin and eosin (H&E) and immunohistochemical (IHC) staining on archived proximal and distal colon. The six criteria for histopathological scoring included (1) disruption of surface colonocytes, (2) crypt loss or disruption, (3) disruption of crypt cells, (4) infiltration of immune cells, (5) dilation of lymphatics and capillaries, and (6) oedema. Overall, we observed that the most severe morphological damage was found in the distal colon as reflected by a significantly higher histopathological score and increased crypt length following neratinib treatment (Fig. 5a, b, and c). In contrast, despite a significantly increase in proliferative Ki67-positive cells, the proximal colon of neratinib-treated rats only displayed a few, small, focal areas of mild mucosal damage without apparent sign of injury in the surface lining colonocytes expressing carbonic anhydrase 1 (CA1) (Fig. 5a-e).

The surface epithelium of the distal colon, where CA1-positive colonocytes reside, of rat treated with neratinib was severely degenerated following neratinib treatment (Fig. 5a * and d). A dramatic increase in the proliferative crypt compartment containing Ki67-positive cells further suggested that a compensatory mechanism was in place with an attempt to regenerate the injured surface epithelium in the distal colon of rat treated with neratinib (Fig. 5d and e).

Inflammatory infiltrate, which was largely comprised of lymphocytes but often with a few polymorphonuclear leukocytes, mainly eosinophils, was prominently observed in the lamina propria in the distal colon (Fig. 5a, Δ). Together with lymphocyte infiltration in the surface epithelium, these histopathological findings were consistent with features of microscopic colitis, specifically lymphocytic colitis [105]. Our current histopathological data collectively substantiated our observations that the injury in the distal colon and its surface lining colonocytes appeared to be more severe than in the proximal colon on day 28 of neratinib treatment.

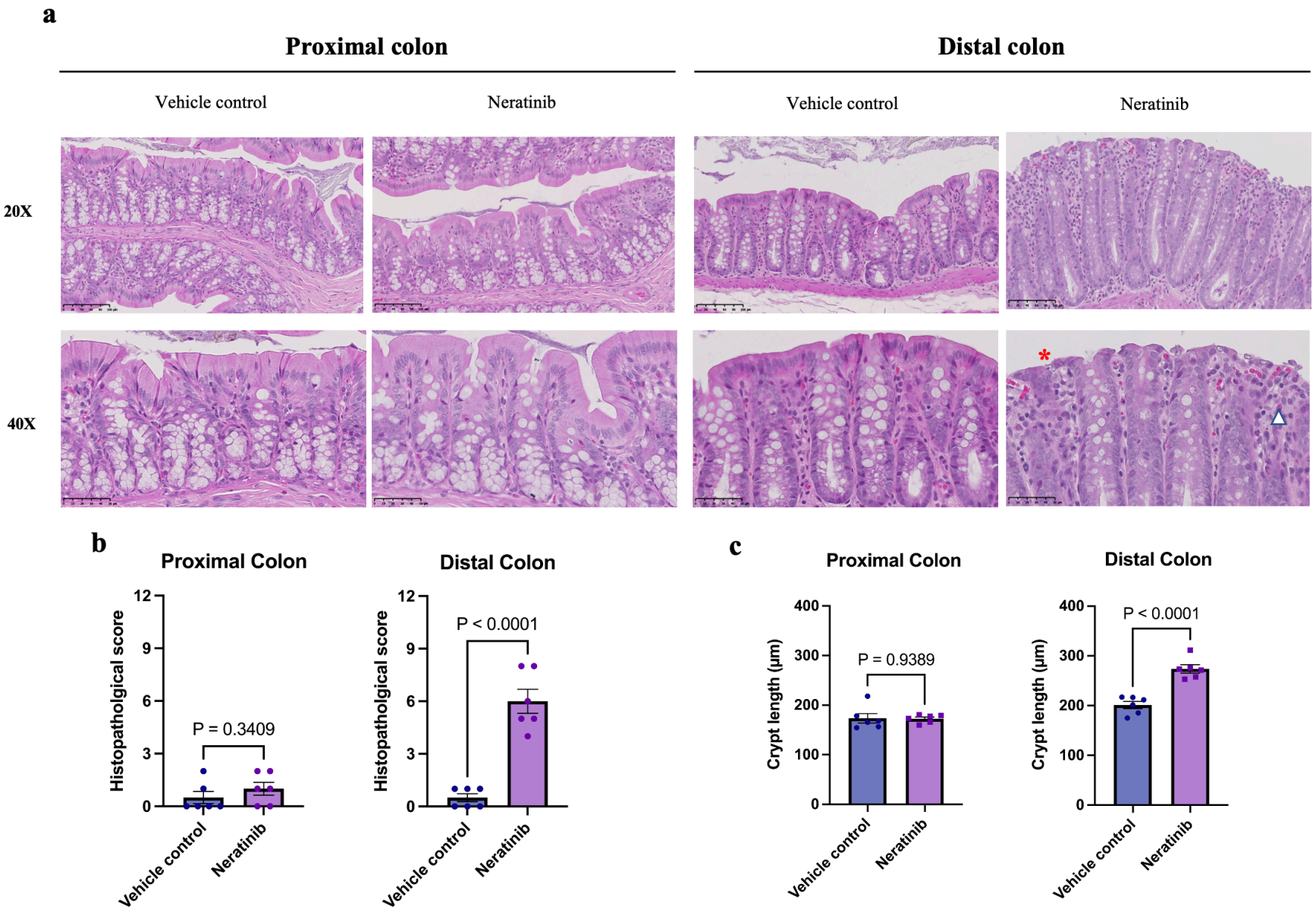
a
Proximal colon
Distal colon
Vehicle control
Neratinib
Vehicle control
Neratinib
20X
40X
b
Proximal Colon
Distal Colon
Histopathological score
P = 0.3409
P < 0.0001
Vehicle control
Neratinib
c
Proximal Colon
Distal Colon
Crypt length (µm)
P = 0.9389
P < 0.0001
Vehicle control
Neratinib

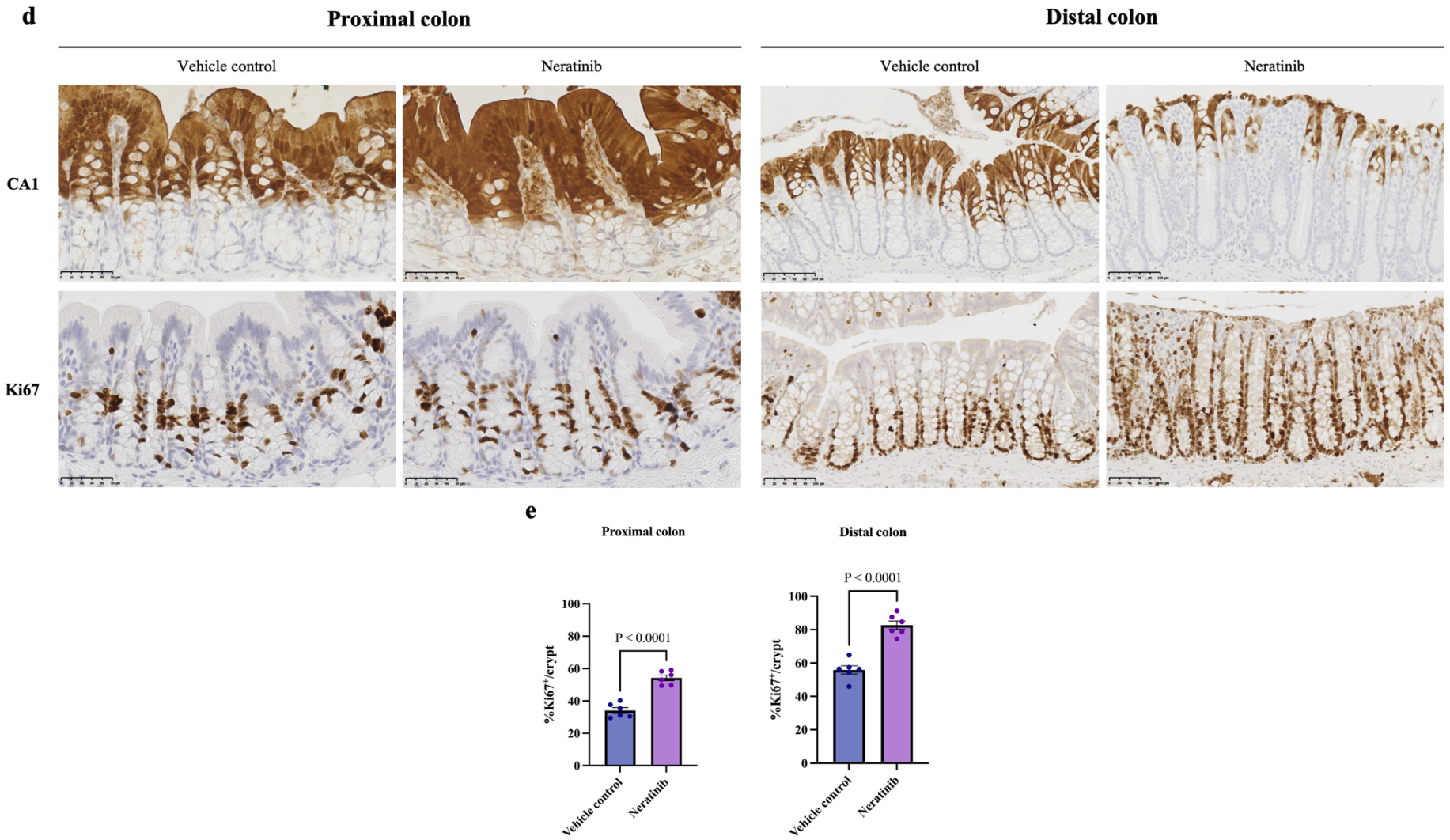
d
Proximal colon
Distal colon
Vehicle control
Neratinib
Vehicle control
Neratinib
CA1
Ki67
e
Proximal colon
Distal colon
P < 0.0001
P < 0.0001
%Ki67+/crypt
%Ki67+/crypt
100
80
60
40
20
0
Vehicle control
Neratinib
Vehicle control
Neratinib

**Figure 5: Histopathological features of neratinib-induced injury in proximal and distal colon. a,** Representative images of H&E panels of proximal and distal colon proximal and distal colon treated with either vehicle control or neratinib at 20X and 40X magnification. In the distal colon of neratinib-treated rat, **(*)** indicates injured surface lining colonocytes and **(Δ)** indicates immune infiltrates. Scale bar, 50 μm (20X) and 100 μm (40X). **b,** Quantification of histopathological scoring. **c,** Quantification of crypt length. **d,** Representative images of IHC (CA1 and Ki67) panels of proximal and distal colon at 40X and 20X magnification, respectively, treated with either vehicle control or neratinib. Scale bar, 50 μm (Proximal colon) and 100 μm (Distal colon) **e,** Quantification of the percentage of Ki67-postive cells per crypt. **For b, c, and 4,** n = 6 rats in each treatment group. Unpaired Student's t-test was used for statistical analysis, where P values below 0.05 were deemed statistical significance. The centre line represents the mean, and the error bar represents s.e.m

## 3.2. Is ferritinophagy-mediated ferroptosis or caspase-3-mediated apoptosis induced by neratinib?

To gain insight into the biological processes underlying neratinib-induced cell death, we performed comprehensive analyses on differential gene expression, KEGG pathway and GO on previously published RNA-sequencing datasets [94,95]. These datasets included TBCP-1 cell line derived from a mouse *HER2*-overexpressed breast cancer brain metastasis treated with neratinib for 24 hours, and intracranial human *EGFR/HER1*-mutant TS895 glioblastoma xenograft treated with neratinib for 3 hours. KEGG pathway analysis revealed that ferroptotic cell death, which is characterised by perturbed iron homeostasis and lipid peroxidation [84], was significantly enriched in both model systems (Fig. 6a). Since a previous study by Nagpal and colleagues confirmed that ferroptosis was induced by neratinib in *HER2*-postive human (SKBR3) and mouse (TBCP1) breast cancer cell lines [94], we hypothesised that neratinib-induced ferroptosis might extend beyond the context of breast cancer.

GO term analyses further uncovered genes involved in autophagy and positive regulation of autophagy were identified among all biological processes in the list of significantly upregulated genes in both neratinib-treated TBCP1 and TS895 cells (Fig. 6b). Autophagy, which is a process mediated by the lysosomal pathway [106], and was previously related to the induction of ferroptosis, especially in the form of ferritinophagy [107,108]. Ferritinophagy is a process of breaking down ferritin, an intracellular iron storage, to release reactive ferrous ion that then accelerates lipid peroxidation [109]. We therefore asked if ferritinophagy-mediated ferroptosis was a likely initiating event of neratinib-induced ferroptosis. Indeed, among all differentially expressed genes contributing to ferroptosis identified from KEGG pathway analysis, only genes involved in iron transport, such as transferrin receptor (*TFRC*), divalent metal transporter 1 (*SLC11A2*) and ferroportin-1 (*SLC40A1*), and ferritinophagy, such as nuclear receptor

coactivator 4 (*NCOA4*) and autophagy related 5 (*ATG5*), were significantly upregulated in TS895 cells following a 3-hour neratinib treatment (Fig. 6c). On the other hand, genes involved in both iron metabolism, such as ferritin heavy chain 1 (*Fth1*) and *Slc40a1*, and lipid peroxidation, such as acyl-CoA synthetase long chain family member 4 and 6 (*Acsl4/6*), were significantly upregulated in TBCP-1 following a 24-hour neratinib treatment (Fig. 6a). Together with a significant increase in iron uptake previously observed in neratinib-treated TBCP-1 cells [94], our bulk RNA-sequencing analyses collectively suggested that *HER1*-mutant TS895 and *HER2*-positive TBCP-1 cancer cells potentially suffered from ferroptotic cell death, which appeared to arise from perturbed iron homeostasis through ferritinophagy, following neratinib treatment.

However, our re-analyses of published bulk RNA-sequencing and CRISPR-screening datasets of neratinib-treated human SF268 glioblastoma cell line suggested that p53-mediated apoptosis, but not ferroptosis, was induced following neratinib treatment (Fig. 6d and e). This then prompted us to propose that a type of cell death induced by neratinib, i.e. ferroptosis or apoptosis, may be cell-type specific. Together with the histopathological assessment from the colon of rats dosed with neratinib, these findings motivated us to explore the biological process, especially the type of cell death and its triggering event, underlying neratinib-induced colon injury.

**a**

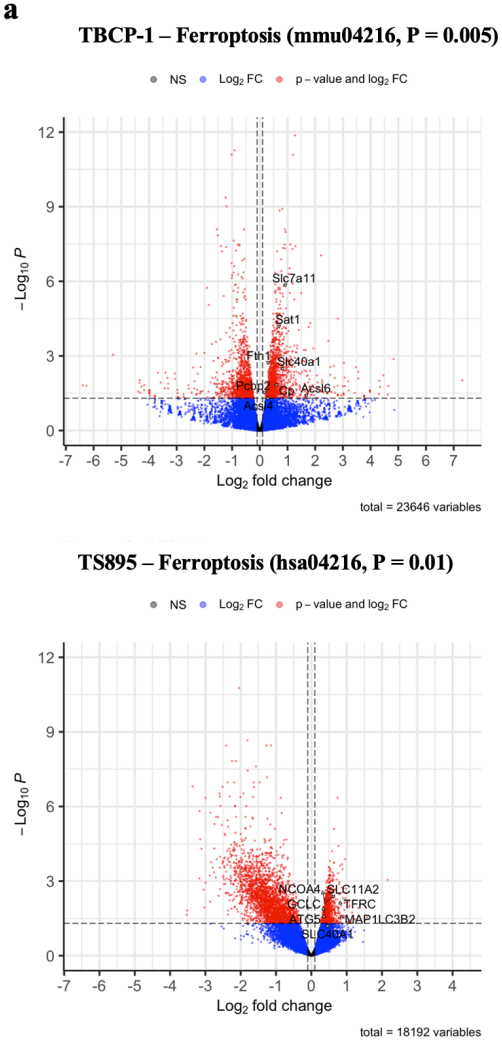


**b**

| | Mouse TBCP-1 cell line | | Human TS895 xenograft | |
|---|---|---|---|---|
| | **Gene set** | **P value** | **Gene set** | **P value** |
| **Autophagy (GO: 0006914 )** | *Xbp1, Wdr47, Stx17, Lrrk2, Vps4b, Vps13a, Fnbp1l, Foxo1, Gpr137b, Tmem59, Herc1, Rb1cc1, Stbd1, Fundc1, Chmp2b, Lamp2, Vps41, Zkscan3, Ulk2, Dram2, Trp53inp1, Trp53inp2* | 0.002 | SH3GLB1, RAB1A, PRKAA1, WDR41, HMGB1, C9ORF72, FOXO1, VMP1, TMEM59, IFI16, RB1CC1, CHMP2B, ATG4A, DRAM2, ATG5, CHMP5 | 0.002 |
| **Positive regulation of autophagy (GO: 0010508)** | *Ufl1, Tmem59, Gsk3b, Xbp1, Ccny, Lrrk2, Rb1cc1, Ulk2, Trp53inp1, Trp53inp2, Foxo1* | 0.02 | SH3GLB1, UFL1, TMEM59, PRKAA1, RB1CC1, HMGB1, FOXO1, TRIM22 | 0.04 |

**c**

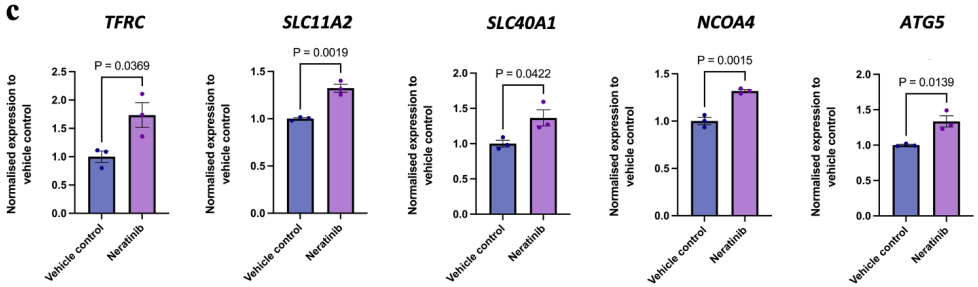


**d**

| | Human SF268 cell line | |
|---|---|---|
| **GO term** | **Genes** | **P value** |
| **Apoptotic process (GO: 0006915)** | *IFI27L1, HRK, CYFIP2, AHCYL1, SH3KBP1, TRADD, ZC3H8, NUDT2, GHITM, TNFAIP1, UBE2Z, HINT2, PEA15, CASP1, BCAP29, MEF2A, UNC5B, DAPK1, AKTIP, IGFBP3, PRKCE, TRAF1, RHOB, NISCH, RNF144B, TMBIM4, SLTM, PACS2, RRAGC, DDIT4, CHMP3, PRKD1, ARHGEF6, PPP1R15A, RTN3, BECN1, BEX2, SGMS1, C5AR1, CDCA7, STK4, GRAMD4, RTN4, PRDX5, DRAM1, BAG1, PTK2B, RIPK1, RNF130, XBP1, GADD45B, GADD45A, RHBDD1, TNFSF12, SIAH2, CFLAR, SULF1, TRIM35, PDCD4, PDCD2, OGT, BCL2L2* | 0.002 |

**e**

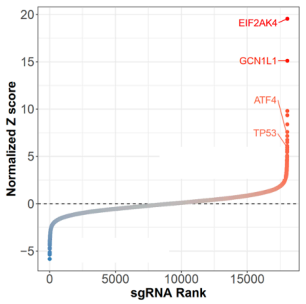

**Figure 6: Whether apoptosis or ferroptosis is induced following neratinib treatment may be cell-type specific. a,** Volcano plot for upregulated key markers of ferroptosis analysed from published bulk RNA-sequencing data of TBCP-1 cell line and TS895 xenograft following 24 hours and 3 hours of neratinib treatment, respectively. **b,** A table of enriched gene sets in autophagy and positive regulation of autophagy following neratinib treatment in TBCP-1 cell line (24 hours) and TS895 xenograft (3 hours). **c,** Differential gene expression of selected markers for iron transport and ferritinophagy in ferroptotic pathway from KEGG pathway analysis in TS895 xenograft. Where P values below 0.05 were considered statistical significance. **d,** A table of enriched gene sets in apoptotic process following neratinib treatment in SF268 cell line (72 hours). **e,** Gene candidates corresponding to neratinib resistant phenotype identified from SF268 CRISPR screen experiment.

### 3.3. Ferritinophagy-mediated ferroptotic cell death is the likely underlying histopathological feature of neratinib-induced colon injury

As our histopathological findings revealed that neratinib stimulated degeneration of surface epithelial cells with strong inflammatory infiltrates in the distal colon (Fig. 5a) and our bulk RNA-sequencing analysis suggested neratinib could trigger either apoptosis or ferroptosis, this prompted us to question which type of cell death was likely induced by neratinib in the rat colon. Through IHC staining for Caspase-3, a marker for apoptosis, in the rat distal colon, we did not detect a significant change in Caspase-3-positive cells between the vehicle-control- and neratinib-treated rats (Fig. 7a and b). This suggested that apoptotic cell death may not be a prominent form of cell death in the rat colon following neratinib treatment.

Next, to determine the presence of ferroptosis, key markers of iron homeostasis and lipid peroxidation were measured using IHC staining and RT-qPCR. Through IHC staining on paraffin-embedded distal colon, a reduction in endogenous FTH1 protein level colocalised with the injured surface epithelium was observed (Fig. 7a). We further observed a significant upregulation of expression of iron absorption gene, *Tfrc*, and downregulation of iron storage gene, *Fth1* (Fig. 7c). Together, these findings may suggest that neratinib perturbed the pool of intracellular iron storage leading to an increase in cytosolic reactive ferrous ($Fe^{2+}$) ion in the rat colon.

Moreover, we found a significant upregulation of gene expression of *Acsl4*, which esterifies polyunsaturated fatty acids (PUFA) making them competent for ferroptosis, and arachidonate 15-lipoxygenase (*Alox15*), which directly causes lipid peroxidation (Fig. 7d) [110,111]. Additionally, the gene expression of *Nox1*, which causes lipid peroxidation by forming a complex with membrane-bound dipeptidyl-peptidase-4 (DPP4) in colorectal cancer and

mediates gut inflammation, was upregulated (Fig. 7d) [110-113]. However, an endogenous 4-hydroxynonenal (4HNE), a marker of lipid peroxide activity in tissues using HNEJ-2 antibody, was not detected. Neratinib also did not alter gene expression of *Gpx4*, which encodes a lipid peroxide scavenger contributing to ferroptotic resistance (Fig. 7d) [114,115]. Collectively, the current findings support the notion that ferroptosis is the potential underlying histopathological features of neratinib-induced colon injury.

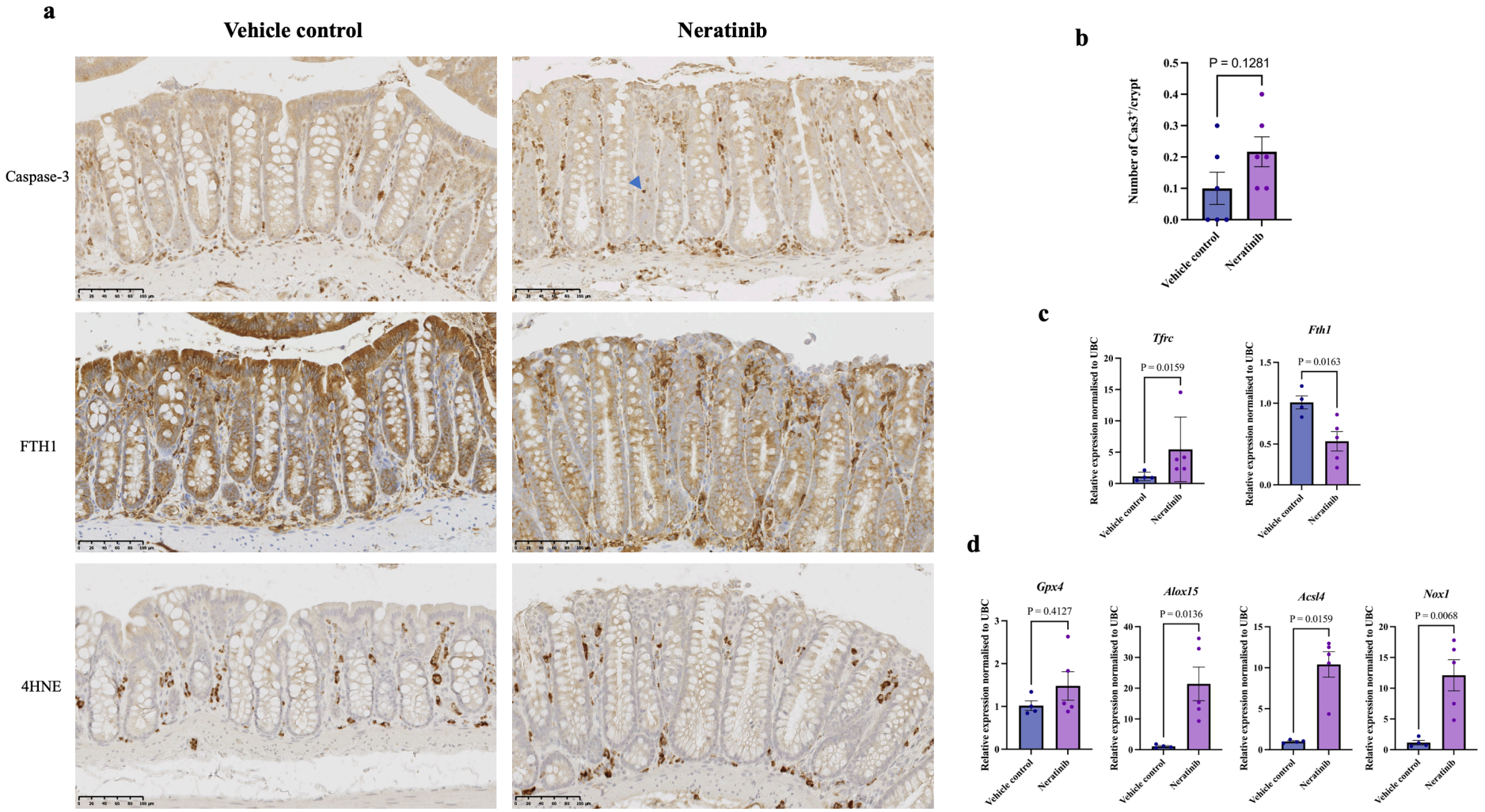
a
Vehicle control
Neratinib
Caspase-3
FTH1
4HNE
b
P = 0.1281
Number of Cas3+/crypt
Vehicle control
Neratinib
c
Tfrc
P = 0.0159
Fth1
P = 0.0163
Relative expression normalised to UBC
d
Gpx4
P = 0.4127
Alox15
P = 0.0136
Acsl4
P = 0.0159
Nox1
P = 0.0068

**Figure 7: Ferroptosis is a potential underlying histopathological feature of neratinib-induced injury in the distal colon. a,** Representative images of IHC-stained (Caspase-3, FTH1, and 4HNE) distal colon treated with either vehicle or neratinib. Scale bar, 100 μm. Arrowhead indicates an apoptotic body. **b,** The quantification of positive Caspase-3 cells per crypt. **c,** The gene expression levels of markers for iron metabolism (*Tfrc* and *Fth1*). **d,** The gene expression levels of markers for lipid peroxidation (*Gpx4*, *Alox15*, and *Acsl4*), superoxide-generating enzyme (*Nox1*). **For b, c, and d,** n = 4 rats in vehicle-control-treated group, and n=5 in neratinib-treated group. The gene expression levels were determined by RT-qPCR and were shown relative to *Ubc* housekeeping gene. Except non-parametric Mann-Whitney test was used for *Tfrc*, *Gpx4*, and *Acsl4*, unpaired Student's t-test was used for statistical analysis, where P values below 0.05 were considered statistical significance. The centre line represents the mean, and the error bar represents s.e.m

## 3.4. The inhibition of MAP4K3 kinase activity by neratinib may be critical for inducing ferroptosis

Structurally similar to neratinib, lapatinib is a pan-HER-TKI that reversibly binds to the ATP-binding pocket of HER1 and HER2 receptors (Fig. 8a) [116,117]. However, rather than ferroptosis, lapatinib promotes apoptotic cell death in human (SKBR3) and mouse (TBCP1) HER2-positive breast cancer cell lines [94,118,119]. Interestingly, patients receiving neratinib experienced a higher incidence of all-grade diarrhoea than with lapatinib, 95% and 65%, respectively [120]. Our preclinical studies in Albino Wistar rats further showed that neratinib caused a more severe grade of diarrhoea than lapatinib did [33,121]. These observations suggest that the difference in severity of diarrhoea might be due to a different type of cell death induced by neratinib compared to lapatinib.

Since both neratinib and lapatinib are second-generation small-molecule TKIs, which target the ATP-binding pocket of kinases, we wondered whether modulating the activity of other kinases by neratinib might be essential for potentiating ferroptosis. To address this question, the publicly available Library of Integrated Network-based Cellular Signatures KINOMEscan (LINCS-KINOMEscan) was utilised to assess the binding affinity ($K_d$, nM) and kinase activity (% to the control) for a panel of 442 kinases following neratinib (10 μM) and lapatinib (10 μM) treatment. To be considered as meaningful binding of a kinase, the cut-off $K_d$ values were determined based on the highest concentration of neratinib (152 nM) and lapatinib (3.67 μM) in human plasma [104,122]. Among all tested kinases, neratinib but not lapatinib strongly bound with a $K_d$ of 7.7 nM against mitogen-activated protein kinase kinase kinase 3 (MAP4K3, M4K3, or GLK) (Fig. 8b). Given that the amino acid sequence of MAP4K3 kinase is conserved in human, mouse, and rat (Appendix Fig.1) and the activation of MAP4K signalling promotes apoptosis and tumour suppression through c-Jun N-terminal kinase (JNK) and Hippo signalling pathways [123-

[125], we conjectured that the inhibition of MAP4K3 by neratinib, but not lapatinib, might perhaps be critical to facilitate a switch from apoptotic to ferroptotic cell death in human and mouse breast cancer cell lines *in vitro* as well as rat colon *in vivo* (Fig. 8c).

To explore the binding of neratinib and lapatinib to the kinase domain of MAP4K3, we utilised a similar approach by Tang et al. [95] to comparatively align the published co-crystal structure of both neratinib-bound and lapatinib-bound EGFR kinase with the co-crystal structure of aminopyrrolopyrimidine-bound MAP4K3 kinase. Aminopyrrolopyrimidine is a model analogue of TKI crizotinib that inhibits MAP4K3 kinase activity by competing at ATP-binding pocket [126]. The alignment suggested that both lapatinib and neratinib can theoretically fit into the ATP-binding pocket of MAP4K3 kinase (Fig. 8d). This appeared contradictory to the experimental data in the LINC KINOMEscan datasets, which reported that only neratinib but not lapatinib could bind to MAP4K3 kinase. Upon close examination of chemical structures of the three inhibitors and their binding conformation inside the ATP-binding pocket of MAP4K3 kinase, we noticed a difference in key functional moieties of the inhibitors that could potentially contribute to variation in binding affinity. Firstly, neratinib and aminopyrrolopyrimidine have the pyridine group in common whereas lapatinib contains a *meta*-fluorobenzyl group inside the binding pocket (Fig. 8a). Though the steric hindrance of the fluorine atom is minimal, fluorine is a highly electronegative atom resulting in a highly polarised carbon-fluorine (C-F) bond which may lead to a poor fit into the binding pocket of MAP4K3 kinase [127]. Secondly, in contrast to neratinib, which contains a substituted diethylamine group, lapatinib has a sulfone group, a polar moiety, that decreases the overall lipophilicity of lapatinib (Fig. 8a). Together, these two different substitution patterns likely lead to the obstruction of lapatinib from binding to the ATP-binding pocket of MAP4K3 kinase. Collectively, these observations are suggestive of why only neratinib but not lapatinib can bind to and inhibit MAP4K3 kinase activity.

**a**

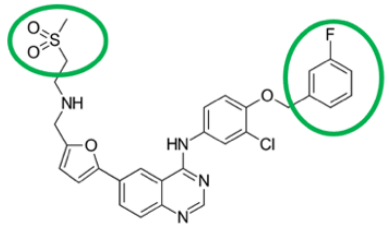

Lapatinib

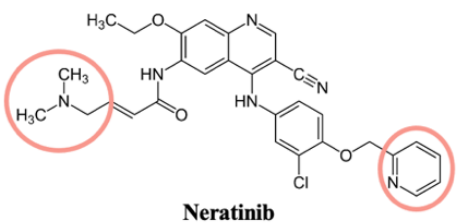

Neratinib

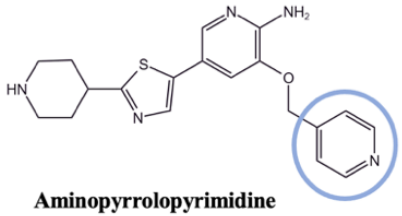

Aminopyrrolopyrimidine

**b**

| | HER1/EGFR$^{wt}$ | HER2$^{wt}$ | HER4$^{wt}$ | MAP4K3$^{wt}$ |
|---|---|---|---|---|
| Neratinib | 1.1 (0.1%) | 6.0 (0%) | 2.4 (0%) | 7.7 (2.1%) |
| Lapatinib | 2.4 (0%) | 7.0 (0%) | 54.0 (0.2%) | > 10,000 (94%) |

*Values are reported in dissociation constant, $K_d$ (nM), and percentage of control (%), where 100% means no inhibition and low percentage means strong inhibition.

**c**

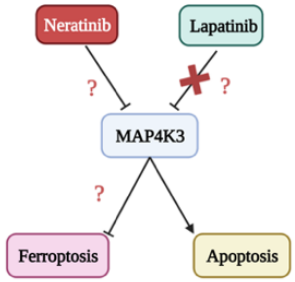


**d**

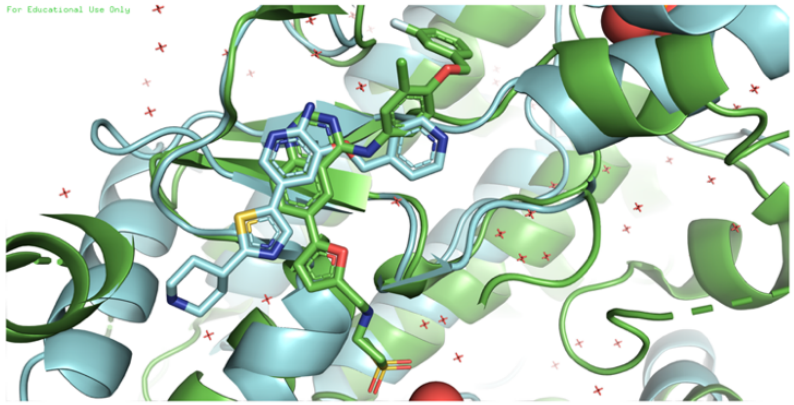


Lapatinib/EGFR: green, Aminopyrrolopyrimidine/MAP4K3: blue

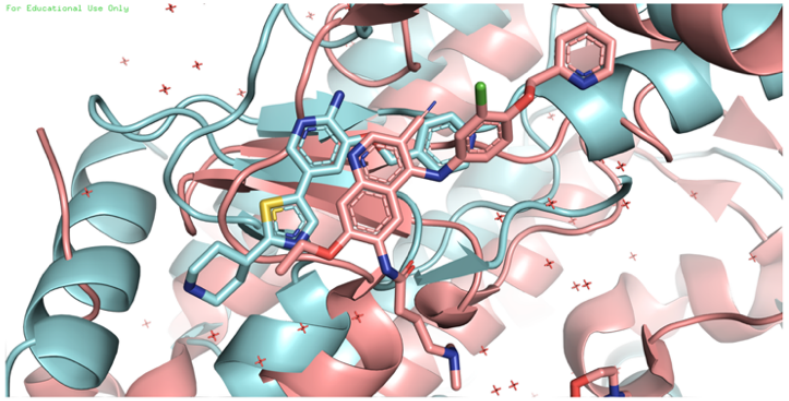


Neratinib/EGFR: pink, Aminopyrrolopyrimidine/MAP4K3: blue

**Figure 8: The modulation of MAP4K3 by neratinib may be essential for potentiating ferroptosis. a,** The chemical structure of neratinib, lapatinib, and aminopyrrolopyrimidine. **b,** A table of $K_d$ values and percentage of control for neratinib and lapatinib to HER1/2/4 and MAP4K3 kinase reported in the LINCS KINOMEscan dataset. **c,** The schematics illustrates of how the modulation of MAP4K3 kinase activity by neratinib might serve as a switch between apoptosis and ferroptosis. **d,** The alignment of crystal structures of published co-crystal structure of MAP4K3 kinase bound with aminopyrrolopyrimidine inhibitor (blue) and either lapatinib (green) or neratinib (pink) bound with EGFR kinase.

## 3.5. Identifying an *in vitro* model suitable for investigating neratinib-induced ferroptosis in colonic epithelial cells

Having identified ferroptosis as the likely feature underlying neratinib-induced colon injury, we wanted to ascertain that ferroptosis was induced by neratinib in colonic epithelial cells and further dissect its underlying mechanism of the early event leading to cell death. We initially attempted to utilise the human $SW48^{wt}$ colorectal cancer cell line, which has genomically wild-type for HER but is mutant for Wnt signalling pathways [128-130], as an *in vitro* model. However, the results from XTT cell viability assay showed that the $IC_{50}$ values of neratinib in $SW48^{wt}$ was approximately 9.73 μM following 24 hours and unable to be calculated following 48 hours of neratinib treatment. These values were significantly higher than the reported plasma concentration of neratinib in human ($C_{max}$ = 152 nM) (Fig. 9a) [122]. Interestingly, our TEM imaging showed extensive vacuoles in the cytosol following the incubation of $SW48^{wt}$ cells with neratinib at a concentration of 10 μM for 4, 12 and 24 hours (Fig. 9b). The formation of vacuoles suggested the cells treated with neratinib likely underwent autophagy-mediated cell death. Nonetheless, as the $IC_{50}$ value of neratinib was significantly higher than human $C_{max}$ value, we concluded that $SW48^{wt}$ cell line was potentially resistant to neratinib treatment and was deemed unsuitable for subsequent mechanistic investigations.

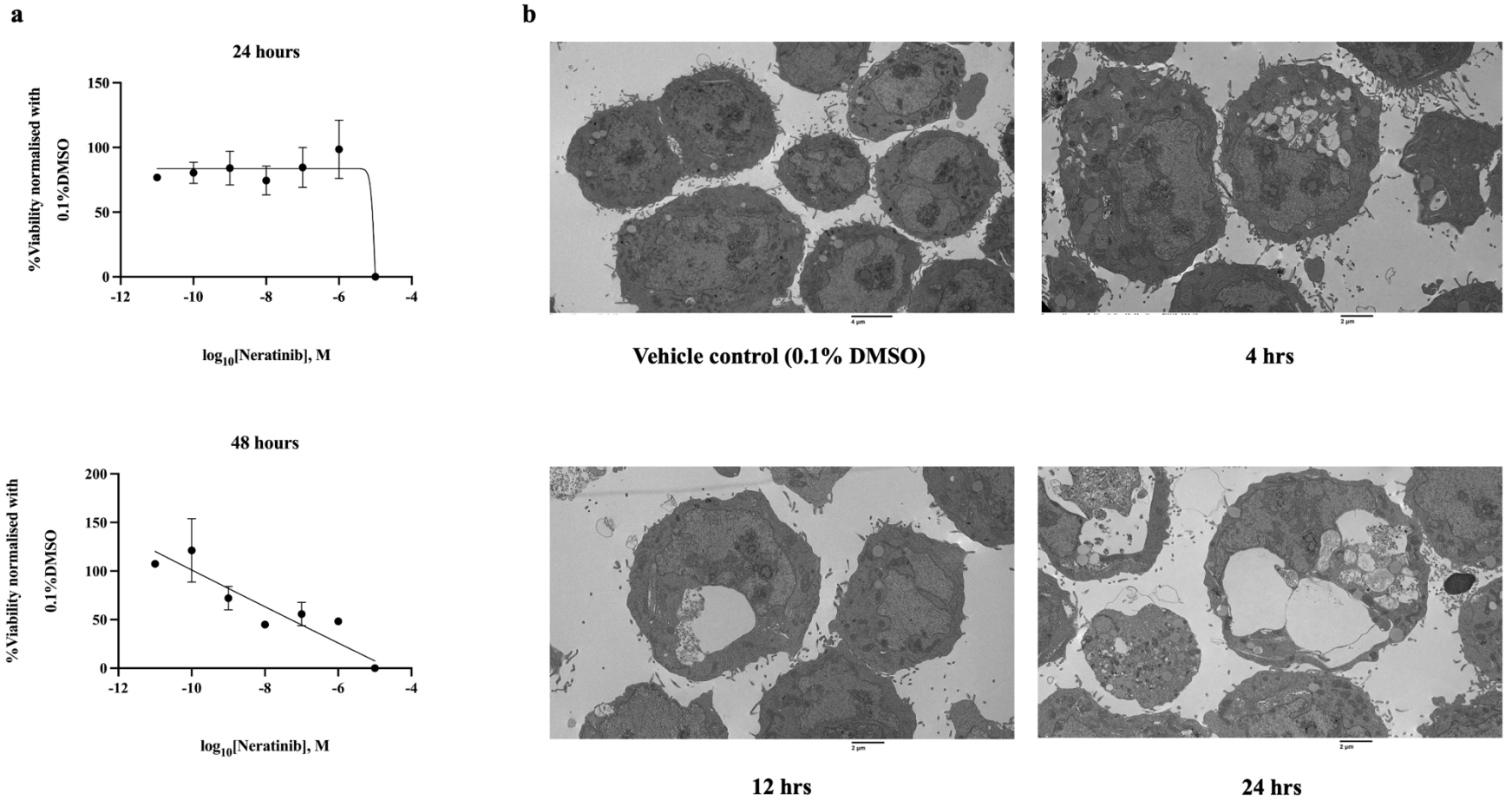


**Figure 9: The effect of neratinib treatment on SW48 cell line. a,** $IC_{50}$ values of neratinib following 24 and 48 hours of drug treatment (n = 2). The centre line represents the mean, and the error bar represents s.e.m. **b,** Representative of TEM images of SW48 cell following 4, 12 and 48 hours of neratinib treatment (10 µM). Scale bar 4 µm for vehicle control (0.1% DMSO) and 2 µm for 4, 12, and 24 hrs.

To overcome the mutation complexities associated with colorectal cancer cell lines, we sought to utilise the *in vitro* wild-type three-dimensional colonic organoid as an alternative model system for subsequent mechanistic investigation. The colonic organoid, which can be grown from isolated intestinal stem cells, recapitulates the complex structure of the intestinal epithelium with physiological relevance [53,58]. The colonic organoid can also be pharmacologically manipulated to differentiate into a specific lineage of interest, such as absorptive colonocytes, critical for dissecting the mechanism of neratinib-induced cell death [62]. Since the above histopathological assessment demonstrated the distal colon and its differentiated surface colonocytes was the major target of neratinib treatment in rats, we conducted a pilot study to stimulate colonic organoids derived from the distal region of a female C57BL/6 mouse colon under $BMP^{low}$ (EN and ENR) and $BMP^{high}$ (E+BMP2 and ER+BMP2) differentiation media to identify the best condition for terminal colonocyte differentiation essential for subsequent mechanistic studies [61,131].

Over the course of a 3-day differentiation period, consistent with previous reports in small intestinal organoids [61,131], colonic organoids grown in $BMP^{high}$ and $BMP^{low}$ differentiation regimes generated compact organoid with thickened and folded epithelial walls in appearance compared to those grown in the complete WENR media (Fig. 10a). Interestingly, colon organoids grown in $BMP^{high}$ media appeared to form a more substantial budding structure than those in $BMP^{low}$ media. To determine if the differentiation was successful, we validated the expression of key markers of differentiated colonocytes (*Ca1*, *Aqp8*, and *Slc6a3*), goblet cells (*Muc2*) and enteroendocrine cells (*Chga*) using RT-qPCR. Compared to complete WENR conditions, organoids in both $BMP^{high}$ and $BMP^{low}$ differentiation conditions appeared to express markers of differentiated epithelial cells noted above (Fig. 10b). This result suggested that $BMP^{high}$ and $BMP^{low}$ conditions, in principle, can trigger organoid differentiation towards

all lineages consistent with previous studies [58,62]. Our current result from this pilot study suggested that differentiated colonic organoids might be a suitable model system to further delineate the underlying mechanism of cell death induced by neratinib in differentiated colon epithelial cells.

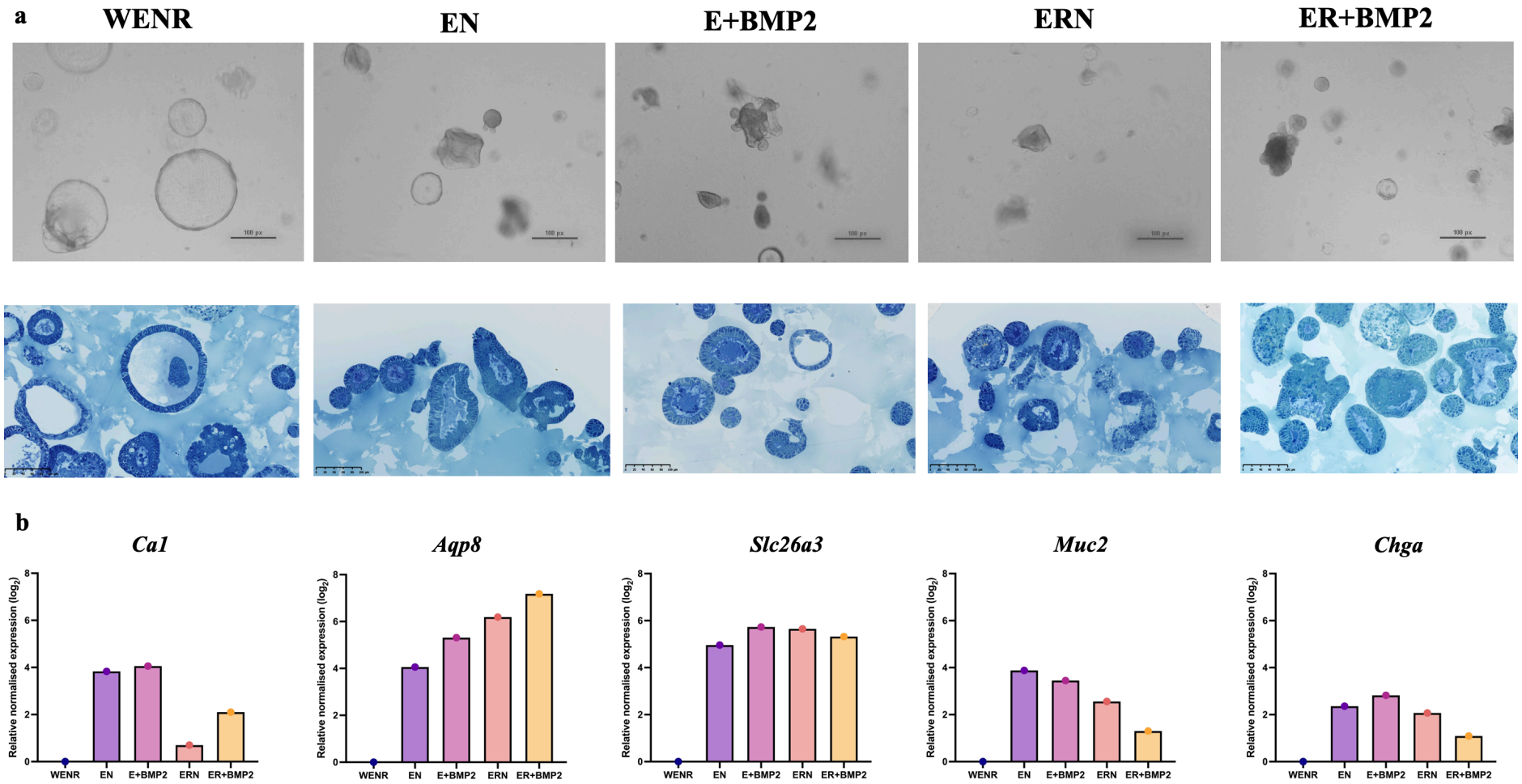
a
WENR
EN
E+BMP2
ERN
ER+BMP2
b
Ca1
Aqp8
Slc26a3
Muc2
Chga
Relative normalised expression (log2)
WENR
EN
E+BMP2
ERN
ER+BMP2

**Figure 10: The effects of BMP-on and BMP-off differentiation regimes on female mouse distal colon organoid: a,** Representative bright-field (top panel) and toluene-blue-stained (bottom panel) images of mouse colon organoid in WENR medium or after 3 days in $BMP^{low}$ (EN and ERN) and $BMP^{high}$ (E+BMP2 and ER+BMP2) differentiation media. Scale bar, 100 px is equivalent to 100 μm. The experiment was independently repeated three times. **b,** The expression levels of markers for colonocytes (*Ca1*, *Slc26a3*, and *Aqp8*), goblet cells (*Muc2*), and enteroendocrine cells (*Chga*) were determined by RT-qPCR and were shown relative to WENR control in $log_2$FoldChange. Sample size represents n = 1 biological experiment.

# Chapter 4: General discussion, limitations, and future direction

Neratinib, a small-molecule pan-HER-TKI, is an adjuvant targeted therapy for patients with HER2-positive breast cancer [132]. In contemporary practice, over 90% of patients receiving neratinib experienced mild-to-severe diarrhoea, which often leads to early dose reduction or discontinuation [32]. Yet, the underlying biological processes leading to neratinib-induced gut toxicity, especially in the colon, remain incomplete. In the present work, we used a previously established clinically relevant *in vivo* Albino Wistar rat model to investigate gut toxicity following neratinib treatment, in which healthy female rats were orally dosed with neratinib (50 mg/kg) daily for 28 consecutive days [33,87]. Overall, our study shows that the injury is spatially located with predominating injury in the distal colon. In particular, the degeneration and morphological changes of CA1-positive colonocytes lining the surface epithelium are more pronounced in the distal colon than in the proximal colon. Ferritinophagy-mediated ferroptosis is a potential histopathological feature of neratinib-induced gut toxicity. Finally, we propose that the inhibition of MAP4K3 kinase activity and its downstream signalling pathway may be essential for inducing ferroptosis in a context of neratinib treatment, but not other TKI such as lapatinib, which promotes apoptosis (Fig. 11).

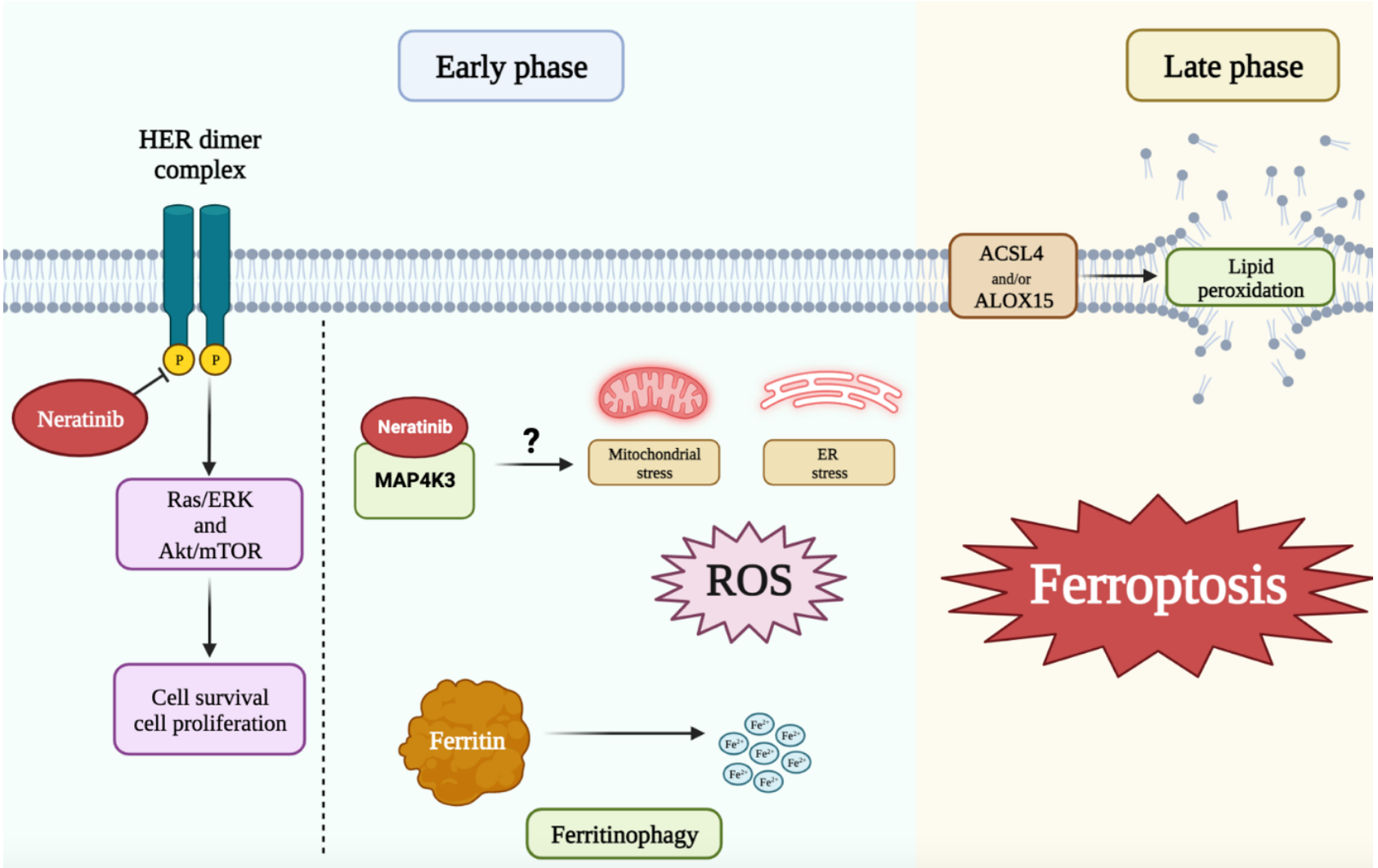


**Figure 11:** A schematic of proposed mechanism of how ferroptosis is induced by neratinib.

## 4.1. Molecular regionalisation may underlie the spatially located neratinib-induced injury in the rat colon

The spatial difference in the severity of injury observed in the proximal and distal colon could be explained on the basis of molecular regionalisation of the colon. Using cutting-edge spatial transcriptomics, a recent study led by Villablanca's team revealed that the difference in the morphology of the proximal and distal colon was governed by molecular regionalisation of gene expression [80]. They further showed that the severity of DSS-induced injury varying between different regions of the colon was likely due to this pattern. As the morphology of the proximal and distal colon of the rat are distinct as observed in representative H&E-stained sections (Fig. 5a), we hypothesised that similar to the mouse colon, there might exist the pattern of molecular regionalisation that potentially implicated the distal colon as the major site of injury following neratinib treatment. For example, factors may contribute to the severity of the injury following neratinib treatment include the different distribution of HER receptors and upregulation of key inflammatory pathways such as JAK-STAT and TNFα pathways between the proximal and distal colon.

On the other hand, since all rats were culled on day 28 of neratinib treatment and a dramatic increase in proliferative Ki67-positive cells in both proximal and distal colon of rats treated with neratinib (Fig. 5e), we cannot exclude the possibility that we might have missed the earlier timepoint, where the mucosal damage may occur in both proximal and distal colon. The proximal colon may possess an intrinsic adaptive mechanism that leads to a more rapid healing rate and a less severely injured phenotypes than the distal colon on day 28 of neratinib treatment. Though the current study does not provide the precise explanation for why the injury in the distal colon appears to be more severe than in the proximal colon, it sheds light on potential consequence of the pathology following neratinib treatment.

## 4.2. Ferritinophagy-mediated ferroptosis may be the underlying feature of neratinib-induced colon injury

Further investigations in rat colon tissues and the integration of published bulk RNA-sequencing analyses revealed that ferritinophagy-mediated ferroptosis may be the underlying feature of not only colon injury, especially in the surface lining colonocytes, but also cell death in the HER2-positive TBCP-1 breast cancer cell line and HER1-mutant TS895 glioblastoma xenografts. However, there are several limitations associated with the current rat models that prevent a conclusive determination that ferroptosis is the causality of neratinib-induced colon injury. Firstly, in IHC staining experiments on rat colon, a positive signal of endogenous 4-hydroxynonenal (4HNE), a marker for detecting lipid peroxide in tissues using HNEJ-2 antibody, was not detected. This could be due to non-specificity of HNEJ-2 antibody to lipid peroxide, which was previously deemed unsuitable for detecting lipid peroxidation underlying ferroptosis, or at least this antibody is not suitable for detecting lipid peroxide in rat colon tissues [84,133]. We suggest that the use of HNEJ-1 or anti-malondialdehyde (MDA) antibodies would be more favourable for IHC staining to detect lipid peroxidation [84,134].

Secondly, a change in *Gpx4* gene expression was additionally not observed in the neratinib-treated group. Previous studies found that transcriptional regulation of *Gpx4* did not seem to correlate with ferroptosis vulnerability, but rather mRNA translation and post-translational regulation of *Gpx4*, which leads to insufficient level or dysfunctional GPX4 enzymatic activity, is implicated in susceptibility to ferroptosis [114,135-137]. In the TBCP-1 breast cancer cell line, neratinib significantly depletes intracellular glutathione, which is essential for the formation and enzymatic function of GPX4 [138]. We suggest that the amount and enzymatic activity of GPX4 might have also been impeded in rat colon following neratinib treatment. To validate the contribution of GPX4, we will determine the presence of GPX4 protein using IHC staining and

measure the reduced/oxidised ratio of glutathione using calorimetric test in the rat colon in a future study.

Finally, the degeneration, or at least changes in the morphology, of surface lining CA1-positive colonocytes and changes in the expression of several markers of ferroptosis following a single endpoint of neratinib treatment are not sufficient to claim that ferroptosis is induced in colonocytes as a direct consequence of neratinib treatment. For example, the degeneration of surface lining epithelial cells could be due to the improper differentiation of stem/progenitor cells that prevents CA1-positive colonocytes to adopt mature phenotypes, such as expressing carcinoembryonic antigen-related cell adhesion molecule 7 (CEACAM7).

Furthermore, following neratinib treatment, there was a dramatic increase in the infiltration of lymphocytes in the lamina propria and intraepithelial of the distal colon that suggested a diagnosis of lymphocytic colitis. A common feature of lymphocytic colitis is the infiltration of CD8+ lymphocytes. Active immune cells, such as $CD8^+$ lymphocytes, are able to stimulate ferroptotic cell death. Two recent studies from Wang et al. [139] and Liao et al. [140] reported that ferroptosis could be induced by active $CD8^+$ T cells. Mechanistically, following the release of interferon gamma (IFNγ) from active $CD8^+$ T cells and interaction with cognate receptors on melanoma and colon cancer cells, the downstream signalling of IFNγ robustly induces ferroptotic cell death by stimulating the uptake of arachidonic acid and upregulation of ACSL4 while suppressing the expression of SLC7A11, which encodes for system $X_c^-$ essential for cysteine uptake [139,140]. As such, based on the current data collected from a single endpoint on day 28 of neratinib treatment, it is possible that ferroptosis is an indirect consequence of neratinib-activated immune cells, such as $CD8^+$ T cells, leading to epithelial cell death.

Future studies require an earlier timepoint of neratinib-treated rats and IHC staining for CEACAM7, a specific marker of mature colonocytes [141] and markers of TH17-related T cells and $CD8^+$ lymphocytes associated with noted microscopic colitis [105,142]. Similar to previous studies done in confirming the presence of ferroptosis in mouse model of DSS-induced colitis, to ascertain if ferroptosis is induced and dependent to ferritinophagy in rat colon, we will co-treat neratinib with liproxstatin-1, a potent spiroquinoxalinamine radical trap of lipid peroxide [134,135], and deferoxamine (DFO) or deferiprone, an iron chelator scavenging reactive ferrous iron, to the rats [143,144]. If liprostatin-1 and DFO/deferiprone can substantially mitigate colon injury and signs of gut toxicity in rats treated with neratinib, then ferroptosis is confirmed as the underlying feature of neratinib-induced colon injury. To further confirm if the death of colonic epithelial cells is a direct consequence of neratinib and ferroptosis is the underlying mechanism, an *in vitro* model system of colonic epithelial cells treated with neratinib is therefore required.

### 4.3. Resistance of SW48 colorectal cancer cell line to neratinib may be due to aberrant Wnt signalling pathway and wild-type *TP53*

Our study demonstrates that the human SW48 colorectal cancer cell line, which bears hyperactivating mutation in *HER1* and wild-type *TP53* gene but intact HER and mutant Wnt signalling pathways, is not suitable for further mechanistic investigation of neratinib-induced ferroptosis [128-130,145]. We suggested the aberrant Wnt signalling pathway and wild-type *TP53* status of SW48 cell line may be the causal of neratinib resistance. First, the resistant phenomenon of SW48 cell line to neratinib could be due to aberrant Wnt signalling pathway. As previously reported in a context of $BRAF^{V600E}$ colorectal cancers treated with BRAF ± HER1 targeted therapy, the aberrant Wnt signalling pathway can activate intrinsic HER1-independent compensatory mechanisms independently from canonical HER-ERK signalling that leads to the resistance of targeted BRAF ± EGFR inhibition [146].

Second, *TP53*$^{wt}$ status in SW48 colorectal cancer cell line might suppress the potentiation of ferroptosis by abolishing lethal lipid peroxidation at the plasma membrane. Nagpal and colleagues recently reported that similar to erastin, neratinib-induced ferroptosis was dependent on the inhibition of cystine/glutamate antiporter (system $X_c^-$) encoded by *SLC7A11/SLC3A2* gene [138,143]. Intriguingly, Xie et al. previously reported that colorectal cancer cell lines with *TP53*$^{wt}$ gene, namely HCT116 and SW48, but not *TP53*$^{mut}$ gene, namely Caco2 and DLD1, completely abolished erastin-induced ferroptosis [113]. Of note, all the colorectal cancer cell lines used in Xie et al.'s study bear genetic mutation in *CNTBB1* and/or *APC* leading to the consecutive activation of Wnt signalling pathway [128-130,145,147]. Mechanistically, TP53$^{wt}$ protein forms a complex with dipeptidyl-peptidase-4 (DPP4) in the cytosol that transcriptionally stabilises the gene expression of *SLC7A11*. On the contrary, in *TP53*$^{mut}$ cell lines, DPP4 translocates to the plasma membrane and forms a complex with NOX1. The active DPP4-NOX1 complex triggers excessive lipid peroxidation resulting in the loss of plasma membrane integrity and inducing ferroptosis [113]. Hence, lethal lipid peroxidation at the plasma membrane induced by neratinib may be driven by NOX1-DPP4 complex and *TP53*$^{wt}$ status may lead to the resistance observed in SW48 colorectal cancer cell line. Collectively, despite intact HER signalling pathway, the resistance to neratinib-induced ferroptosis of colorectal cancer cell lines may depend on both the aberrant Wnt signalling arisen from *CNTBB1* and/or *APC* mutations and wild-type *TP53*.

However, it should be noted that ferroptosis can be induced in cells bearing wild-type *TP53* and intact Wnt signalling, such as HT1080 fibrosarcoma cell line [114,143,148-150]. Given that colonic epithelial cells express wild-type *TP53* and intact Wnt signalling pathway, we argue that ferroptosis may also be induced in the colon following neratinib treatment. Collectively, an alternative *in vitro* model system, which can recapitulate the physiologically relevant phenotype

of differentiated colonic epithelial cells and is amendable to a wide range of experimental methods, to immortal colorectal cancer cell lines is needed.

### 4.4. 3D organoids may be a suitable *in vitro* model for future mechanistic investigations

As an alternative to SW48 colorectal cancer cell line, differentiated 3D colonic organoids appeared to be a more suitable *in vitro* model system for subsequent studies with neratinib. The colonic organoids were chosen because they can be derived from isolated colonic stem cells and self-organise into a 3D tissue-like structure that recapitulates the complex structure and functions of the colonic epithelium *in vivo* [53,151]. Here, we suggest that the 3D colon organoids would be suitable for (1) determining if ferroptosis is induced by neratinib and which differentiating lineage and cell population were affected by neratinib treatment; and (2) dissecting the mechanisms underlying the early event of neratinib-induced cell death by integrating genetic and pharmacological manipulation, imaging, and -omics techniques.

So far, we tested two different differentiation conditions, namely $BMP^{high}$ and $BMP^{low}$, to identify which was the best conditions for stimulating terminally differentiated mouse colon organoids. We found that both BMP conditions promoted the differentiation of colon organoids towards goblet cells (*Muc2*), enteroendocrine cells (*Chga*), and terminally differentiated colonocytes (*Ca1*, *Aqp8*, and *Slc26a3*). However, due to small sample size (n = 1), we cannot confidently conclude at this stage which phenotype, such as mature versus immature, and which differententiation lineages were more favourably enriched under $BMP^{high}$ and $BMP^{low}$ conditions as previously reported by Clevers' group in small intestinal organoid [61,131]. As such, future research will need to increase the sample size (n = 3) to address the outstanding questions on $BMP^{low}$- and $BMP^{high}$-driven organoid differentiation.

To probe ferroptosis, we additionally consider modifying the composition of the current organoid culture media, specifically B27 supplement. Though B-27 supplement contains transferrin, which is essential for ferroptosis [152], it also contains several anti-ferroptotic compounds such as α-tocopherol, catalase, SOD, glutathione, and selenite [153]. Hence, B27 supplement may hinder the induction of ferroptosis by neratinib in colonic organoids as previously observed in cortical organoids [154]. Therefore, it is essential for future studies to be cautious about the potential anti-ferroptotic effect of B27 supplement, and perhaps to consider culturing organoids in a condition of B27-depletion with or without FBS supplement, which has been proven essential for ferroptotic progression [152], for a few days before treating the organoids with neratinib and other known ferroptotic inducers such as erastin or RSL3, which serve as the control for ferroptotic induction. To further confirm that ferroptosis can be induced by neratinib in colonic organoids, similar to the approach discussed in section 5.2, we will co-treat the organoid with neratinib and liproxstatin-1 and DFO. Only if liproxstatin-1 and DFO can substantially rescue cell death, we can then confidently conclude that the colonic epithelial cells can undergo ferroptosis following neratinib treatment.

In addition, we proposed that the inhibition of MAP4K3 kinase activity by neratinib but not lapatinib might be essential for ferroptotic induction. Future studies should exploit the use of X-ray crystallography to explore how neratinib but not lapatinib binds to the active ATP-binding pocket of MAP4K3 kinase and to determine any additional allosteric binding sites that might be important for modulating kinase activity as outlined in the context of RSL3-bound GPX4 by Stockwell's group [136]. The use of *in vitro* 3D colonic organoids can be integrated to validate of the activity of MAP4K3 kinase and its downstream signalling pathway leading to apoptosis. Here, we suggest performing immunoblotting experiments similar to Lam et al. [123] to determine

the presence of phospho-MAP4K3, phospho-JNK, phospho-cJun and cleaved caspase-3 following a titration of a series concentration of neratinib and lapatinib.

Furthermore, emerging evidence from recent literatures has demonstrated that the distinct subcellular partition of chemically related inhibitors correlates with distinct therapeutic outcomes. As a proof of concept, using fluorescent confocal microscopy, Fryman and colleagues revealed that the partitioning of closely related heat shock proteins 70 (Hsp70) inhibitors to mitochondria, ER or vesicles can exert either anti-cancer or anti-viral therapeutic outcomes [155]. We therefore hypothesise that neratinib and lapatinib may localise at distinct subcellular compartments that may be essential to fuel ferroptosis and apoptosis, respectively.

## 4.5. Limitations of the current study

Though our current rat study suggests that ferroptosis is a potential underlying feature of neratinib-induced colonic injury, there are several technical limitations associated with the current models and analyses which in our opinion are essential to be address in future studies. An earlier timepoint of neratinib treatment in the rat model is needed (1) to fully understand the difference in response to neratinib treatment in proximal versus distal colon and to conclude that apoptosis is not induced by neratinib; (2) to determine if mature colonocyte is a major target of neratinib treatment; and (3) to determine whether the death of colonic epithelial cell is due to either the direct or indirect consequence of neratinib treatment.

Besides the use of *in vitro* SW48 as a model system, we also attempted to use LIM1215 colorectal cancer cell line, which expresses intact HER but mutant Wnt signalling pathway [156,157]. The viability of LIM1215 was determined by MTT cell viability assay in collaboration with Professor Ross Bathgate and Dr. Brad Hoare from the Florey Institute of Neuroscience

and Mental Health. Our results demonstrated that culturing LIM1215 cell lines in RMPI-1640 media was not suitable for testing neratinib because of neratinib resistance and extensive cell death in the negative control (DMSO-treated) group (Fig. 12a and b).

Culturing conditions of *in vitro* colonic organoids derived from both human and mouse as a model system as an alternative to colorectal cancer cell lines should be further optimised. These optimisations include identifying appropriate culturing condition for both undifferentiated and differentiated models critical for probing neratinib-induced ferroptosis. Finally, the initiating event of how neratinib induces ferroptosis remains unclear, in which we postulate is due to perturbed redox regulation at specific subcellular compartment, such as mitochondria or endoplasmic reticulum (ER).

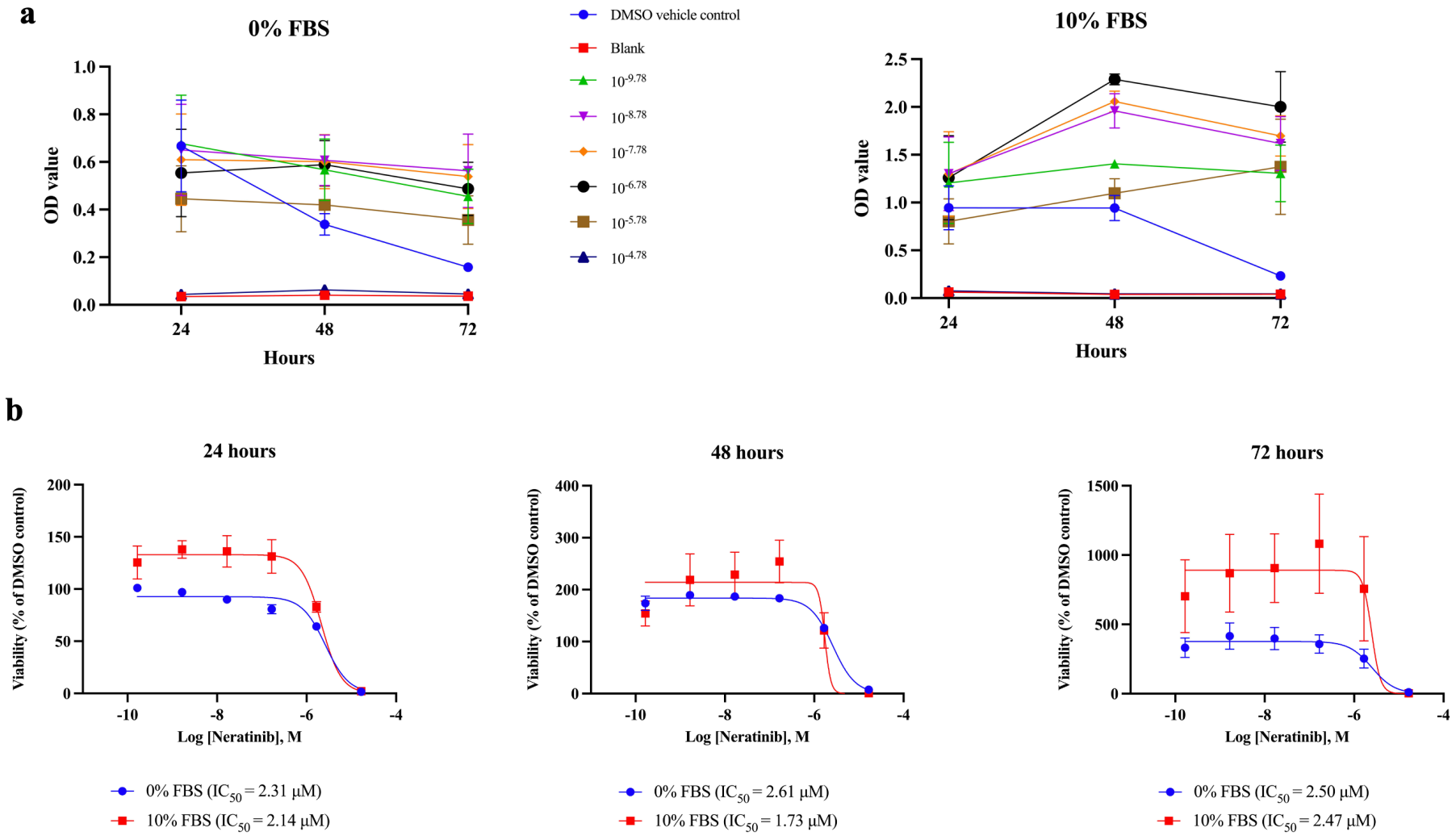
a
0% FBS
10% FBS
OD value
Hours
DMSO vehicle control
Blank
10-9.78
10-8.78
10-7.78
10-6.78
10-5.78
10-4.78
b
24 hours
48 hours
72 hours
Viability (% of DMSO control)
Log [Neratinib], M
0% FBS (IC50 = 2.31 µM)
10% FBS (IC50 = 2.14 µM)
0% FBS (IC50 = 2.61 µM)
10% FBS (IC50 = 1.73 µM)
0% FBS (IC50 = 2.50 µM)
10% FBS (IC50 = 2.47 µM)

**Figure 12: The response of LIM1215 colorectal cancer cell line to neratinib treatment.** **a,** Mitochondrial metabolic activity of Lim1215 measured by MTT assay and plotted against the absorbance optical density (O.D.) value. **b,** $IC_{50}$ values of neratinib for LIM1215 after 24, 48, and 72 hours of neratinib treatment. **For a, and b,** data are presented from n = 2 biologically independent experiments. The centre line represents the mean, and the error bar represents s.e.m.

## 4.6. Future direction – Towards understanding the spatiotemporal dynamics of ROS at specific subcellular compartments – a mini-review

### 4.6.1. Pleiotropic role of ROS in mediating intestinal health and injury

The biological functions of ROS are pleiotropic in intestinal epithelial cells. The study of the precise spatiotemporal regulation of ROS at specific compartments of the cell is a fast-evolving field. To date, ample evidence has uncovered a more complex physiological-relevant functions of ROS in intestinal homeostasis by mediating various signalling and metabolic pathways, gene expression and cell cycle [158-161]. For example, ROS generated from NAPDH oxidase (NOX) enzymes located at the plasma membrane (PM) control the activity of the gut bacteria [162,163] and potentiate HER signalling pathway [164]. Mitochondrial ROS, which are mainly the by-product metabolites of complex I and II from the electron transport chain [165-167], have emerged as signalling mediators critical for orchestrating the normal functions of intestinal stem cells. In active intestinal stem cells, mitochondrial $H_2O_2$ activates p38-MAPK signalling pathway and oxidises cyclin dependent kinases (CDK) which thereby drive the proliferation and differentiation of stem cells [168-170].

However, sustained elevation or reduction of intracellular ROS level, which are referred to as oxidative and reductive stress, respectively, can cause both reversible and irreversible damage to biomolecules, such as lipids, proteins, and nucleic acids [82,171]. Unless the physiological concentration of ROS is restored, dysfunctional biomolecules can potentially impede critical signalling and metabolic pathways while inducing cell cycle arrest and growth inhibition and activating death-accelerating mechanisms [82,172,173]. For example, uncontrolled peroxidation of polyunsaturated fat (PUFA) at the endoplasmic reticulum (ER), PM, and mitochondrial membrane following the treatment of ferroptosis inducers such as dihydroorotate dehydrogenase (DHODH) inhibitor brequinar, $FINO_2$, and erastin, leads to lethal membrane

permeabilization – the hallmark of ferroptotic cell death [143,174,175]. On the other hand, the treatment of chemotherapy, such as cisplatin, or peroxiredoxin (PRDX) inhibitor, such as ainsliadimer A, results in the rapid accumulation of mitochondrial $H_2O_2$ and permeabilization of the mitochondrial outer membrane that subsequently releases cytochrome c and activates a cascade of caspase leading to apoptosis [176-180]. This evidence collectively suggests that a type of cell death triggered by aberrant ROS signalling is context-specific that strongly depends on the type of stimulus, specific ROS species, and their corresponding subcellular compartments.

As ROS can be both essential and lethal to the cell, the production, activity, and degradation of ROS must be precisely regulated and compartmentalised to specific subcellular compartments, such as PM or mitochondria, critical for driving cellular physiology. To compartmentalise and neutralise ROS, an intricate antioxidant defence system has evolved ranging from small molecules, such as vitamins and coenzyme Q (CoQ or ubiquinone), to large biomolecules, such as thiol-containing enzymes namely PRDX and glutathione peroxidases (GPX). Following the neutralisation of ROS, the thiol-containing enzymes can be regenerated from their oxidised state by their counterpart reductase enzymes, which requires the $NADP^+$/NADPH system [181,182]. For instance, GPX4, CoQ10, and vitamin K act in parallel to scavenge lipid peroxides, protect the PUFA from being peroxidised at the membrane, and thus prevent ferroptotic cell death [114,183-185]. Mitochondrial ROS are primarily controlled by mitochondrial membrane potential [186] and PRDX enzymes [180,187]. E3 ligase Culin-2-Fem-1-homolog-B ($CUL2^{FEM1B}$) and its target folliculin-interacting protein 1 (FNIP1) is a newly discovered core machinery of reductive stress response by regulating mitochondrial ROS [188,189]. Under homeostatic and oxidative stress condition, brain-expressed X-linked (BEX) proteins bind to and inhibits $CUL2^{FEM1B}$ complex and release free FNIP1. FNIP1 plays a critical role in removing damaged mitochondria via mitophagy to prevent excessive mitochondrial ROS production [188,190]. However, under

reductive stress, to restore physiological levels of mitochondrial ROS via oxidative phosphorylation, the $CUL2^{FEM1B}$ complex detects and binds to the conserved cysteine residues of FNIP1 through zinc ions. FNIP1 is subsequently ubiquitylated and degraded via a proteasome-dependent mechanism [188,189]. Together, the tight regulation of ROS at their corresponding subcellular compartments is pivotal to the health of intestinal epithelial cells, whereas perturbation to the precision of spatiotemporal redox regulation, such as by chemotherapy or targeted cancer therapy, may trigger intestinal cell death that implicating intestinal injury.

Emerging in the current literature is that rather than functioning autonomously, the cell forms an intricate interconnected network of communication among different subcellular compartments to adapt with internal and external challenges [191,192]. Despite current knowledge of the significance of ROS for cellular homeostasis and injury, biological questions central to ROS as the mediator for intercompartmental communication remains incomplete. Specifically, in the present work, we proposed that aberrant redox signalling is a potential initiating event of neratinib-induced ferroptosis, but which ROS species, as well as where and how ROS are initiated and propagated following neratinib treatment remains unclear.

Recent studies in the field of ferroptosis discovered that almost all ferroptotic inducers, at least in cancerous cell lines *in vitro*, first trigger the lipid peroxidation at specific compartments of the cell. For example, brequinar and $FINO_2$ trigger extensive lipid peroxidation at the inner membrane of the mitochondria and ER, respectively [174,175]. Subsequently, lipid peroxide is rapidly spread to the PM where lipid peroxide exerts its lethality to the cell [99,193]. Aligning with this observation, we herein conjecture that neratinib may first perturb redox regulation of at specific subcellular compartment, such as ER and/or mitochondria, which then rapidly

propagates and triggers a massive lipid peroxidation at the PM leading to ferroptosis. Yet, the underlying mechanism of how lipid peroxide is spread from the internal subcellular compartments to the plasma membrane remains unclear. It is plausible that the spread of lipid peroxide is carried out by vesicular transport, such as peroxisome [194], or direct membrane contact sites, e.g. mitochondria-PM and ER-PM. Consequently, investigating how the dynamics of ROS are spatially and temporally modulated in their native form following a perturbation, such as neratinib treatment, necessitates the integration of cutting-edge technologies, namely organoids, light-sheet microscopy (LSM), and fluorescent probe/sensors. We previously discussed the utility of 3D organoids as an *in vitro* model system for studying physiological and disease states of the colonic epithelium in section 1.6. Here, we will discuss the utility of LSM and the next-generation fluorescent probes/sensors for illuminating the spatiotemporal dynamics of specific ROS species at a specific compartment of the cell in the 3D intestinal organoids.

### 4.6.2. Imaging strategies for illuminating the spatiotemporal dynamics of ROS

#### 4.6.2.1. Light-sheet microscopy (LSM)

Imaging-based fluorescent technologies that provide single-cell resolution for visualising and constructing the 3D dynamic structure of thick samples such as organoids are blossoming. We argue that the key criteria for the choice of microscopy suitable for studying ROS dynamics should be associated with low level of unwanted phototoxicity and photobleaching that may potentially obscure the ROS read-outs. One such candidate is the state-of-the-art light-sheet microscope (LSM). LSM, which utilises ultra-thin single illuminating plane, has revolutionised the field of microscopy for imaging thick objects including whole tissues, animals, and organoids in live-cell 3D imaging [195-198]. While the whole object is illuminated in the conventional wide-field and confocal fluorescent microscopes, only a section of the sample

corresponding to the plane of light is illuminated at any given time in LSM. As the result, LSM allows fast in-depth tissue-penetration volumetric scanning while reducing out-of-focus light scattering to enhance signal-to-noise ratio [199,200]. As the illuminating plane is restricted to the region of the light sheet, the exposure time is significantly reduced resulting in reducing the exciting time for a fluorophore and thus reducing photobleaching and phototoxicity for continuous live-cell imaging in an extended period of time. Therefore, the use of LSM could potentially be applicable for illuminating the spatiotemporal ROS dynamics in organoids.

Subcellular resolution of images can be greatly enhanced by integrating the LSM with other cutting-edge microscopic technologies. Firstly, by incorporating the adaptive objective, which correct wavefront distortion travelling through different environment causing blurry images [201], to the lattice LSM, Betzig and colleagues successfully constructed high-resolution 3D videos of the dynamics of mitochondria throughout different stages of the zebrafish embryogenesis [196]. Notably, they observed that during mitosis, the mitochondria are re-organised to near the plasma membrane demonstrated the direct contact between the mitochondria and plasma membrane may be essential for cell division. Secondly, super-resolution imaging technologies, which significantly improve the imaging resolution of subcellular compartments by breaking the diffraction limit imposed by the characteristic of light wave [202], can also be integrated into the LSM. For instance, incorporating structured illumination microscopy (SIM) and single-molecule stochastic optical reconstruction microscopy (STORM) to the 3-dimensional interferometric lattice light-sheet (3D-iLLS) microscope allows the investigators to visualise and study the precise expression patterns of receptors at the plasma membrane and illuminate dynamics of microtubules and mitochondria at subcellular level [203-205].

#### 4.6.2.2. Fluorescent probes and sensors

The use of fluorescent probes and sensors is considered as a direct method for visualising and quantifying ROS in a cellular system. Previous reviews have summarised and provided expert recommendation for the choice of different types of probes/sensors, including small-molecule probes and genetically encoded sensors, for detecting various different ROS species *in vitro* and *in vivo* [206,207]. Here, we exclusively focus on the design of probes/sensors suitable for illuminating specific ROS species at subcellular compartments of interest with an example of $H_2O_2$. We recommend that this type of fluorescent probes/sensors should have at least three main desired characteristics – (1) not perturbing the normal cellular system; (2) demonstrating ROS species sensitivity and selectivity; and (3) only targeting specific subcellular compartments of interest.

##### *4.6.2.2.1. Genetically encoded sensors (GES)*

The use of genetically encoded sensors (GES) has long been regarded as the most sensitive approach for spatiotemporal visualisation and quantification of subcellular $H_2O_2$ [206-208]. However, no current GES for $O_2^{\cdot -}$ and lipid peroxide is available. The advantage of GES is that it can be stably or transiently expressed in cell lines and intestinal organoids using genetically engineered approaches, namely lentiviral gene transduction [209]. In general, the sensors from the HyPer and roGFP series contains a mutant $H_2O_2$-sensitive thiol and a site-specific domain in a fluorescent protein (e.g., green, or red fluorescent proteins) to direct the sensor to specific subcellular compartments of interest such as mitochondria or cytoplasmic microtubules [68,210,211]. For instance, in HEK293 and HeLa cells, the use of HyPer7 sensors revealed that under normal condition, mitochondrial $H_2O_2$ accumulates at membrane and is compartmentalised by cytosolic PRDXs and thioredoxin reductase (TXNRD), and that perturbed this antioxidant system leads to an increase in both mitochondrial and cytosolic ROS [187,211].

#### *4.6.2.2.2. Small-molecule fluorescent probes*

Though the use of current commercially available or in-house small-molecule probes can demonstrate ROS species selectivity such as boronate probes for $H_2O_2$ [212,213] and dual ROS species, such as $^{\cdot}OH$ and hypochlorous acid (HClO) [214] or $H_2O_2$ and nitric oxide (NO) [215]. However, due to the lack of spatial resolution, these probes can be problematic in illuminating the precise subcellular localisation of a specific ROS species of interest [206,207]. To circumvent current challenges, innovative technologies, such as nucleic acids and nanoparticles as delivery system, for precisely targeting specific subcellular compartments have attracted considerable attentions and have been discussed in great detailed elsewhere [216]. Here, we exclusively focus on tethered conjugates that can direct the small-molecule probes to specific compartments of the cell, thus, achieving the spatial single-cell resolution.

The first approach is to use the luciferin-based bioluminescent system. A previous study from Chang's group demonstrated that co-injecting peroxy caged luciferin-2 (PCL-2) and z-Ile-Glu-ThrAsp-d-Cys (IETDC) into the mice can simultaneously detect $H_2O_2$ and caspase-8 activity following lipopolysaccharides (LPS) treatment [217]. Mechanistically, PCL-2 reacts with $H_2O_2$ to release 6-hydroxy-2-cyanobenzothiazole (HCBT). HCBT subsequently reacts with D-cysteine, which is the product from the interaction between IETDC and active caspase 8, to produce firefly luciferin bioluminescent signal. By using the similar principle, one could theoretically target ROS species at specific subcellular compartments to achieve spatial imaging resolution.

The second approach is to directly tag additional moiety to the fluorescent probe to direct the probe to a specific subcellular compartment. For example, the use of dihydrotetrazine-diacylphospholipid and a TCO-modified dye (TCO-Dye) for targeting the plasma membrane [218] or triphenylphosphonium lipophilic cation moiety of the MitoNeoD probe for targeting

mitochondrial $O_2^{\bullet -}$ [219]. Furthermore, the similar principle to photoswitchable $BGAG_{12,400}$ probe, which precisely targets metabotropic glutamate receptor (mGluR) and modulate the binding of glutamate to mGluR developed by Gutzeit et al. [220], could also be exploited for illuminating the dynamics of ROS of a targeted protein. In brief, $BGAG_{12,400}$ contains two key functional moieties – (1) the SNAP-tag direct to direct the probe to specific protein of target [221,222], such as mGluR; and (2) the photoswitchable moiety, azobenzene-400, tethered with glutamate (hereafter referred to as A400-Glu) to control the binding of glutamate to the mGluR. Inspired by $BGAG_{12,400}$ probe, we can theoretically replace the A400-Glu moiety with the ROS-selective moiety and SNAP-tag to other known protein expressed at a specific subcellular compartment such as NOX enzymes at the plasma membrane. Hence, this type of probe may potentially be the direct approach for not only visualising the spatial dynamics but also quantifying the amount of specific ROS species and a targeted protein of interest at a particular subcellular compartment of interest.

## 4.7. Concluding remarks

The overarching goal of this thesis was to better understand the biological processes underlying neratinib-induced gut injury, especially in the colon. The research carried out in this thesis suggests ferritinophagy-mediated ferroptosis as a potential underlying histopathological feature of not only neratinib-induced colon injury in an *in vivo* rat model, but also in *in vitro HER2*-positive mouse TCBP-1 breast cancer cells and xenografted *HER1*-mutant human TS895 glioblastoma cells. However, neratinib-induced ferroptosis is context specific. In the context of neratinib-induced ferroptosis, we propose that the modulation of MAP4K3 signalling by neratinib, but not by lapatinib, may serve as a critical switch from apoptotic to ferroptotic cell death. For future mechanistic investigation in the colon, we recommend the use of differentiated colon organoids as a model system rather than cell lines because the organoids precisely recapitulate the complex structure and functions of the *in vivo* colonic epithelium. Altogether, we hope that our study will inspire future research to offer a thorough understanding of the molecular mechanism underlying neratinib-induced ferroptosis in the colon, especially perturbed redox regulation at a specific subcellular compartment as the initiating event of cell death. We believe that the integration of cutting-edge technologies, namely 3D organoids, LSM, fluorescent probes/sensors, and multi-omics, will provide a holistic profile of compartmental-specific regulation of ROS and its underlying biological processes following neratinib treatment. A thorough understanding of this early event of neratinib-induced cell death may serve as an exciting new platform for future supportive therapies and discovery of redox compartmental-specific therapies to mitigate gut toxicity while enhancing the efficacy of similar or emerging anti-cancer therapeutics.

# Appendix

```
CLUSTAL O(1.2.4) multiple sequence alignment

sp|Q8IVH8|M4K3_HUMAN      MNPGFDLSRRNPQEDFELIQRIGSGTYGDVYKARNVNTGELAAIKVIKLEPGEDFAVVQQ  60
sp|Q99JP0|M4K3_MOUSE      MNPGFDLSRRNPQEDFELIQRIGSGTYGDVYKARNVNTGELAAIKVIKLEPGEDFAVVQQ  60
sp|Q924I2|M4K3_RAT        MNPGFDLSRRNPQEDFELIQRIGSGTYGDVYKARNVNTGELAAIKVIKLEPGEDFAVVQQ  60
                          ************************************************************

sp|Q8IVH8|M4K3_HUMAN      EIIMMKDCKHPNIVAYFGSYLRRDKLWICMEFCGGGSLQDIYHVTGPLSELQIAYVSRET  120
sp|Q99JP0|M4K3_MOUSE      EIIMMKDCKHPNIVAYFGSYLRRDKLWICMEFCGGGSLQDIYHVTGPLSELQIAYVSRET  120
sp|Q924I2|M4K3_RAT        EIIMMKDCKHANIVAYFGSYLRRDKLWICMEFCGGGSLQDIYHVTGPLSELQIAYVSRET  120
                          ********** ************************************************

sp|Q8IVH8|M4K3_HUMAN      LQGLYYLHSKGKMHRDIKGANILLTDNGHVKLADFGVSAQITATIAKRKSFIGTPYWMAP  180
sp|Q99JP0|M4K3_MOUSE      LQGLYYLHSKGKMHRDIKGANILLTDNGHVKLADFGVSAQITATIAKRKSFIGTPYWMAP  180
sp|Q924I2|M4K3_RAT        LQGLYYLHSKGKMHRDIKGANILLTDNGHVKLADFGVSAQITATIAKRKSFIGTPYWMAP  180
                          ************************************************************

sp|Q8IVH8|M4K3_HUMAN      EVAAVERKGGYNQLCDLWAVGITAIELAELQPPMFDLHPMRALFLMTKSNFQPPKLKDKM  240
sp|Q99JP0|M4K3_MOUSE      EVAAVERKGGYNQLCDLWAVGITAIELAELQPPMFDLHPMRALFLMTKSNFQPPKLKDKL  240
sp|Q924I2|M4K3_RAT        EVAAVERKGGYNQLCDLWAVGITAIELAELQPPMFDLHPMRALFLMTKSNFQPPKLKDKL  240
                          ************************************************************:

sp|Q8IVH8|M4K3_HUMAN      KWSNSFHHFVKMALTKNPKKRPTAEKLLQHPFVTQHLTRSLAIELLDKVNNPDHSTYHDF  300
sp|Q99JP0|M4K3_MOUSE      KWSNSFHHFVKMALTKNPKKRPNAEKLLQHPFVTQPLTRSLAIELLDKVNNPDHSTYHDF  300
sp|Q924I2|M4K3_RAT        KWSNSFHHFVKMALTKNPKKRPTAEKLLQHPFVTQPLTRSLAIELLDKVNNPDHSTYHDF  300
                          **********************.************ ************************
```

**Appendix figure 1: Result for the alignment sequences of human, mouse, and rat MAP4K3 kinase (aa 16-273) using the Alignment function in https://www.uniprot.org/.** The sequence from 16$^{th}$ to 273$^{rd}$ amino acid in human MAP4K3 encodes for the kinase domain. An * (asterisk) is denoted for fully conserved residue; an : (colon) is denoted for highly conserved residue; a blank space ( ) is denoted for not conserved sequence.

# Reference list


1 Beumer, J. & Clevers, H. Cell fate specification and differentiation in the adult mammalian intestine. *Nat. Rev. Mol. Cell Biol.* **22**, 39-53, doi:10.1038/s41580-020-0278-0 (2021).

2 Sung, H. *et al.* Global Cancer Statistics 2020: GLOBOCAN Estimates of incidence and mortality worldwide for 36 cancers in 185 countries. *CA Cancer J Clin* **71**, 209-249, doi:10.3322/caac.21660 (2021).

3 Cancer in Australia Statistics. (Australian Government - Cancer Australia, Canberra, Australia, 2021).

4 Prati, R., Apple, S. K., He, J., Gornbein, J. A. & Chang, H. R. Histopathologic characteristics predicting HER-2/neu amplification in breast cancer. *Breast J* **11**, 433-439, doi: 10.1111/j.1075-122X.2005.00125.x (2005).

5 Altundag, K. *et al.* Clinicopathologic characteristics and prognostic factors in 420 metastatic breast cancer patients with central nervous system metastasis. *Cancer* **110**, 2640-2647, doi: 10.1002/cncr.23088 (2007).

6 Gonzalez-Angulo, A. M. *et al.* High risk of recurrence for patients with breast cancer who have human epidermal growth factor receptor 2–positive, node-negative tumors 1 cm or smaller. *J Clin Oncol* **27**, 5700-5706, doi: 10.1200/JCO.2009.23.2025 (2009).

7 Goyette, M.-A. *et al.* The receptor tyrosine kinase AXL is required at multiple steps of the metastatic cascade during HER2-positive breast cancer progression. *Cell Rep* **23**, 1476-1490, doi: 10.1016/j.celrep.2018.04.019 (2018).

8 Harper, K. L. *et al.* Mechanism of early dissemination and metastasis in Her2+ mammary cancer. *Nature* **540**, 588-592, doi: 10.1038/nature20609 (2016).

9 Xue, B., Krishnamurthy, K., Allred, D. C. & Muthuswamy, S. K. Loss of Par3 promotes breast cancer metastasis by compromising cell–cell cohesion. *Nat Cell Biol* **15**, 189-200, doi: 10.1038/ncb2663 (2013).

10 Oh, D.-Y. & Bang, Y.-J. HER2-targeted therapies — a role beyond breast cancer. *Nat Rev Clin Oncol* **17**, 33-48, doi: 10.1038/s41571-019-0268-3 (2020).

11 Yarden, Y. & Sliwkowski, M. X. Untangling the ErbB signalling network. *Nat Rev Mol Cell Biol* **2**, 127-137, doi: 10.1038/35052073 (2001).

12 Garrett, T. P. J. *et al.* The crystal structure of a truncated ErbB2 ectodomain reveals an active conformation, poised to interact with other ErbB receptors. *Mol Cell* **11**, 495-505, doi: 10.1016/s1097-2765(03)00048-0 (2003).

13 Feng, Z., Zhang, H., Levine, A. J. & Jin, S. The coordinate regulation of the p53 and mTOR pathways in cells. *Proc Natl Acad Sci U S A* **102**, 8204-8209, doi: 10.1073/pnas.0502857102 (2005).

14 Oh, D. Y. & Bang, Y. J. HER2-targeted therapies - a role beyond breast cancer. *Nat Rev Clin Oncol* **17**, 33-48, doi:10.1038/s41571-019-0268-3 (2020).

15 Badache, A. & Hynes, N. E. A new therapeutic antibody masks ErbB2 to its partners *Cancer Cell* **5**, 299-301, doi: 10.1016/s1535-6108(04)00088-1 (2004).

16 Goldhirsch, A. *et al.* 2 years versus 1 year of adjuvant trastuzumab for HER2-positive breast cancer (HERA): an open-label, randomised controlled trial. *Lancet* **382**, 21-27, doi: 10.1016/S0140-6736(13)61094-6 (2013).

17 Slamon, D. *et al.* Adjuvant trastuzumab in HER2-positive breast cancer. *N Engl J Med* **365**, 1273-1283, doi: 10.1056/NEJMoa0910383 (2011).

18 Slamon, D. J. *et al.* Use of chemotherapy plus a monoclonal antibody against HER2 for metastatic breast cancer that overexpresses HER2. *N Engl J Med* **344**, 783-792, doi: 10.1056/NEJM200103153441101 (2001).

19 Cizkova, M. *et al.* Outcome impact of PIK3CA mutations in HER2-positive breast cancer patients treated with trastuzumab. *Br J Cancer* **108**, 1807-1809, doi: 10.1038/bjc.2013.164 (2013).

20 Spector, N. L. & Blackwell, K. L. Understanding the mechanisms behind trastuzumab therapy for human epidermal growth factor receptor 2-positive breast cancer. *J Clin Oncol* **27**, 5838-5847, doi: 10.1200/JCO.2009.22.1507 (2009).

21 Perez, E. A. *et al.* Trastuzumab plus adjuvant chemotherapy for human epidermal growth factor receptor 2-positive breast cancer: planned joint analysis of overall survival from NSABP B-31 and NCCTG N9831. *J Clin Oncol* **32,** 3744-3752, doi: 10.1200/JCO.2014.55.5730 (2014).

22 Goldhirsch, A. *et al.* 2 years versus 1 year of adjuvant trastuzumab for HER2-positive breast cancer (HERA): an open-label, randomised controlled trial. *Lancet* **382**, 1021-1028, doi: 10.1016/S0140-6736(13)61094-6 (2013).

23 Truong, T. H. *et al.* Molecular basis for redox activation of epidermal growth factor receptor kinase. *Cell Chem Biol* **23,** 837-848, doi: 10.1016/j.chembiol.2016.05.017 (2016).

24 Tsou, H.-R. *et al.* Optimization of 6,7-disubstituted-4-(arylamino)quinoline-3-carbonitriles as orally active, irreversible inhibitors of human epidermal growth factor receptor-2 kinase activity. *J Med Chem* **48**, 1107-1131, doi: 10.1021/jm040159c (2005).

25 Deeks, E. D. Neratinib: First Global Approval. *Drugs* **77**, 1695-1704, doi:10.1007/s40265-017-0811-4 (2017).

26 Conlon, N. T. *et al.* Comparative analysis of drug response and gene profiling of HER2-targeted tyrosine kinase inhibitors. *Br J Cancer* **124**, 1249-1259, doi: 10.1038/s41416-020-01257-x (2021).

27 Chan, A. *et al.* Neratinib after trastuzumab-based adjuvant therapy in patients with HER2-positive breast cancer (ExteNET): a multicentre, randomised, double-blind, placebo-controlled, phase 3 trial. *Lancet Oncol* **17**, 367-377, doi: 10.1016/S1470-2045(15)00551-3 (2016).

28 Martin, M. *et al.* Neratinib after trastuzumab-based adjuvant therapy in HER2-positive breast cancer (ExteNET): 5-year analysis of a randomised, double-blind, placebo-controlled, phase 3 trial. *Lancet Oncol* **18**, 1688-1700, doi: 10.1016/S1470-2045(17)30717-9 (2017).

29 TGA. Australian Public Assessment Report for Neratinib (as maleate). (Therapeutic Goods Administration, Canberra, Australia, 2020).

30 FDA. *FDA approves neratinib for metastatic HER2-positive breast cancer*, <https://www.fda.gov/drugs/resources-information-approved-drugs/fda-approves-neratinib-metastatic-her2-positive-breast-cancer> (2020).

31 Chen, P., Chen, F. & Zhou, B. Risk of gastrointestinal events during neratinib therapy in patients with cancer: a systematic review and meta-analysis of clinical trials. *Int J Clin Exp Med* **12**, 3546-3557 (2019).

32 Mortimer, J., Palma, J. D., Schmid, K., Ye, Y. & Jahanzeb, M. Patterns of occurrence and implications of neratinib-associated diarrhea in patients with HER2-positive breast

cancer: analyses from the randomized phase III ExteNET trial. *Breast Cancer Res* **21**, 1-9, https://doi.org/10.1186/s13058-019-1112-5 (2019).

33 Secombe, K. R. *et al.* Pathophysiology of neratinib-induced diarrhea in male and female rats: microbial alterations a potential determinant. *Breast Cancer* **28**, 99-109, doi:10.1007/s12282-020-01133-9 (2021).

34 Wong, K. K. *et al.* A phase I study with neratinib (HKI-272), an irreversible pan ErbB receptor tyrosine kinase inhibitor, in patients with solid tumors. *Clin Cancer Res* **15**, 2552-2558, doi:10.1158/1078-0432.Ccr-08-1978 (2009).

35 Abud, H. E., Chan, W. H. & Jardé, T. Source and impact of the EGF family of ligands on intestinal stem cells. *Front Cell Dev Biol* **9**, 1-9, doi: 10.3389/fcell.2021.685665 (2021).

36 Yamaoka, T. *et al.* Transactivation of EGF receptor and ErbB2 protects intestinal epithelial cells from TNF-induced apoptosis. *Proc Natl Acad Sci U S A* **105**, 11772-11777, doi: 10.1073/pnas.0801463105 (2008).

37 Xiang, J. *et al.* EGFR-dependent TOR-independent endocycles support Drosophila gut epithelial regeneration. *Nat Commun* **8**, 1-13, doi: 10.1038/ncomms15125 (2017).

38 Yang, Y.-P. *et al.* A chimeric Egfr protein reporter mouse reveals Egfr localization and trafficking *In vivo*. *Cell Rep* **19**, 1257-1267, doi: 10.1016/j.celrep.2017.04.048 (2017).

39 Hirsh, V., Blais, N., Burkes, R., Verma, S. & Croitoru, K. Management of diarrhea induced by epidermal growth factor receptor tyrosine kinase inhibitors. *Curr Oncol* **21**, 329-336, doi:10.3747/co.21.2241 (2014).

40 Sandhu, B. K., Tripp, J. H., Candy, D. C. & Harries, J. T. Loperamide: studies on its mechanism of action. *Gut* **22**, 658-662, doi:10.1136/gut.22.8.658 (1981).

41 Pannemans, J. & Corsetti, M. Opioid receptors in the GI tract: targets for treatment of both diarrhea and constipation in functional bowel disorders? *Curr Opin Pharmacol* **43**, 53-58, doi:10.1016/j.coph.2018.08.008 (2018).

42 Hurvitz, S. *et al.* Abstract P3-14-01: Effects of adding budesonide or colestipol to loperamide prophylaxis on neratinib-associated diarrhea in patients with HER2+ early-stage breast cancer: The CONTROL trial. *Cancer Res* **78,** doi: 10.1158/1538-7445.SABCS17-P3-14-01 (2018).

43 Barcenas, C. H. *et al.* Improved tolerability of neratinib in patients with HER2-positive early-stage breast cancer: the CONTROL trial. *Ann Oncol* **31**, 1123-1230, doi: 10.1016/j.annonc.2020.05.012 (2020).

44 Barker, N. *et al.* Identification of stem cells in small intestine and colon by marker gene Lgr5. *Nature* **449**, 1003-1007, doi:10.1038/nature06196 (2007).

45 Vereecke, L., Beyaert, R. & van Loo, G. Enterocyte death and intestinal barrier maintenance in homeostasis and disease. *Trends Mol Med* **17**, 584-593, doi:10.1016/j.molmed.2011.05.011 (2011).

46 Sasaki, N. *et al.* Reg4+ deep crypt secretory cells function as epithelial niche for Lgr5+ stem cells in colon. *Proc Natl Acad Sci U S A* **113**, E5399-5407, doi:10.1073/pnas.1607327113 (2016).

47 Schumacher, M. A. *et al.* Deep crypt secretory cell differentiation in the colonic epithelium is regulated by Sprouty2 and Interleukin 13. *Cell Mol Gastroenterol Hepatol* **15**, 971-984, doi:10.1016/j.jcmgh.2022.11.004 (2023).

48 Martens, E. C., Neumann, M. & Desai, M. S. Interactions of commensal and pathogenic microorganisms with the intestinal mucosal barrier. *Nat Rev Microbiol* **16**, 457-470, doi:10.1038/s41579-018-0036-x (2018).

49 Yao, Y. *et al.* Mucus sialylation determines intestinal host-commensal homeostasis. *Cell* **185**, 1172-1188.e1128, doi:10.1016/j.cell.2022.02.013 (2022).

50 Worthington, J. J., Reimann, F. & Gribble, F. M. Enteroendocrine cells-sensory sentinels of the intestinal environment and orchestrators of mucosal immunity. *Mucosal Immunol* **11**, 3-20, doi:10.1038/mi.2017.73 (2018).

51 Gribble, F. M. & Reimann, F. Function and mechanisms of enteroendocrine cells and gut hormones in metabolism. *Nat Rev Endocrinol* **15**, 226-237, doi:10.1038/s41574-019-0168-8 (2019).

52 Watnick, P. I. & Jugder, B. E. Microbial control of intestinal homeostasis via enteroendocrine cell innate immune signaling. *Trends Microbiol* **28**, 141-149, doi:10.1016/j.tim.2019.09.005 (2020).

53 Sato, T. *et al.* Single Lgr5 stem cells build crypt-villus structures in vitro without a mesenchymal niche. *Nature* **459**, 262-265, doi:10.1038/nature07935 (2009).

54 Spence, J. R. *et al.* Directed differentiation of human pluripotent stem cells into intestinal tissue in vitro. *Nature* **470**, 105-109, doi:10.1038/nature09691 (2011).

55 Múnera, J. O. *et al.* Differentiation of Human Pluripotent Stem Cells into Colonic Organoids via Transient Activation of BMP Signaling. *Cell Stem Cell* **21**, 51-64.e56, doi:10.1016/j.stem.2017.05.020 (2017).

56 Lau, H. C. H., Kranenburg, O., Xiao, H. & Yu, J. Organoid models of gastrointestinal cancers in basic and translational research. *Nat Rev Gastroenterol Hepatol* **17**, 203-222, doi:10.1038/s41575-019-0255-2 (2020).

57 Qu, M. *et al.* Establishment of intestinal organoid cultures modeling injury-associated epithelial regeneration. *Cell Res* **31**, 259-271, doi:10.1038/s41422-020-00453-x (2021).

58 Sato, T. *et al.* Long-term expansion of epithelial organoids from human colon, adenoma, adenocarcinoma, and Barrett's epithelium. *Gastroenterology* **141**, 1762-1772 (2011).

59 Artegiani, B. *et al.* Fast and efficient generation of knock-in human organoids using homology-independent CRISPR-Cas9 precision genome editing. *Nat Cell Biol* **22**, 321-331, doi:10.1038/s41556-020-0472-5 (2020).

60 Lin, S. C., Haga, K., Zeng, X. L. & Estes, M. K. Generation of CRISPR-Cas9-mediated genetic knockout human intestinal tissue-derived enteroid lines by lentivirus transduction and single-cell cloning. *Nat Protoc* **17**, 1004-1027, doi:10.1038/s41596-021-00669-0 (2022).

61 Beumer, J. *et al.* BMP gradient along the intestinal villus axis controls zonated enterocyte and goblet cell states. *Cell Rep* **38**, 110438, doi:10.1016/j.celrep.2022.110438 (2022).

62 Yin, X. *et al.* Niche-independent high-purity cultures of Lgr5+ intestinal stem cells and their progeny. *Nat. Methods* **11**, 106-112 (2014).

63 Basak, O. *et al.* Induced quiescence of Lgr5+ stem cells in intestinal organoids enables differentiation of hormone-producing enteroendocrine cells. *Cell Stem Cell* **20**, 177-190 (2017).

64 Sanman, L. E. *et al.* Transit-Amplifying Cells Coordinate Changes in Intestinal Epithelial Cell-Type Composition. *Dev Cell* **56**, 356-365.e359, doi:10.1016/j.devcel.2020.12.020 (2021).

65 Gu, W. *et al.* SATB2 preserves colon stem cell identity and mediates ileum-colon conversion via enhancer remodeling. *Cell Stem Cell* **29**, 101-115.e110, doi:10.1016/j.stem.2021.09.004 (2022).

66 Qin, X. *et al.* Cell-type-specific signaling networks in heterocellular organoids. *Nat Methods* **17**, 335-342, doi:10.1038/s41592-020-0737-8 (2020).

67 Replogle, J. M. *et al.* Mapping information-rich genotype-phenotype landscapes with genome-scale Perturb-seq. *Cell* **185**, 2559-2575.e2528, doi:10.1016/j.cell.2022.05.013 (2022).

68 Albrecht, S. C., Barata, A. G., Grosshans, J., Teleman, A. A. & Dick, T. P. In vivo mapping of hydrogen peroxide and oxidized glutathione reveals chemical and regional specificity of redox homeostasis. *Cell Metab* **14**, 819-829, doi:10.1016/j.cmet.2011.10.010 (2011).

69 Fujikawa, Y. *et al.* Mouse redox histology using genetically encoded probes. *Sci Signal* **9**, rs1, doi:10.1126/scisignal.aad3895 (2016).

70 Sufi, J. *et al.* Multiplexed single-cell analysis of organoid signaling networks. *Nat Protoc* **16**, 4897-4918, doi:10.1038/s41596-021-00603-4 (2021).

71 Holloway, E. M. *et al.* Mapping development of the human intestinal niche at single-sell resolution. *Cell Stem Cell* **28**, 568-580, doi: 10.1016/j.stem.2020.11.008 (2021).

72 Abud, H. E., Chan, W. H. & Jardé, T. Source and Impact of the EGF Family of Ligands on Intestinal Stem Cells. *Front Cell Dev Biol* **9**, 685665, doi:10.3389/fcell.2021.685665 (2021).

73 Frey, M. R., Edelblum, K. L., Mullane, M. T., Liang, D. & Polk, D. B. The ErbB4 growth factor receptor is required for colon epithelial cell survival in the presence of TNF. *Gastroenterology* **136**, 217-226, doi: 10.1053/j.gastro.2008.09.023 (2009).

74 Schumacher, M. A. *et al.* ErbB4 signaling stimulates pro-inflammatory macrophage apoptosis and limits colonic inflammation. *Cell Death Dis* **8**, 1-12, doi: 10.1038/cddis.2017.42 (2017).

75 Jardé, T. *et al.* Mesenchymal niche-derived Neuregulin-1 drives intestinal stem cell proliferation and regeneration of damaged epithelium. *Cell Stem Cell* **27**, 646-662.e647, doi: 10.1016/j.stem.2020.06.021 (2020).

76 Martin, M. *et al.* Neratinib after trastuzumab-based adjuvant therapy in HER2-positive breast cancer (ExteNET): 5-year analysis of a randomised, double-blind, placebo-controlled, phase 3 trial. *Lancet Oncol.* **18**, 1688-1700, doi: 10.1016/S1470-2045(17)30717-9 (2017).

77 Mortimer, J., Palma, J. D., Schmid, K., Ye, Y. & Jahanzeb, M. Patterns of occurrence and implications of neratinib-associated diarrhea in patients with HER2-positive breast cancer: analyses from the randomized phase III ExteNET trial. *Breast Cancer Res.* **21**, 1-9, doi: 10.1186/s13058-019-1112-5 (2019).

78 Elmentaite, R. *et al.* Cells of the human intestinal tract mapped across space and time. *Nature* **597**, 250-255, doi: 10.1038/s41586-021-03852-1 (2021).

79 Burclaff, J. *et al.* A proximal-to-distal survey of healthy adult human small Intestine and colon epithelium by single-cell transcriptomics. *Cell. Mol. Gastroenterol. Hepatol.* **13**, 1554-1589, doi: 10.1016/j.jcmgh.2022.02.007 (2022).

80 Parigi, S. M. *et al.* The spatial transcriptomic landscape of the healing mouse intestine following damage. *Nat Commun* **13**, 828, doi:10.1038/s41467-022-28497-0 (2022).

81 Fox, D. B. *et al.* NRF2 activation promotes the recurrence of dormant tumour cells through regulation of redox and nucleotide metabolism. *Nat Metab* **2**, 318-334, doi: 10.1038/s42255-020-0191-z (2020).

82 Sies, H., Berndt, C. & Jones, D. P. Oxidative Stress. *Annu Rev Biochem* **86**, 715-748, doi:10.1146/annurev-biochem-061516-045037 (2017).

83 Nagpal, A. *et al.* Neoadjuvant neratinib promotes ferroptosis and inhibits brain metastasis in a novel syngeneic model of spontaneous HER2+ve breast cancer metastasis. *Breast Cancer Res* **21**, 1-19, doi: 10.1186/s13058-019-1177-1 (2021).

84 Stockwell, B. Ferroptosis turns 10: Emerging mechanisms, physiological functions, and therapeutic applications. *Cell* **185**, 2401-2421, doi: 10.1016/j.cell.2022.06.003 (2022).

85 Secombe, K. R. *et al.* Targeting neratinib-induced diarrhea with budesonide and colesevelam in a rat model. *Cancer Chemother Pharmacol* **83**, 531-543, doi: 10.1007/s00280-018-3756-8 (2019).

86 Secombe, K. R. *et al.* Pathophysiology of neratinib-induced diarrhea in male and female rats: microbial alterations a potential determinant. *Breast Cancer* **28**, 99-109, doi: 10.1007/s12282-020-01133-9 (2021).

87 Secombe, K. R. *et al.* Antibiotic treatment targeting gram negative bacteria prevents neratinib-induced diarrhea in rats. *Neoplasia* **30**, 100806, doi:10.1016/j.neo.2022.100806 (2022).

88 Howarth, G. S. *et al.* Milk growth factors enriched from cheese whey ameliorate intestinal damage by methotrexate when administered orally to rats. *J Nutr* **126**, 2519-2530, doi:10.1093/jn/126.10.2519 (1996).

89 Schmittgen & Livak. Analyzing real-time PCR data by the comparative CT method. *Nat Protoc* **3**, 1101-1108, doi: 10.1038/nprot.2008.73 (2008).

90 Al-Dasooqi, N. *et al.* Selection of housekeeping genes for gene expression studies in a rat model of irinotecan-induced mucositis. *Chemotherapy* **57**, 43-53, doi:10.1159/000321477 (2011).

91 Zain, W. N. I. Z. W. M., Bowen, J., Bateman, E. & Keefe, D. Cytotoxic effects of the dual ErbB tyrosine kinase inhibitor, lapatinib, on walker 256 eat Breast tumour and IEC-6 rat normal small intestinal cell lines. *Biomedicines* **8**, 1-14, doi: 10.3390/biomedicines8010002 (2019).

92 Mahe, M. M. *et al.* Establishment of gastrointestinal epithelial organoids. *Curr Protoc Mouse Biol* **3**, 217-240, doi: 10.1002/9780470942390.mo130179 (2013).

93 Lannagan, T. R. M. *et al.* Genetic editing of colonic organoids provides a molecularly distinct and orthotopic preclinical model of serrated carcinogenesis. *Gut* **68**, 684-692, doi:10.1136/gutjnl-2017-315920 (2019).

94 Nagpal, A. *et al.* Neoadjuvant neratinib promotes ferroptosis and inhibits brain metastasis in a novel syngeneic model of spontaneous HER2+ve breast cancer metastasis. *Breast Cancer Res.* **21**, 1-19, doi: 10.1186/s13058-019-1177-1 (2019).

95 Tang, C. P. *et al.* GCN2 kinase activation by ATP-competitive kinase inhibitors. *Nat Chem Biol* **18**, 207-215, doi:10.1038/s41589-021-00947-8 (2022).

96 Love, M. I., Huber, W. & Anders, S. Moderated estimation of fold change and dispersion for RNA-seq data with DESeq2. *Genome Biol* **15**, 550, doi:10.1186/s13059-014-0550-8 (2014).

97 Huang da, W., Sherman, B. T. & Lempicki, R. A. Bioinformatics enrichment tools: paths toward the comprehensive functional analysis of large gene lists. *Nucleic Acids Res* **37**, 1-13, doi:10.1093/nar/gkn923 (2009).

98 Huang da, W., Sherman, B. T. & Lempicki, R. A. Systematic and integrative analysis of large gene lists using DAVID bioinformatics resources. *Nat Protoc* **4**, 44-57, doi:10.1038/nprot.2008.211 (2009).

99 Magtanong, L. *et al.* Context-dependent regulation of ferroptosis sensitivity. *Cell Chem Biol* **29**, 1409-1418.e1406, doi:10.1016/j.chembiol.2022.06.004 (2022).

100 Huang, D. W. *et al.* The DAVID Gene Functional Classification Tool: a novel biological module-centric algorithm to functionally analyze large gene lists. *Genome Biol* **8**, R183, doi:10.1186/gb-2007-8-9-r183 (2007).

101 Fabian, M. A. *et al.* A small molecule-kinase interaction map for clinical kinase inhibitors. *Nat Biotechnol* **23**, 329-336, doi:10.1038/nbt1068 (2005).

102 Davis, M. I. *et al.* Comprehensive analysis of kinase inhibitor selectivity. *Nat Biotechnol* **29**, 1046-1051, doi:10.1038/nbt.1990 (2011).

103 Keyvanjah, K. *et al.* Pharmacokinetics of neratinib during coadministration with lansoprazole in healthy subjects. *Br J Clin Pharmacol* **83**, 554-561, doi:10.1111/bcp.13132 (2017).

104 Burris, H. A., 3rd *et al.* Phase I safety, pharmacokinetics, and clinical activity study of lapatinib (GW572016), a reversible dual inhibitor of epidermal growth factor receptor tyrosine kinases, in heavily pretreated patients with metastatic carcinomas. *J Clin Oncol* **23**, 5305-5313, doi:10.1200/jco.2005.16.584 (2005).

105 Burke, K. E. *et al.* Microscopic colitis. *Nat Rev Dis Primers* **7**, 39, doi:10.1038/s41572-021-00273-2 (2021).

106 Dikic, I. & Elazar, Z. Mechanism and medical implications of mammalian autophagy. *Nat Rev Mol Cell Biol* **19**, 349-364, doi:10.1038/s41580-018-0003-4 (2018).

107 Gao, M. *et al.* Ferroptosis is an autophagic cell death process. *Cell. Res.* **26**, 1021-1032 (2016).

108 Hou, W. *et al.* Autophagy promotes ferroptosis by degradation of ferritin. *Autophagy* **12**, 1425-1428 (2016).

109 Dixon, S. J. & Pratt, D. A. Ferroptosis: A flexible constellation of related biochemical mechanisms. *Mol Cell*, doi:10.1016/j.molcel.2023.03.005 (2023).

110 Doll, S. *et al.* ACSL4 dictates ferroptosis sensitivity by shaping cellular lipid composition. *Nat Chem Biol* **13**, 91-98, doi:10.1038/nchembio.2239 (2017).

111 Wenzel, S. E. *et al.* PEBP1 Wardens Ferroptosis by Enabling Lipoxygenase Generation of Lipid Death Signals. *Cell* **171**, 628-641.e626, doi:10.1016/j.cell.2017.09.044 (2017).

112 Yasuda, M. *et al.* Potential role of the NADPH oxidase NOX1 in the pathogenesis of 5-fluorouracil-induced intestinal mucositis in mice. *Am J Physiol Gastrointest Liver Physiol* **302**, G1133-1142, doi:10.1152/ajpgi.00535.2011 (2012).

113 Xie, Y. *et al.* The Tumor Suppressor p53 Limits Ferroptosis by Blocking DPP4 Activity. *Cell Rep* **20**, 1692-1704, doi:10.1016/j.celrep.2017.07.055 (2017).

114 Yang, W. S. *et al.* Regulation of ferroptotic cancer cell death by GPX4. *Cell* **156**, 317-331, doi:10.1016/j.cell.2013.12.010 (2014).

115 Yang, W. S. *et al.* Peroxidation of polyunsaturated fatty acids by lipoxygenases drives ferroptosis. *Proc Natl Acad Sci U S A* **113**, E4966-4975, doi:10.1073/pnas.1603244113 (2016).

116 Wood, E. R. *et al.* A unique structure for epidermal growth factor receptor bound to GW572016 (Lapatinib): relationships among protein conformation, inhibitor off-rate, and receptor activity in tumor cells. *Cancer Res* **64**, 6652-6659, doi:10.1158/0008-5472.Can-04-1168 (2004).

117 Konecny, G. E. *et al.* Activity of the dual kinase inhibitor lapatinib (GW572016) against HER-2-overexpressing and trastuzumab-treated breast cancer cells. *Cancer Res* **66**, 1630-1639, doi:10.1158/0008-5472.Can-05-1182 (2006).

118 Tanizaki, J. *et al.* Roles of BIM induction and survivin downregulation in lapatinib-induced apoptosis in breast cancer cells with HER2 amplification. *Oncogene* **30**, 4097-4106, doi:10.1038/onc.2011.111 (2011).

119 Eustace, A. J. *et al.* Development of acquired resistance to lapatinib may sensitise HER2-positive breast cancer cells to apoptosis induction by obatoclax and TRAIL. *BMC Cancer* **18**, 965, doi:10.1186/s12885-018-4852-1 (2018).

120 Rugo, H. S. *et al.* The characterization, management, and future considerations for ErbB-family TKI-associated diarrhea. *Breast Cancer Res Treat* **175**, 5-15, doi:10.1007/s10549-018-05102-x (2019).

121 Bowen, J. M. *et al.* Determining the mechanisms of lapatinib-induced diarrhoea using a rat model. *Cancer Chemother Pharmacol* **74**, 617-627, doi:10.1007/s00280-014-2519-4 (2014).

122 Keyvanjah, K. *et al.* Pharmacokinetics of neratinib during coadministration with lansoprazole in healthy subjects. *Br. J. Clin. Pharmacol.* **83**, 554-561 (2017).

123 Lam, D. *et al.* MAP4K3 modulates cell death via the post-transcriptional regulation of BH3-only proteins. *Proc Natl Acad Sci U S A* **106**, 11978-11983, doi:10.1073/pnas.0900608106 (2009).

124 Wu, C., Watts, M. E. & Rubin, L. L. MAP4K4 Activation Mediates Motor Neuron Degeneration in Amyotrophic Lateral Sclerosis. *Cell Rep* **26**, 1143-1156.e1145, doi:10.1016/j.celrep.2019.01.019 (2019).

125 Seo, G. *et al.* MAP4K Interactome Reveals STRN4 as a Key STRIPAK Complex Component in Hippo Pathway Regulation. *Cell Rep* **32**, 107860, doi:10.1016/j.celrep.2020.107860 (2020).

126 Marcotte, D. *et al.* Germinal-center kinase-like kinase co-crystal structure reveals a swapped activation loop and C-terminal extension. *Protein Sci* **26**, 152-162, doi:10.1002/pro.3062 (2017).

127 Gillis, E. P., Eastman, K. J., Hill, M. D., Donnelly, D. J. & Meanwell, N. A. Applications of Fluorine in Medicinal Chemistry. *J Med Chem* **58**, 8315-8359, doi:10.1021/acs.jmedchem.5b00258 (2015).

128 Chen, R. H. & McCormick, F. Selective targeting to the hyperactive beta-catenin/T-cell factor pathway in colon cancer cells. *Cancer Res* **61**, 4445-4449 (2001).

129 Wu, Z. Q. *et al.* Canonical Wnt suppressor, Axin2, promotes colon carcinoma oncogenic activity. *Proc Natl Acad Sci U S A* **109**, 11312-11317, doi:10.1073/pnas.1203015109 (2012).

130 Ahmed, D. *et al.* Epigenetic and genetic features of 24 colon cancer cell lines. *Oncogenesis* **2**, e71, doi:10.1038/oncsis.2013.35 (2013).

131 Beumer, J. *et al.* Enteroendocrine cells switch hormone expression along the crypt-to-villus BMP signalling gradient. *Nat Cell Biol* **20**, 909-916, doi:10.1038/s41556-018-0143-y (2018).

132 Martin, M. *et al.* Neratinib after trastuzumab-based adjuvant therapy in HER2-positive breast cancer (ExteNET): 5-year analysis of a randomised, double-blind, placebo-controlled, phase 3 trial. *Lancet Oncol* **18**, 1688-1700, doi:10.1016/s1470-2045(17)30717-9 (2017).

133 Zheng, H., Jiang, L., Tsuduki, T., Conrad, M. & Toyokuni, S. Embryonal erythropoiesis and aging exploit ferroptosis. *Redox Biol* **48**, 102175, doi:10.1016/j.redox.2021.102175 (2021).

134 Chen, Y., Zhang, P., Chen, W. & Chen, G. Ferroptosis mediated DSS-induced ulcerative colitis associated with Nrf2/HO-1 signaling pathway. *Immunol Lett* **225**, 9-15, doi:10.1016/j.imlet.2020.06.005 (2020).

135 Friedmann Angeli, J. P. *et al.* Inactivation of the ferroptosis regulator Gpx4 triggers acute renal failure in mice. *Nat Cell Biol* **16**, 1180-1191, doi:10.1038/ncb3064 (2014).

136 Liu, H. *et al.* Small-molecule allosteric inhibitors of GPX4. *Cell Chem Biol* **29**, 1680-1693.e1689, doi:10.1016/j.chembiol.2022.11.003 (2022).

137 Zhao, J. *et al.* Human hematopoietic stem cell vulnerability to ferroptosis. *Cell* **186**, 732-747.e716, doi:10.1016/j.cell.2023.01.020 (2023).

138 Nagpal, A. *et al.* Integrin αvβ3 Is a Master Regulator of Resistance to TKI-Induced Ferroptosis in HER2-Positive Breast Cancer. *Cancers (Basel)* **15**, doi:10.3390/cancers15041216 (2023).

139 Wang, W. *et al.* CD8(+) T cells regulate tumour ferroptosis during cancer immunotherapy. *Nature* **569**, 270-274, doi:10.1038/s41586-019-1170-y (2019).

140 Liao, P. *et al.* CD8(+) T cells and fatty acids orchestrate tumor ferroptosis and immunity via ACSL4. *Cancer Cell* **40**, 365-378.e366, doi:10.1016/j.ccell.2022.02.003 (2022).

141 Kanke, M. *et al.* Single-Cell Analysis Reveals Unexpected Cellular Changes and Transposon Expression Signatures in the Colonic Epithelium of Treatment-Naïve Adult Crohn's Disease Patients. *Cell Mol Gastroenterol Hepatol* **13**, 1717-1740, doi:10.1016/j.jcmgh.2022.02.005 (2022).

142 Hou, G. & Bishu, S. Th17 Cells in Inflammatory Bowel Disease: An Update for the Clinician. *Inflamm Bowel Dis* **26**, 653-661, doi:10.1093/ibd/izz316 (2020).

143 Dixon, S. J. *et al.* Ferroptosis: an iron-dependent form of nonapoptotic cell death. *Cell* **149**, 1060-1072 (2012).

144 Ablin, J., Shalev, O., Okon, E., Karmeli, F. & Rachmilewitz, D. Deferiprone, an oral iron chelator, ameliorates experimental colitis and gastric ulceration in rats. *Inflamm Bowel Dis* **5**, 253-261, doi:10.1097/00054725-199911000-00003 (1999).

145 Ilyas, M., Tomlinson, I. P., Rowan, A., Pignatelli, M. & Bodmer, W. F. Beta-catenin mutations in cell lines established from human colorectal cancers. *Proc Natl Acad Sci U S A* **94**, 10330-10334, doi:10.1073/pnas.94.19.10330 (1997).

146 Ruiz-Saenz, A. *et al.* A reversible SRC-relayed COX2 inflammatory program drives resistance to BRAF and EGFR inhibition in BRAF(V600E) colorectal tumors. *Nat Cancer* **4**, 240-256, doi:10.1038/s43018-022-00508-5 (2023).

147 Voloshanenko, O. *et al.* Wnt secretion is required to maintain high levels of Wnt activity in colon cancer cells. *Nat Commun* **4**, 2610, doi:10.1038/ncomms3610 (2013).

148 Pellegata, N. S., Antoniono, R. J., Redpath, J. L. & Stanbridge, E. J. DNA damage and p53-mediated cell cycle arrest: a reevaluation. *Proc Natl Acad Sci U S A* **93**, 15209-15214, doi:10.1073/pnas.93.26.15209 (1996).

149 Chu, B. *et al.* ALOX12 is required for p53-mediated tumour suppression through a distinct ferroptosis pathway. *Nat. Cell Biol.* **21**, 579-591 (2019).

150 Vijayakumar, S. *et al.* High-frequency canonical Wnt activation in multiple sarcoma subtypes drives proliferation through a TCF/β-catenin target gene, CDC25A. *Cancer Cell* **19**, 601-612, doi:10.1016/j.ccr.2011.03.010 (2011).

151 Zhao, Z. *et al.* Organoids. *Nature Reviews Methods Primers* **2**, 94, doi:10.1038/s43586-022-00174-y (2022).

152 Gao, M., Monian, P., Quadri, N., Ramasamy, R. & Jiang, X. Glutaminolysis and Transferrin Regulate Ferroptosis. *Mol Cell* **59**, 298-308, doi:10.1016/j.molcel.2015.06.011 (2015).

153 *Technical Resources: B-27 Serum-Free Supplement (50X) liquid*, <https://www.thermofisher.com/au/en/home/technical-resources/media-formulation.250.html>

154 Tschuck, J. *et al.* Suppression of ferroptosis by vitamin A or antioxidants is essential for neuronal development. *bioRxiv*, 2023.2004.2005.535746, doi:10.1101/2023.04.05.535746 (2023).

155 Shao, H. *et al.* A campaign targeting a conserved Hsp70 binding site uncovers how subcellular localization is linked to distinct biological activities. *Cell Chem Biol* **29**, 1303-1316.e1303, doi:10.1016/j.chembiol.2022.06.006 (2022).

156 Misale, S. *et al.* Emergence of KRAS mutations and acquired resistance to anti-EGFR therapy in colorectal cancer. *Nature* **486**, 532-536, doi:10.1038/nature11156 (2012).

157 Woolston, A. *et al.* Genomic and Transcriptomic Determinants of Therapy Resistance and Immune Landscape Evolution during Anti-EGFR Treatment in Colorectal Cancer. *Cancer Cell* **36**, 35-50.e39, doi:10.1016/j.ccell.2019.05.013 (2019).

158 D'Autréaux, B. & Toledano, M. B. ROS as signalling molecules: mechanisms that generate specificity in ROS homeostasis. *Nat Rev Mol Cell Biol* **8**, 813-824, doi:10.1038/nrm2256 (2007).

159 Holmström, K. M. & Finkel, T. Cellular mechanisms and physiological consequences of redox-dependent signalling. *Nat Rev Mol Cell Biol* **15**, 411-421, doi:10.1038/nrm3801 (2014).

160 Zhang, L. *et al.* Biochemical basis and metabolic interplay of redox regulation. *Redox Biol* **26**, 101284, doi:10.1016/j.redox.2019.101284 (2019).

161 Sies, H. & Jones, D. P. Reactive oxygen species (ROS) as pleiotropic physiological signalling agents. *Nat. Rev. Mol. Cell Biol.* **21**, 363-383 (2020).

162 Sommer, F. & Bäckhed, F. The gut microbiota engages different signaling pathways to induce Duox2 expression in the ileum and colon epithelium. *Mucosal Immunol* **8**, 372-379, doi:10.1038/mi.2014.74 (2015).

163 Makhezer, N. *et al.* NOX1-derived ROS drive the expression of Lipocalin-2 in colonic epithelial cells in inflammatory conditions. *Mucosal Immunol* **12**, 117-131, doi:10.1038/s41385-018-0086-4 (2019).

164 Post, S. v. d., Birchenough, G. M. H. & Held, J. M. NOX1-dependent redox signaling potentiates colonic stem cell proliferation to adapt to the intestinal microbiota by linking EGFR and TLR activation. *Cell Reports* **35**, 1-18 (2021).

165 Muller, F. L., Liu, Y. & Van Remmen, H. Complex III releases superoxide to both sides of the inner mitochondrial membrane. *J Biol Chem* **279**, 49064-49073, doi:10.1074/jbc.M407715200 (2004).

166 Murphy, M. P. How mitochondria produce reactive oxygen species. *Biochem J* **417**, 1-13, doi:10.1042/bj20081386 (2009).

167 Palma, F. R. *et al.* Mitochondrial Superoxide Dismutase: What the Established, the Intriguing, and the Novel Reveal About a Key Cellular Redox Switch. *Antioxid Redox Signal* **32**, 701-714, doi:10.1089/ars.2019.7962 (2020).

168 Rodríguez-Colman, M. J. *et al.* Interplay between metabolic identities in the intestinal crypt supports stem cell function. *Nature* **543**, 424-427 (2017).

169 Ludikhuize, M. C. *et al.* Mitochondria Define Intestinal Stem Cell Differentiation Downstream of a FOXO/Notch Axis. *Cell Metab* **32**, 889-900.e887, doi:10.1016/j.cmet.2020.10.005 (2020).

170 Kirova, D. G. *et al.* A ROS-dependent mechanism promotes CDK2 phosphorylation to drive progression through S phase. *Dev Cell* **57**, 1712-1727.e1719, doi:10.1016/j.devcel.2022.06.008 (2022).

171 Xiao, W. & Loscalzo, J. Metabolic Responses to Reductive Stress. *Antioxid Redox Signal* **32**, 1330-1347, doi:10.1089/ars.2019.7803 (2020).

172 Dixon, S. J. & Stockwell, B. R. The role of iron and reactive oxygen species in cell death. *Nat Chem Biol* **10**, 9-17, doi:10.1038/nchembio.1416 (2014).

173 Patterson, J. C. *et al.* ROS and Oxidative Stress Are Elevated in Mitosis during Asynchronous Cell Cycle Progression and Are Exacerbated by Mitotic Arrest. *Cell Syst* **8**, 163-167.e162, doi:10.1016/j.cels.2019.01.005 (2019).

174 Mao, C. *et al.* DHODH-mediated ferroptosis defence is a targetable vulnerability in cancer. *Nature* **593**, 586-590, doi:10.1038/s41586-021-03539-7 (2021).

175 Gaschler, M. M. *et al.* FINO(2) initiates ferroptosis through GPX4 inactivation and iron oxidation. *Nat Chem Biol* **14**, 507-515, doi:10.1038/s41589-018-0031-6 (2018).

176 Guerra-Castellano, A. *et al.* Oxidative stress is tightly regulated by cytochrome c phosphorylation and respirasome factors in mitochondria. *Proc Natl Acad Sci U S A* **115**, 7955-7960, doi:10.1073/pnas.1806833115 (2018).

177 Kleih, M. *et al.* Direct impact of cisplatin on mitochondria induces ROS production that dictates cell fate of ovarian cancer cells. *Cell Death Dis* **10**, 851, doi:10.1038/s41419-019-2081-4 (2019).

178 Bock, F. J. & Tait, S. W. G. Mitochondria as multifaceted regulators of cell death. *Nat Rev Mol Cell Biol* **21**, 85-100, doi:10.1038/s41580-019-0173-8 (2020).

179 Niu, X. *et al.* Cytosolic and mitochondrial NADPH fluxes are independently regulated. *Nature Chemical Biology*, doi:10.1038/s41589-023-01283-9 (2023).

180 Lv, C. *et al.* Ainsliadimer A induces ROS-mediated apoptosis in colorectal cancer cells via directly targeting peroxiredoxin 1 and 2. *Cell Chem Biol* **30**, 295-307.e295, doi:10.1016/j.chembiol.2023.02.003 (2023).

181 Rhee, S. G., Woo, H. A., Kil, I. S. & Bae, S. H. Peroxiredoxin functions as a peroxidase and a regulator and sensor of local peroxides. *J Biol Chem* **287**, 4403-4410, doi:10.1074/jbc.R111.283432 (2012).

182 Brigelius-Flohé, R. & Flohé, L. Regulatory Phenomena in the Glutathione Peroxidase Superfamily. *Antioxid Redox Signal* **33**, 498-516, doi:10.1089/ars.2019.7905 (2020).

183 Bersuker, K. *et al.* The CoQ oxidoreductase FSP1 acts parallel to GPX4 to inhibit ferroptosis. *Nature* **575**, 688-692, doi:10.1038/s41586-019-1705-2 (2019).

184 Doll, S. *et al.* FSP1 is a glutathione-independent ferroptosis suppressor. *Nature* **575**, 693-698, doi:10.1038/s41586-019-1707-0 (2019).

185 Mishima, E. *et al.* A non-canonical vitamin K cycle is a potent ferroptosis suppressor. *Nature* **608**, 778-783, doi:10.1038/s41586-022-05022-3 (2022).

186 Martínez-Reyes, I. *et al.* TCA Cycle and Mitochondrial Membrane Potential Are Necessary for Diverse Biological Functions. *Mol Cell* **61**, 199-209, doi:10.1016/j.molcel.2015.12.002 (2016).

187 Hoehne, M. N. *et al.* Spatial and temporal control of mitochondrial H(2) O(2) release in intact human cells. *Embo j* **41**, e109169, doi:10.15252/embj.2021109169 (2022).

188 Manford, A. G. *et al.* A Cellular Mechanism to Detect and Alleviate Reductive Stress. *Cell* **183**, 46-61.e21, doi:10.1016/j.cell.2020.08.034 (2020).

189 Manford, A. G. *et al.* Structural basis and regulation of the reductive stress response. *Cell* **184**, 5375-5390.e5316, doi:10.1016/j.cell.2021.09.002 (2021).

190 Heo, J. M. *et al.* RAB7A phosphorylation by TBK1 promotes mitophagy via the PINK-PARKIN pathway. *Sci Adv* **4**, eaav0443, doi:10.1126/sciadv.aav0443 (2018).

191 Gottschling, D. E. & Nyström, T. The Upsides and Downsides of Organelle Interconnectivity. *Cell* **169**, 24-34, doi:10.1016/j.cell.2017.02.030 (2017).

192 Redhai, S. & Boutros, M. The Role of Organelles in Intestinal Function, Physiology, and Disease. *Trends Cell Biol* **31**, 485-499, doi:10.1016/j.tcb.2021.01.003 (2021).

193 von Krusenstiern, A. N. *et al.* Identification of essential sites of lipid peroxidation in ferroptosis. *Nat Chem Biol*, doi:10.1038/s41589-022-01249-3 (2023).

194 Zou, Y. *et al.* Plasticity of ether lipids promotes ferroptosis susceptibility and evasion. *Nature* **585**, 603-608, doi:10.1038/s41586-020-2732-8 (2020).

195 Keller, P. J. & Ahrens, M. B. Visualizing whole-brain activity and development at the single-cell level using light-sheet microscopy. *Neuron* **85**, 462-483, doi:10.1016/j.neuron.2014.12.039 (2015).

196 Liu, T. L. *et al.* Observing the cell in its native state: Imaging subcellular dynamics in multicellular organisms. *Science* **360**, doi:10.1126/science.aaq1392 (2018).

197 Dekkers, J. F. *et al.* High-resolution 3D imaging of fixed and cleared organoids. *Nat Protoc* **14**, 1756-1771, doi:10.1038/s41596-019-0160-8 (2019).

198 Kumar, M., Rauthan, R., Chakraborty, D. & Arumugam, S. in *Brain Organoid Research* (ed Jay Gopalakrishnan) 43-66 (Springer US, 2023).

199 Strobl, F., Schmitz, A. & Stelzer, E. H. K. Improving your four-dimensional image: traveling through a decade of light-sheet-based fluorescence microscopy research. *Nat Protoc* **12**, 1103-1109, doi:10.1038/nprot.2017.028 (2017).

200 Stelzer, E. H. K. *et al.* Light sheet fluorescence microscopy. *Nature Reviews Methods Primers* **1**, 73, doi:10.1038/s43586-021-00069-4 (2021).

201 Ji, N. Adaptive optical fluorescence microscopy. *Nat Methods* **14**, 374-380, doi:10.1038/nmeth.4218 (2017).

202 Huang, B., Babcock, H. & Zhuang, X. Breaking the diffraction barrier: super-resolution imaging of cells. *Cell* **143**, 1047-1058, doi:10.1016/j.cell.2010.12.002 (2010).

203 Wäldchen, F. *et al.* Whole-cell imaging of plasma membrane receptors by 3D lattice light-sheet dSTORM. *Nat Commun* **11**, 887, doi:10.1038/s41467-020-14731-0 (2020).

204 Cao, B., Coelho, S., Li, J., Wang, G. & Pertsinidis, A. Volumetric interferometric lattice light-sheet imaging. *Nat Biotechnol* **39**, 1385-1393, doi:10.1038/s41587-021-01042-y (2021).

205 Chen, B. *et al.* Resolution doubling in light-sheet microscopy via oblique plane structured illumination. *Nat Methods* **19**, 1419-1426, doi:10.1038/s41592-022-01635-8 (2022).

206 Murphy, M. P. *et al.* Guidelines for measuring reactive oxygen species and oxidative damage in cells and in vivo. *Nat Metab* **4**, 651-662, doi:10.1038/s42255-022-00591-z (2022).

207 Sies, H. *et al.* Defining roles of specific reactive oxygen species (ROS) in cell biology and physiology. *Nat Rev Mol Cell Biol* **23**, 499-515, doi:10.1038/s41580-022-00456-z (2022).

208 Erard, M., Dupré-Crochet, S. & Nüße, O. Biosensors for spatiotemporal detection of reactive oxygen species in cells and tissues. *Am J Physiol Regul Integr Comp Physiol* **314**, R667-r683, doi:10.1152/ajpregu.00140.2017 (2018).

209 Van Lidth de Jeude, J. F., Vermeulen, J. L., Montenegro-Miranda, P. S., Van den Brink, G. R. & Heijmans, J. A protocol for lentiviral transduction and downstream analysis of intestinal organoids. *J Vis Exp*, doi:10.3791/52531 (2015).

210 Ermakova, Y. G. *et al.* Red fluorescent genetically encoded indicator for intracellular hydrogen peroxide. *Nat Commun* **5**, 5222, doi:10.1038/ncomms6222 (2014).

211 Pak, V. V. *et al.* Ultrasensitive Genetically Encoded Indicator for Hydrogen Peroxide Identifies Roles for the Oxidant in Cell Migration and Mitochondrial Function. *Cell Metab* **31**, 642-653.e646, doi:10.1016/j.cmet.2020.02.003 (2020).

212 Lippert, A. R., Van de Bittner, G. C. & Chang, C. J. Boronate oxidation as a bioorthogonal reaction approach for studying the chemistry of hydrogen peroxide in living systems. *Acc Chem Res* **44**, 793-804, doi:10.1021/ar200126t (2011).

213 Purdey, M. S. *et al.* Biological hydrogen peroxide detection with aryl boronate and benzil BODIPY-based fluorescent probes. *Sensors and Actuators B: Chemical* **262**, 750-757, doi:https://doi.org/10.1016/j.snb.2018.01.198 (2018).

214 Zhang, R. *et al.* Real-Time Discrimination and Versatile Profiling of Spontaneous Reactive Oxygen Species in Living Organisms with a Single Fluorescent Probe. *J Am Chem Soc* **138**, 3769-3778, doi:10.1021/jacs.5b12848 (2016).

215 Yuan, L., Lin, W., Xie, Y., Chen, B. & Zhu, S. Single fluorescent probe responds to H2O2, NO, and H2O2/NO with three different sets of fluorescence signals. *J Am Chem Soc* **134**, 1305-1315, doi:10.1021/ja2100577 (2012).

216 Saminathan, A., Zajac, M., Anees, P. & Krishnan, Y. Organelle-level precision with next-generation targeting technologies. *Nature Reviews Materials* **7**, 355-371, doi:10.1038/s41578-021-00396-8 (2022).

217 Van de Bittner, G. C., Bertozzi, C. R. & Chang, C. J. Strategy for dual-analyte luciferin imaging: in vivo bioluminescence detection of hydrogen peroxide and caspase activity in a murine model of acute inflammation. *J Am Chem Soc* **135**, 1783-1795, doi:10.1021/ja309078t (2013).

218 Liu, L., Zhang, D., Johnson, M. & Devaraj, N. K. Light-activated tetrazines enable precision live-cell bioorthogonal chemistry. *Nat Chem* **14**, 1078-1085, doi:10.1038/s41557-022-00963-8 (2022).

219 Shchepinova, M. M. *et al.* MitoNeoD: A Mitochondria-Targeted Superoxide Probe. *Cell Chem Biol* **24**, 1285-1298.e1212, doi:10.1016/j.chembiol.2017.08.003 (2017).

220 Gutzeit, V. A. *et al.* A fine-tuned azobenzene for enhanced photopharmacology in vivo. *Cell Chem Biol* **28**, 1648-1663.e1616, doi:10.1016/j.chembiol.2021.02.020 (2021).

221 Keppler, A. *et al.* A general method for the covalent labeling of fusion proteins with small molecules in vivo. *Nat Biotechnol* **21**, 86-89, doi:10.1038/nbt765 (2003).

222 Xue, L., Karpenko, I. A., Hiblot, J. & Johnsson, K. Imaging and manipulating proteins in live cells through covalent labeling. *Nat Chem Biol* **11**, 917-923, doi:10.1038/nchembio.1959 (2015).